ANL-7219

ANL-7219

Argonne National Laboratory

REACTOR DEVELOPMENT PROGRAM

PROGRESS REPORT

May 1966

LEGAL NOTICE

Printed in USA. Price $4.00 . Available from the Clearinghouse for Federal Scientific and Technical Information, National Bureau of Standards, U. S. Department of Commerce, Springfield, Virginia 22151

ANL-7219
Reactor Technology
(TID-4500)
AEC Research and
Development Report

ARGONNE NATIONAL LABORATORY
9700 South Cass Avenue
Argonne, Illinois 60439

REACTOR DEVELOPMENT PROGRAM PROGRESS REPORT

May 1966

Albert V. Crewe, Laboratory Director
Stephen Lawroski, Associate Laboratory Director

Division	Director
Chemical Engineering	R. C. Vogel
Idaho	M. Novick
Metallurgy	M. V. Nevitt
Reactor Engineering	L. J. Koch
Reactor Physics	R. Avery
Remote Control	R. C. Goertz

Report coordinated by
R. M. Adams and A. Glassner

Issued June 30, 1966

Operated by The University of Chicago
under
Contract W-31-109-eng-38
with the
U. S. Atomic Energy Commission

FOREWORD

The Reactor Development Program Progress Report, issued monthly, is intended to be a means of reporting those items of significant technical progress which have occurred in both the specific reactor projects and the general engineering research and development programs. The report is organized in a way which, it is hoped, gives the clearest, most logical overall view of progress. The budget classification is followed only in broad outline, and no attempt is made to report separately on each sub-activity number. Further, since the intent is to report only items of significant progress, not all activities are reported each month. In order to issue this report as soon as possible after the end of the month editorial work must necessarily be limited. Also, since this is an informal progress report, the results and data presented should be understood to be preliminary and subject to change unless otherwise stated.

The issuance of these reports is not intended to constitute publication in any sense of the word. Final results either will be submitted for publication in regular professional journals or will be published in the form of ANL topical reports.

The last six reports issued in this series are:

November 1965	ANL-7122
December 1965	ANL-7132
January 1966	ANL-7152
February 1966	ANL-7176
March 1966	ANL-7193
April 1966	ANL-7204

REACTOR DEVELOPMENT PROGRAM

Highlights of Project Activities for May, 1966

EBR-II

Two reactor runs were completed during the month. In addition, a short run (No. 17A) was made to evaluate the performance of a fuel element rupture detector and fission gas monitor. One experimental subassembly containing oxide and cermet fuel capsules for GE, PNL, and ANL was loaded into the reactor.

Run No. 18, scheduled for 875 MWd, was begun.

With the exception of 4.5 days required for fuel handling, the reactor ran continuously this month.

ZPPR

After a meeting with the Advisory Committee on Reactor Safeguards in Washington, D. C., on May 6, permission was received to solicit bids for the construction contract.

Bid packages on certain components, which had been allowed to expire because of the lengthy hold order on procurement, are being newly assembled for solicitation to vendors.

ZPR-3

A final series of experiments with the SEFOR mockup involved measurements of total reactivity changes due to heating of samples to obtain the Doppler effect.

"Hot sample-cold reactor" measurements were made with oxide samples of U^{238}, U^{235}, Pu^{239} and mixed U^{238}-Pu^{239} in the normal core, core voided of sodium, and in a boron sleeve.

U^{238} gave the expected large negative effect. A pure plutonium sample in the normal core and in the boron sleeve was negative in the first case and positive in the second. A U^{235} sample in the normal core was increasingly positive with temperature increase.

EBWR Plutonium Recycle Program

Measurements were made of the boric acid worth, nine-rod bank worth, and minimum boric acid concentration required for eight-rod shutdown for the full fuel loading at room temperature. The shutdown margin of the unpoisoned, fully rodded reactor was estimated as 6 ± 3% k. The computed shutdown margin, however, is 3.4% k, which will limit the reactor to about 30 MW. The use of spike assemblies as a means of reducing the shutdown margin to allow operation at higher power is being investigated.

TABLE OF CONTENTS

TABLE OF CONTENTS

TABLE OF CONTENTS

I. LIQUID-METAL-COOLED REACTORS

A. EBR-II

1. Operations

Reactor Runs No. 16 (775 MWdt) and No. 17 (475 MWdt) were completed during the month. Total integrated power is now 7,615 MWdt.

Run No. 17-A, "bare pin fuel element test #2," was carried out to evaluate the performance of the fuel-element-rupture detector and the fission gas monitor (see Sect. I.A.4). The response of both detection systems was excellent.

Fuel unloading for Run No. 17 involved the installation of experimental irradiation subassembly X011 in grid position 2-F-1. This subassembly is jointly occupied by fuel specimens from GE, PNL, and ANL. In addition to X011, seven driver subassemblies were removed and replaced.

At the conclusion of Run No. 16, a test was performed to determine the capabilities of the EBR-II turbine-generator automatic transfer system. This test involved separating the EBR-II power-distribution system from the NRTS 138-kV system with the reactor at 25 and 45 MWt, generating approximately 7 and 14.5 MWe, respectively. Under such circumstances, the turbine switches from the initial pressure regulator to speed control. The electrical load drops to approximately 3 MWe and the excess steam is taken up by the bypass system. The test was conducted to determine the following:

a. the transient behavior of the bypass steam system and its controls;

b. the voltage and frequency transient produced by rapid load reduction;

c. the effects, if any, upon continued operation of the reactor under these conditions.

The test results were completely satisfactory at both power levels. Electrical-load reduction was accompanied by an increase in both voltage and frequency; however, the magnitude was small and caused no problems in reactor instrumentation. The steam bypass system assumed the increased steam flow with an increase of only 130 psi during the transient.

This test demonstrated that EBR-II can continue to operate uninterruptedly, even though separated from the NRTS electrical-distribution system by a fault or a failure in that system.

Four rod-drop tests were performed at 45 MWe and four at 500 kW during Run No. 16 to obtain further data on the feedback characteristics of the reactor and its associated heat transfer systems.

During Run No. 17, subassembly C-166, which had been removed from the grid at the conclusion of Run No. 16, was transferred to the Fuel Cycle Facility for surveillance examination. This subassembly, a Mark I-A type, is the first of this type to achieve 0.95% burnup.

Fuel loading for Run No. 18, scheduled for 875 MWdt, was started, involving the exchange of eight enriched core types, two control, and one inner blanket subassemblies. This run is scheduled for the purpose of irradiating a selected Mark I-A surveillance subassembly (C-182) to a burnup of 1.2 a/o.

2. Maintenance and Modification

Installation of the new door on the Reactor Building end of the equipment air lock has been satisfactorily completed. Leakage during the standard leak rate test was smaller than previously recorded and well within the specified limits.

A load test of the auxiliary primary sodium pump batteries was made to test the discharge characteristics in the event of a complete power failure. In every category tested, the results indicate some loss in capacity, but all minimum requirements specified were exceeded. Chemical analysis showed that the electrolyte requires replacement, and procurement has been initiated.

3. Reactor Improvements

a. Oscillator System Mark II. Fabrication of the mechanical components of the oscillator rod (see Progress Report for October 1965 ANL-7115, pp. 3-6) was completed. The rod drive subassembly has been completed and operated successfully. After an inspection of the drive-shaft assembly for straightness, the rod drive unit, the shaft subassembly, and the dummy oscillator rod with its thimble were assembled and installed in the sodium test tank.

The temporary operating console and drive-unit wiring have been completed and are being checked in preparation for the operational, elevated-temperature test runs.

The investigation of hydraulic design of the oscillator rod by water-flow tests gave satisfactory results.

b. Sodium Surveillance Periscope. The Sodium Surveillance periscope was removed from the primary tank due to malfunction of the optical system. Inspection after disassembly disclosed that one of the pitch-cemented achromat lenses located in the lower end of the periscope had overheated and the cement had melted. This lens was replaced by an air-spaced type of achromat, which should eliminate the temperature problem.

In addition, a small leak had occurred at the seal on the screw-on type of cap located at the lower end of the periscope. Inleakage of sodium vapor past this seal resulted in a thin film of sodium on some of the noncoated-type lenses. To eliminate the leakage, the lower end of the periscope was redesigned for a bolted flange-type end cap, and the metallic seal will be replaced with a high-temperature, reinforced Teflon gasket. Also, the operating instructions are being changed to assure a constant positive argon pressure of 5 in. of water at all times inside the periscope to reduce possibility of inleakage.

The redesign has been completed and fabrication of new parts is approximately 50% complete.

4. Bare Pin Experiment No. 2

A measure of the signal strength expected from the Fuel Element Rupture Detection (FERD) monitoring system in the event of fuel-pin failure was established from simulation studies in which an unclad fuel pin, contained in a standard control-rod subassembly, was deliberately inserted into the core. A graphic record of significant results is given in Fig. 1 for one of the three counting channels (similar results were obtained with two other independent channels). The amplitude of the trace at the right-hand side gives the total signal, 49 cps, with the bare pin fully inserted in the core. The background component due to Na^{24} was established by turning off the flow through the loop. As expected, delayed-neutron-emitting species remaining at the detection point decayed rapidly. The counting rate, after

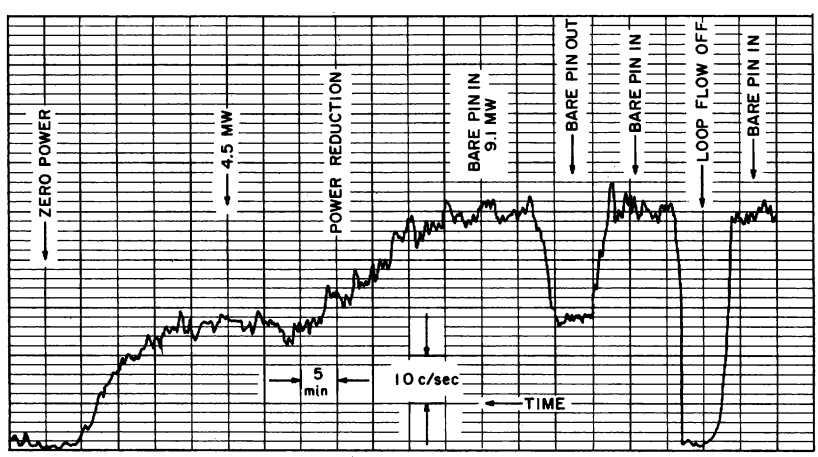

Fig. 1. Signal from Channel 2A of Delayed-neutron Monitor

complete decay of the delayed-neutron-emitting species, consisted primarily of events caused by the Na^{24} activity, the signal amounting to approximately one cps.

Upon the reinitiation of flow, the counting rate increased to its original level. After reaching equilibrium, the control element was driven downward to approximately 2.20 in. The gross counting rate, accordingly, decreased to 28 cps, a value which reflected fissions in the unclad pin at this elevation. Following a period of approximately 10 min with the pin fully inserted, the power was reduced from 9.1 MW to 4.5 MW. As evident from Fig. 1, the gross counting rate decreased by a factor of two. Upon reducing power to zero, the counting rate decreased to 1 cpm, a rate attributable primarily to Na^{24} activity.

The only important counting rate component not established in these measurements is the effect of "tramp uranium," defined as fissionable material present in the system either as an impurity in the coolant or as a contamination on fuel-element surfaces. The magnitude of this effect, 5.5 cps, was established at a corresponding power level after the modified control assembly had been removed from the system. The signal intrinsically associated with the full insertion of the unclad pin thus amounts to 42.5 cps. Since the combined unavoidable background from tramp uranium and Na^{24} activity is only 6.5 cps, the true signal-over-background ratio is given by 42.5/6.5, or 6.5, a value sufficiently high to permit the detection of an actual fuel-pin failure which results in the exposure of bare fuel approaching that of a single pin in area.

5. Experimental Irradiations

Experimental subassembly XO11, containing seven and nine mixed-oxide fuel capsules from the ANL and GE, respectively, and three cermet capsules from Battelle Northwest, was loaded into reactor position 2-F-1. Alpha-measurement subassembly C222X was removed from position 5-B-4 after completing the desired exposure.

A flowmeter of higher range for flow testing subassemblies at rates equivalent to the maximum in driver fuel subassemblies is now on hand. The recently available Mark-B experimental subassembly design will allow fuel loading and required flow rates comparable to that of adjacent driver fuel. The new flowmeter will allow the flow testing of the Mark-B subassembly with maximum fuel loading.

6. Fuel Cycle Facility

a. Vertical Assembler-Dismantler. A specific-purpose machine, the Vertical Assembler-Dismantler (VAD), is being developed which will vertically assemble or disassemble EBR-II experimental core subassemblies.

This will enable experimental capsules or elements to be replaced or regrouped within a subassembly as desired for further irradiation. Vertical handling is needed so that liquid metal bonds are not disrupted.

The very restricted viewing and manipulation available in the FCF Air Cell has emphasized the need for a detailed configurational study of the VAD. To aid in the study, a full-sized wooden partial mockup has been built and modified to achieve the desired viewing and manipulator access. The conceptual arrangement of the ducting for the suction cooling system is also being worked on by means of this mockup. Basically the machine consists of a long vertical carriage which supports the core subassembly, subassembly rotational drive, and horizontal cooling plenum. This carriage can be positioned vertically to bring the desired areas of the subassembly into convenient working position. The carriage moves down into a pit in the floor for operation on the upper end.

The VAD will require the use of extended-reach mechanical master-slaves in order to achieve sufficient vertical reach. One each of a heavy-duty and standard-duty manipulator, not used now in the FCF Air Cell, are being purchased for use in future mockup and final machine tests. They will later be installed in the cell.

Detailed design of the main frame of the machine, and major subassemblies, e.g., the core subassembly rotational drive, the carriage-elevating drive, and hex tube cutter has been started. Fabrication of the prototype fuel-element remover and loader is nearly complete.

The welding of the hexagonal sheath to the pole piece of the subassembly has given some trouble with the present assembly machine. It is planned to determine the operating range of the critical welding parameters, e.g., part clearances, electrode spacing and temperature, gas flow and pressure, and welding current profile. All parts for these tests are being procured or fabricated.

b. Investigation of Process Conditions. A continuation of studies aimed at defining minimum process conditions in melt refining has investigated the effect of liquation temperature on fission product removal. A series of 2-hr runs were made in which the liquation temperature was varied between 1300 and 1400°C. At 1350°C, removal of cerium dropped to 89-96%, compared with 99.9% removal obtained at 1400°C. Removal of barium and cesium was unaffected. At 1300°C, removal of cerium decreased further, and the removal of barium dropped from 99.9 to 97% and of cesium from 99.9 to 99.5%.

c. Comparison of FCF- and Chicago-produced Fuel Pins. Correlation of data from bond testing of FCF-produced and Chicago-produced Mark-I-A fuel pins shows that the reject rate resulting from gas-void

formation in the sodium within the jacket (voids along the length of the pin, bubbles between the pin and the restrainer, and trapped sodium on the restrainer) is significantly higher for FCF-produced pins: 57 per 1000 versus 21 per 1000 for Chicago-produced pins. Two variations which would affect the surface condition on the pins are: (1) a thoria wash is used on the FCF injection-casting molds, whereas a yttria wash was used in Chicago; (2) the Chicago-produced pins were all wiped clean of the mold wash after they were removed from the molds, while the FCF pins are processed as produced in the injection-casting operation. Both variables will be investigated in an effort to increase the acceptance rate from bonding. In conjunction with this, the average number of bonding runs required for Chicago-produced pins is 1.3 per element, whereas the FCF pins require 1.5 per element. This is a result of rebonding runs made to increase the acceptance rate, but which reduce the productivity of the machine.

Axial profiles of burnup from Mark-I-A fuel elements obtained by gamma scanning indicate no significant difference in axial or radial burnup distribution between the Mark-I and the Mark-I-A fuel. This may change when all of the remaining Mark-I fuel, comprising more than half the core at present, has been removed from the reactor.

Measurements of sodium level made with two Chicago-manufactured Mark-I-A irradiated subassemblies (0.62 and 0.95% maximum burnup) show slightly higher levels than those obtained from Mark-I fuel of comparable burnup values. This may result from less pneumatic restraint because of the larger gas space in the Mark-I-A jacket, which would allow a greater swelling of the fuel at low burnup values. Surveillance of Mark-I-A fuel is continuing.

Measurements of sodium level of recycled Mark-I irradiated fuel have shown abnormal axial growth of the fuel pins produced from two FCF casting batches. All examined pins from these two batches showed this growth. Detailed chemical and metallurgical examinations of these pins will be made to try to isolate the cause of this behavior.

TABLE I. Production Summary for May 1966

Subassemblies received	13 plus 6 unirradiated natural uranium for storage		
Subassemblies dismantled			12
Subassemblies fabricated			8
Subassemblies transferred to reactor			20
Pins decanned			1044
Melt refining	5 irradiated	6 recycle	
Avg pour yield	92.7%	93.2%	
Injection casting runs			13
Pin Processing			
Accepts			1107
Rejects			254
Pins welded			800
Leak testing			
Accepts			816
Rejects			20
Bond testing (complete runs)			
Accepts			386
Rejects			34
Surveillance	C-191, C-165, C-194, C-166, XA01		

B. General Fast Reactor Physics

1. ZPR-3

a. Doppler Measurements. A series of "hot sample-cold reactor" measurements were performed with the SEFOR mockup in ZPR-3. Since the total reactivity change due to heating the samples was measured, expansion effects must first be calculated and subtracted from the measurements to obtain the Doppler effect.

The experiments were performed with 0.5-in.-dia oxide samples of 70% theoretical density. These samples were small enough not to perturb the spectrum greatly but, at the same time, were large enough to give sufficient reactivity signals.

The measurements were performed in three environments in an attempt to isolate different effects. A natural uranium sample was measured in the normal core environment, the core voided in sodium, and in a boron sleeve. The results (see Fig. 2) were increasingly negative with increasing temperature. Preliminary calculations give values which are 86% of that measured in the normal core and 75% of that in the sodium-voided core, indicating that the calculations did not provide sufficiently negative values. The measurement in the boron sleeve (0.5-in.-thick natural boron carbide) indicates that the measured reactivity signal was primarily due to low-energy neutrons.

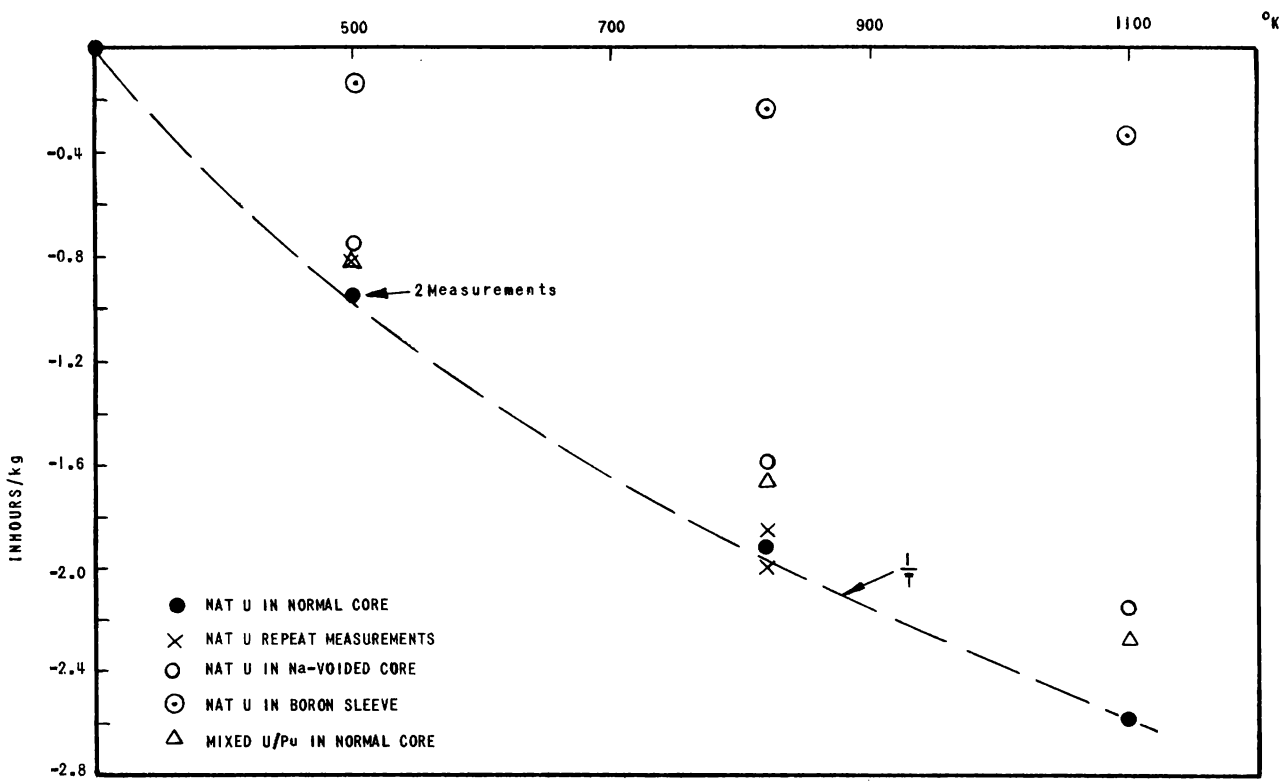

Fig. 2. Measured Reactivity Changes in the SEFOR Mockup due to Heating

A 7:1 atomic ratio mixed natural uranium:plutonium sample was also measured in the normal core. As expected, the large U^{238} signal overwhelmed the smaller Pu^{239} signal and any interaction effects between the two elements.

The measured values of the natural uranium and mixed samples are given in Table II relative to the natural uranium measurement in the normal core. It is encouraging that the measured reduction in the reactivity signal due to voiding the core of sodium is less than the calculated reduction of about 27%.

TABLE II. Measured Change Relative to Natural Uranium in Normal Core

Sample and Environment	Temperature (°K)		
	500	800	1100
Natural Uranium in Sodium Void	0.818	0.825	0.831
Natural Uranium in Boron Sleeve	0.133	0.119	0.129
Mixed U/Pu in Normal Core	0.886	0.861	0.882

A pure plutonium sample was measured in the boron sleeve and in the normal core. In both cases, the results varied monotonically to 800°K with a negative measured reactivity change in the normal core and a positive change in the sleeve (see Fig. 3). Above 800°K, curves for both cases have an increasing positive slope, that for the normal core changing

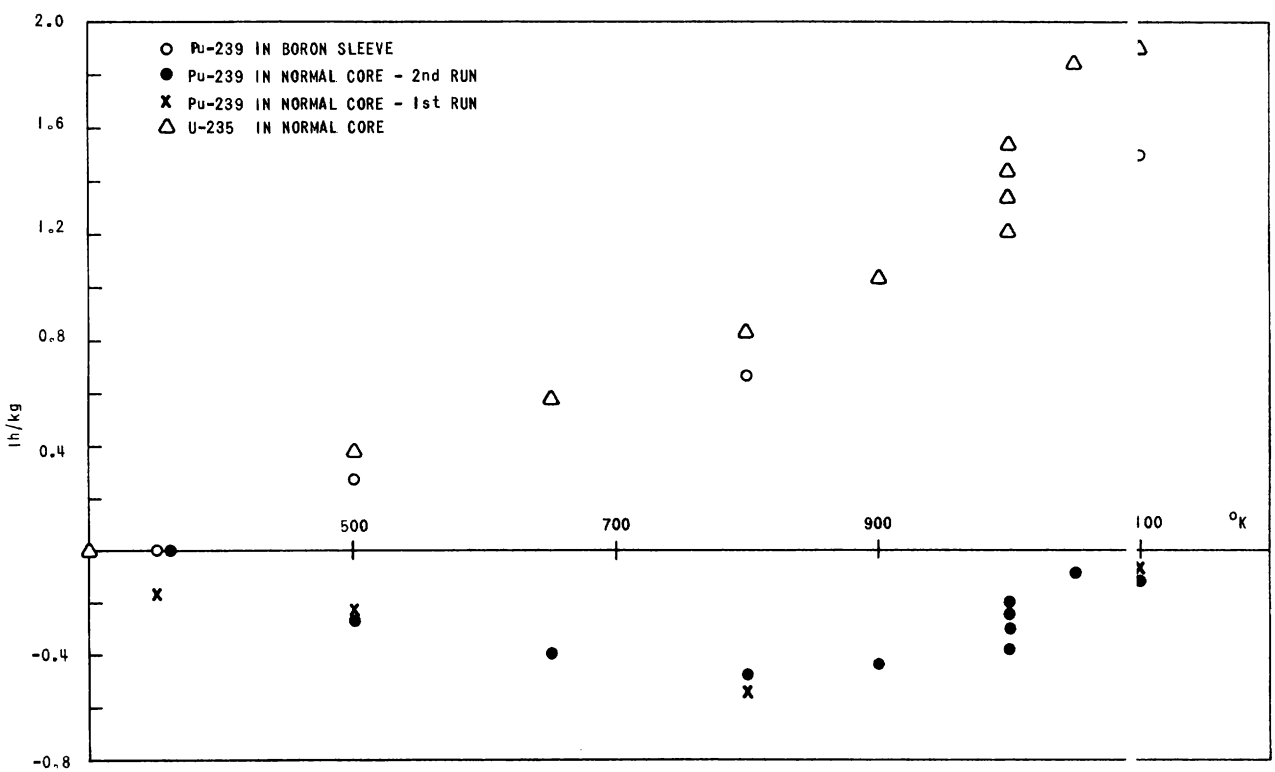

Fig. 3. Measured Reactivity Changes for Fissile Samples

from negative to positive. In particular, the reactivity signal varied as a function of time at 1000°K and did not stabilize during the course of the measurement at that temperature. The temperature was then raised to 1050°K, at which point the signal became stable. A U^{235} sample was then run to determine if changes in slope of the signal and time variation of response were due to the sample construction or were peculiar to the plutonium sample. The same type of behavior was observed with the U^{235} sample, particularly the changing reactivity signal at 1000°K.

Previous out-of-core experiments indicated that the samples became slightly plastic above 800°K. Repeat measurements of the Pu^{239} and U^{235} samples at the reference temperature indicated a permanent positive reactivity change in the samples. However, this change is only about 20% of the change due to the increased slope, indicating that the effect, whatever it is, is mostly reversible. Out-of-core X-ray measurements will be made to determine the type and magnitude of the physical changes in the samples.

b. Instrument and Technique Development. The DDP-24 computer at the Illinois site has been used for on-line processing of data from the ZPR-3 fast critical in Idaho with the aid of a Dataphone link. Two Dataphones, Type 202-C, were installed at each location so that two quantities could be monitored simultaneously.

One set of Dataphones was used for the transmission of pulses whose rate was proportional to the reactor flux. To obtain these pulses, the output of an ion chamber and current amplifier was taken to a voltage-to-frequency converter, whose output in turn was scaled by a factor of 100. The output of the prescaler had a maximum rate of 1000 pulses/sec, which should have been within the transmission capacity of the Dataphones. It was found, however, that such a rate could not be transmitted over the circuits between Illinois and Idaho. Therefore, the output of the prescaler was run into a flip-flop which would make one transition for each pulse and thus halve the rate. This pulse rate could be transmitted without error.

At the Illinois end, the received pulses were differentiated. Each spike from the differentiator represented 100 counts from the voltage-to-frequency converter. Alternate spikes were of opposite polarity, but the input circuits to the DDP-24 data scalers will accept pulses of either polarity, so that the counts could be recorded accurately.

The flux signals were used both for period and rod-calibration measurements. The least-count error introduced by the prescaling did not cause noticable dispersion in the rod-calibration traces.

The other pairs of Dataphones was used for the transmission of rod-position information. This was obtained from an optical disk encoder connected to the rod-position indicator, which transmitted one pulse for every 0.025 in. of rod motion.

Excellent agreement for both period measurements and rod calibrations was obtained with the results of previous measurements that had been done using off-line methods.

The 600-line/min printer obtained from the recently decommissioned GUS Computer System has been connected to the DDP-24 computer and is now in routine use.

2. ZPR-6

The preliminary loading of Assembly No. 5 has been completed. The degree of misalignment between the stationary half and the movable half has been measured. One quadrant in each half of the reactor has been unloaded and the Doppler experiment drawer will be aligned by shimming techniques.

The solid wiring to the stationary-half rod-drive mechanisms has been replaced by stranded-wire cables to reduce the problem of wire breakage at the rod connectors. All B^{10} and dual-purpose rods have been inspected and serviced where necessary.

All power supplies for the ionization chambers have been checked and repaired to bring their performance within specifications. In addition, the linear and log reading instruments have been checked. Hum and noise pickup in the operating instruments have been reduced by eliminating multiple ground loops and by installing a new instrument ground line

A pulsed neutron generator was delivered by KAMAN NUCLEAR and installed in the basement of Building 316. The machine is capable of producing about 2×10^{11} neutrons/sec in continuous operation. It has provisions for microsecond pulsing with a minimum pulse width of 1 microsecond and for nanosecond pulsing with a minimum pulse width of 10 nanoseconds. Prompt-neutron decay measurements and possibly time-of-flight measurements will be performed with this generator for ZPR-6 and -9 assemblies, and measurements will be made for non-multiplying assemblies of various reactor materials.

At present the various modes of operation of the machine are being tested. So far, it has been operated at a yield of about 5×10^{9} neutrons/sec in the continuous mode and with microsecond pulsing. Operation with full yield and with the nanosecond pulser will be performed after some modifications are made to the pulsing component.

3. ZPR-9

ZPR-9 Assembly 11A went critical on May 19. This assembly is a zoned system with the central region of the core having a composition typical of a dilute U^{235}-fueled carbide fast reactor, and identical in composition but smaller than the central region in ZPR-6 Assemblies 4Z and 5. The primary purpose of the study is to determine the U^{238} and U^{235} Doppler effect in the spectra over a wide range of variations of the central core composition.

Initial spectrum measurements with Assembly 11A were made using hydrogen-recoil proportional counters. Two types of proportional counters were used in each spectrum measurement; both types were made with stainless steel walls 0.8 mm thick. One counter was pressurized to 5 atm of hydrogen, and had an effective counting length of 3.1 cm and a diameter of 1.6 cm. This detector was used to span the energy region below 300 keV. Since hydrogen-filled counters show prohibitive wall and end-effect distortions above this energy level, the second and larger counter, having a 5.0-cm effective length and a diameter of 2.5 cm, was filled to a pressure of 5 atm of methane. No corrections were made for wall and end effects in the measured spectrum. These effects could contribute about a 20% systematic error, at most, to the data at 1 MeV and correspondingly less with decreasing energy.

Systematic errors may also be present at very low energies (below 5 keV) due to several unrelated effects. However, the spectra at these energies are not expected to be distorted by more than 25%, either in energy or amplitude.

The energy resolution of the measurements was about 20% (fullwidth at half maximum) and the statistics were within $\pm 3\%$ of the maximum observed neutron-flux value. About 7 hr was required to perform each measurement.

Spectra were measured in the central drawer at a counter position 4 in. back from the reactor midplane at about 7% and 0.1% $\Delta k/k$ subcritical. The results show no significant differences in the spectra as a function of subcriticality in this range. The results are in very close agreement with the spectra from ZPR-6 Assembly 4Z. Figure 4 shows a comparison of the measured spectra at 0.1% $\Delta k/k$ subcritical with the group spectra calculated by means of the MACH-1 code and ELMOE-corrected cross sections.

4. ZPPR

After a meeting of ZPPR personnel with the full committee of the Advisory Committee on Reactor Safeguards in Washington to review the Preliminary Safety Analysis Report, the Laboratory received permission informally to solicit bids for the construction contract.

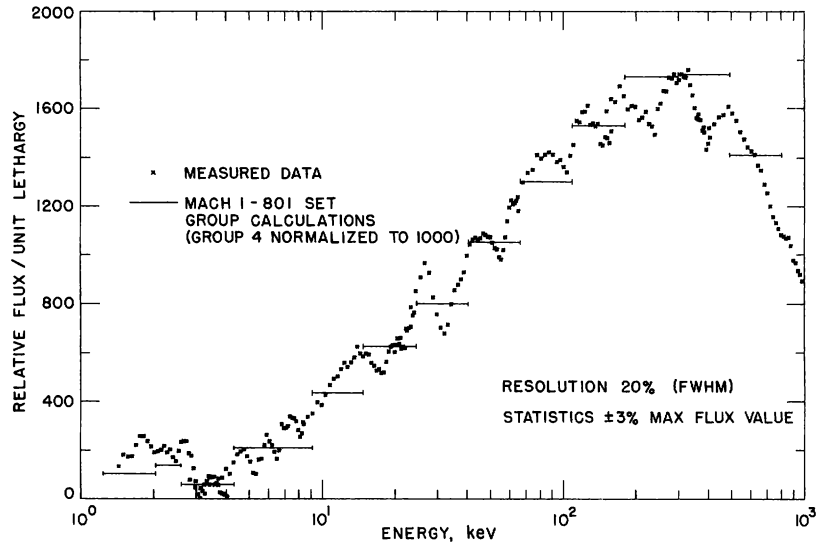

Fig. 4. Spectra as Measured in the Central Drawer at the Midplane in ZPR-9 Assembly 11A at 0.1% Δk/k Subcritical. The experimental results are compared with calculated values obtained from use of the MACH-1 code and ELMOE-corrected cross sections.

Work on all items except the bed and tables and the reactor matrix drawers had been at a standstill to this time because of instructions from the AEC to hold up procurement. The fuel-rod drives and reactor matrix tubes have been fabricated to specification and have been accepted.

Bids had been received and evaluated previously on the poison safety-rod drives, the reactor knees, safety blades and sheaths, and the rear support structures for the rod drives. The time limits on these bids have been allowed to expire on the basis of the hold order on procurement. Complete new bid packages are being assembled to send out to vendors.

The following is the present status of reactor components in the procurement phase:

a. Reactor Bed and Tables: The schedule for delivery of the bed and tables has been extended to August 30 instead of May 31. All castings have been received from the foundry. The castings were visually inspected on April 28 for major defects such as voids, cracks, and discontinuities in all accessible areas. These castings appeared to be good and were quite straight and true for their size. Analyses of the chemical and physical characteristics of the castings are in progress. Machining of the other components, such as the ball screw and transmission, is approximately 35% complete.

b. Matrix Drawers. All of the 2-in.-wide drawer blanks have been perforated. Six hundred have the front weld complete. Of these, approximately 500 have had the front face milled and finished. The next step in the operation is the welding of the rear portion of the drawer and subsequent stretching to size.

C. General Fast Reactor Fuel Development

1. Jacket Development

a. Tube-burst Tests. Tube-burst tests of 0.74-cm-OD x 0.04-cm-wall tubing of Type 304 stainless steel and V-15 w/o Ti-7.5 w/o Cr were made. Both at room temperature and 650°C, the stainless steel was tested in an as-drawn condition (~40% cold work) and in an annealed (15 min at 1090°C and rapid cool) condition. Tubes of V-Ti-Cr alloy were tested at room temperature in the as-drawn condition (~40% cold work) and in the annealed condition (1 hr at 850°C). At 650°C, the Vi-Ti-Cr alloy was tested in an as-drawn condition and two annealed conditions: the standard anneal of one hour at 850°C, and a high-temperature anneal of one hour at 1250°C.

For the room-temperature tests, the tubes were pressurized with oil. For tests at 650°C, the tubes were heated in a flowing helium atmosphere and pressurized with argon. Since the tubes were heated for a relatively short time (15 to 30 min), the helium atmosphere provided adequate protection against contamination at 650°C. Three tubes were tested for each set of conditions.

Calculations of hoop stress were based on the thick-wall tube formula using pretest tube dimensions. After rupture, an average tube diameter was measured at a location near the failure to obtain a rough measure of the deformation just prior to failure. Comparison of the tube diameters before and after testing yielded an approximation of the expansion of the tubes prior to rupture.

The results of the tube-burst tests are summarized in Table III which gives the burst pressures, calculated hoop stresses, and approximate

TABLE III. Results of Tube-burst Tests at Room Temperature and 650°C on Type 304 Stainless Steel and V-15 w/o Ti-7.5 w/o Cr Tubing

(Nominal tube size of 0.292-in. OD x 0.016-in. wall thickness)

	Room Temperature			650°C		
Material and Condition	Burst Pressure (psi)	Calculated Hoop Stress (psi)	Approx Radial Expansion (%)	Burst Pressure (psi)	Calculated Hoop Stress (psi)	Approx Radial Expansion (%)
Type 304 SS, As drawn						
Average	21,600	188,200	1.6	11,600	101,300	1.6
Range	21,050-21,950	183,200-191,000	1.5-1.7	11,300-11,800	99,700-102,400	1.3-1.8
Type 304 SS, Annealed						
Average	9,200	80,000	24.4	5,330	46,500	16.4
Range	8,950-9,450	78,000-82,400	23.0-25.1	5,300-5,400	46,200-47,100	15.8-17.6
V-15 Ti-7.5 Cr, As drawn						
Average	19,000	168,100	1.2	14,300	125,800	3.0
Range	18,850-19,300	166,200-170,700	1.0-1.3	14,100-14,500	123,600-127,400	2.2-3.7
V-15 Ti-7.5 Cr, 850°C Anneal						
Average	14,200	124,800	8.6	10,800	95,100	6.9
Range	13,850-14,400	122,100-126,900	7.3-10.4	10,600-11,000	93,400-96,600	5.6-8.6
V-15 Ti-7.5 Cr, 1250°C Anneal						
Average	-	-	-	10,700	93,800	5.7
Range				10,600-10,750	92,900-94,800	4.8-6.3

elongations. The range is given along with the average values. The V-15 w/o Ti-7.5 w/o Cr alloy proved significantly stronger than Type 304 stainless steel for all cases except the room-temperature tests with the materials in an as-drawn condition. In this case, the stainless steel was about 10% stronger. In the annealed condition, the V-Ti-Cr alloy was about 50% stronger than Type 304 stainless steel in the room-temperature tests. In the tube-burst tests at 650°C, the V-Ti-Cr alloy was about 25% stronger than Type 304 stainless steel in the as-drawn condition, and stronger by a factor of about two in the annealed condition.

Expansion as measured by diameter increase was roughly comparable between the two materials in the as-drawn condition, but the stainless steel showed much more radial expansion than the vanadium alloy in the annealed condition. The Type 304 stainless steel suffered significantly more degradation of strength in going from room temperature to 650°C than did the vanadium alloy. Calculated hoop stresses at failure dropped approximately 40% for Type 304 stainless steel but only about 25% for the vanadium alloy. Annealing the vanadium alloy at 1250°C instead of at 850°C yielded an insignificant drop in hoop stress and a slight drop in expansion.

2. Refractory-metal Alloys for Service in Oxygen-contaminated Sodium

The dynamic test of annealed V-20 w/o Ti and V-15 w/o Ti-7.5 w/o Cr in sodium flowing at 6.1 m/sec at 650°C and containing 10 to 12 ppm of oxygen by weight is continuing (see Progress Report for April 1966, ANL-7204, p. 24). After 53 days of exposure the V-20 w/o Ti samples still show no external change (except for a slight brown color) and the weight-gain data can be expressed by the equation

$$\Delta W\ (mg/cm^2) = 0.278\ t^{0.278}, \qquad (1)$$

with t in days. The weight gains of V-15 w/o Ti-7.5 w/o Cr samples are only about 60% of those for V-20 w/o Ti.

The exponent 0.209 in Eq. (1) has no known theoretical significance, but it does represent very protective kinetics. There is always the possibility that loss of corrosion product could account for such a low value, but there is no sign of such loss as judged by thickness measurements or appearance of the samples.

A number of alloys prepared in sheet form have been exposed for seven days to 650°C sodium containing about 15 ppm oxygen. The data are shown in Table IV.

A test of levitation-melted alloy cylinders under the same conditions was completed to fill in missing data for the V-Cr-Al system. The results are shown in Table V.

TABLE IV. Corrosion of Vanadium-base Alloys in Sodium at 650°C

Alloy (w/o)	ΔW (mg/cm²)
V-5 Cr, As Rolled	9.1
V-10 Cr, As Rolled	9.3
V-15 Ti-7.5 Cr-1 Y, Annealed*	14.6
V-40 Ti-5 Cr, Annealed*	9.3
V-40 Ti-10 Cr, Annealed	9.3
V-20 Ti, Annealed	9.7

*Annealed one hour in vacuum at 900°C.

TABLE V. Experimental Castings Exposed to Sodium at 650°C

Alloy (w/o)	ΔW (mg/cm²)
V-30 Cr-5 Al	4.0
V-30 Cr-7.5 Al	1.8
V-40 Cr	1.6
V-40 Cr-10 Al	0.2
V-20 Ti, Annealed Sheet	8.4

3. Irradiation of Materials for Fast Reactors

a. Examination of Irradiated EBR-II Fuel Cladding. Specimens of Type 304L stainless steel, about 3.5 in. long, taken from the tubular jackets of irradiated EBR-II fuel rods are being used for burst tests. Argon is the pressurizing medium.

In addition to the tests previously reported (see Progress Report for April 1966, ANL-7024, pp. 19-20), five specimens from the jacket of fuel rod C142-E78 have been tested at 600°C. The calculated tangential rupture strength varied from a minimum of 59,100 psi at the top of the jacket to a maximum of 67,100 psi slightly below the center of the fuel column. The range of rupture strength values along the length of the jacket compared to previously reported values for 500 and 700°C indicate that some annealing is occurring at the 600°C test temperature.

Circumferential elongations were determined from diameter measurements on each specimen. The average elongations ranged 0.3 to 3.1%, values that in general are between those obtained from the tests at 500 and 700°C. The ductility minimum apparently is in the neighborhood of 500°C, which is the approximate maximum jacket temperature in the reactor.

b. Uranium-Plutonium Alloys. Capsule ANL-55-8 was irradiated in the MTR from June 8, 1964 to January 10, 1966. The capsule contained three experimental metallic fuel rods, whose fuel composition is given in Table VI and whose cladding is identified in Table VII. The calculated burnup, based on reported flux, was 3.3 a/o. Maximum jacket temperatures during irradiation were 555°C.

TABLE VI. Identification of Fuel in Capsule ANL-55-8

Specimen Number	Fuel Composition (w/o)	Uranium Enrichment (%)	Length of Fuel (in.)	Diameter of Fuel (in.)
CK01	U-10 Pu-10 Fz	15.5	12.999	0.145
CE03	U-15 Pu-10 Fz	7.7	13.000	0.145
EC01	U-15 Pu-10 Fz	7.7	13.001	0.143

TABLE VII. Identification of Cladding in Capsule ANL-55-8

Specimen Number	Composition (w/o)	Condition	OD (in.)	Wall Thickness (in.)	Gas Expansion Volume (%)
CK01	Nb-1 Zr	Annealed	0.186	0.015	22
CE03	Nb-1 Zr	Annealed	0.186	0.015	23
EC01	V	Annealed	0.186	0.015	24

The capsule was opened in the Metallurgy Alpha-Gamma Hot Cell in Building 212. Fuel rods CK01 and CE03 jacketed in Nb-1 w/o Zr alloy were found to have brittle-appearing ruptures in the jackets. Fuel rod EC01 with vanadium cladding was apparently in excellent condition.

A volume determination by the method of immersion indicated that the fuel rod EC01 was intact and had increased in volume 1.5%. Further examination is in progress.

A total of 20 full-length (14 in.) metal fuel rods are undergoing irradiation in EBR-II. Eighteen rods are of U-Pu-Zr alloys clad in either V-20 w/o Ti, Type 304 stainless steel, Type 316 stainless steel, Hastelloy-X, or Hastelloy-X-280 tubings. These rods are subject to maximum cladding temperatures of 650°C and at present have reached a calculated maximum 2.5 a/o burnup. Two additional rods are fueled with U-Pu-Ti alloy and clad in V-20 w/o Ti alloy tubing. The rods are being irradiated at maximum cladding temperatures of 540°C and have attained a maximum burnup of 2.7 a/o. Additional details on the design of the fuel rods and the irradiation conditions are summarized in Table VIII.

Five instrumented temperature-controlled capsules, which contain several different types of experimental alloy fuels are being irradiated in CP-5 (see Table VIII).

TABLE VIII. Status of Metal Fuel Irradiations in Progress

Test Reactor	Capsule or S/A No.	Specimen Number	Design Parameters: Fuel Composition (w/o)	Effective Density (%)	Cladding Composition (w/o)	Cladding OD (in.)	Cladding Thickness (in.)	Operating Conditions: kW/cc[a]	Max Cladding Temp (°C)	Burnup to Date: a/o (U + Pu)	Burnup to Date: fiss/cc x 10^{-20}[a]
CP-5	CP-45	1N15	U-19 Pu-14 Zr	66	V-20 Ti	0.208	0.015	2.6	640	7.9	17.1
EBR-II	XG06	ND23	U-15 Pu-10 Zr	66	V-20 Ti	0.209	0.016	1.7	540	2.6	6.2
EBR-II	XG05	ND24	U-15 Pu-10 Zr	66	V-20 Ti	0.209	0.016	1.7	535	2.5	6.0
EBR-II	XA07	ND28	U-15 Pu-9 Zr	75	304 SS	0.208	0.021	2.0	650	2.5	7.0
EBR-II	XA07	ND41	U-15 Pu-9 Zr	75	304 SS	0.208	0.021	2.0	650	2.4	6.7
EBR-II	XA07	ND32	U-15 Pu-9 Zr	75	316 SS	0.196	0.015	2.0	645	2.3	6.4
EBR-II	XA07	ND43	U-15 Pu-9 Zr	75	Hastelloy-X	0.196	0.015	2.0	645	2.4	6.7
CP-5	CP-48	1L18	U-15 Pu-12 Zr	75	Hastelloy-X	0.196	0.015	1.9	600	1.7	4.3
CP-5	CP-48	2F35	U-15 Pu-12 Zr	75	304 SS	0.196	0.015	1.9	600	1.7	4.3
CP-5	CP-48	3F37	U-15 Pu-12 Zr	75	316 SS	0.196	0.015	1.9	600	1.7	4.3
CP-5	CP-48	4L19	U-15 Pu-12 Zr	75	Hastelloy-X	0.196	0.015	1.9	660	1.7	4.3
CP-5	CP-48	5F36	U-15 Pu-12 Zr	75	304 SS	0.196	0.015	1.9	660	1.7	4.3
CP-5	CP-48	6F38	U-15 Pu-12 Zr	75	316 SS	0.196	0.015	1.9	660	1.7	4.3
EBR-II	XA07	ND25	U-14 Pu-12 Zr	76	304 SS	0.208	0.021	1.9	630	2.2	5.7
EBR-II	XA07	ND27	U-14 Pu-12 Zr	76	304 SS	0.208	0.021	1.9	630	2.2	5.7
EBR-II	XA07	ND26	U-14 Pu-12 Zr	76	316 SS	0.196	0.015	1.8	625	2.1	5.5
EBR-II	XA07	ND29	U-14 Pu-12 Zr	76	316 SS	0.196	0.015	1.8	625	2.2	5.7
EBR-II	XA07	ND30	U-14 Pu-12 Zr	76	316 SS	0.196	0.015	1.9	635	2.4	6.2
EBR-II	XA07	ND31	U-14 Pu-12 Zr	76	316 SS	0.196	0.015	1.9	635	2.3	6.0
EBR-II	XA07	ND33	U-14 Pu-12 Zr	76	Hastelloy-X	0.196	0.015	1.9	630	2.3	6.0
EBR-II	XA07	ND34	U-14 Pu-12 Zr	76	Hastelloy-X	0.196	0.015	1.9	635	2.4	6.2
EBR-II	XA07	ND35	U-14 Pu-12 Zr	76	Hastelloy-X	0.196	0.015	1.9	640	2.4	6.2
EBR-II	XA07	ND37	U-14 Pu-12 Zr	66	Hastelloy-X-280	0.208	0.015	1.8	635	2.4	6.0
EBR-II	XA07	ND39	U-14 Pu-12 Zr	66	Hastelloy-X-280	0.208	0.015	1.8	635	2.4	6.0
EBR-II	XA07	ND44	U-14 Pu-12 Zr	66	Hastelloy-X-280	0.208	0.015	1.8	635	2.3	5.7
CP-5	CP-44	1N14	U-15 Pu-10 Ti	69	V-20 Ti	0.203	0.015	2.4	560	6.8	15.6
EBR-II	XG05	NC17	U-15 Pu-10 Ti	63	V-20 Ti	0.209	0.016	1.6	540	2.6	5.7
EBR-II	XG06	NC23	U-15 Pu-10 Ti	63	V-20 Ti	0.209	0.016	1.6	540	2.7	5.9
CP-5	CP-41	4N10	U-10 Pu-10 Fz	77	V-20 Ti	0.196	0.016	1.9	530	6.7	19.7
CP-5	CP-41	5N11	U-10 Pu-10 Fz	79	V-20 Ti	0.193	0.016	2.0	530	6.7	20.1
CP-5	CP-41	6N12	U-10 Pu-10 Fz	84	V-20 Ti	0.189	0.016	2.1	530	6.7	21.4
CP-5	CP-46	1T3	U-15 Pu-10 Fz	57*	Nb-1 Zr	0.174	0.009	1.5	500	3.8	8.2
CP-5	CP-46	2C152	U-15 Pu-10 Fz	58*	Nb-1 Zr	0.174	0.009	1.5	500	3.8	8.3
CP-5	CP-46	3C153	U-15 Pu-10 Fz	59*	Nb-1 Zr	0.174	0.009	1.5	500	3.8	8.5
CP-5	CP-46	4C155	U-15 Pu-10 Fz	58*	Nb-1 Zr	0.174	0.009	1.5	510	3.8	8.3
CP-5	CP-46	5C156	U-15 Pu-10 Fz	61*	Nb-1 Zr	0.174	0.009	1.5	510	3.8	8.7
CP-5	CP-46	6C159	U-15 Pu-10 Fz	59*	Nb-1 Zr	0.174	0.009	1.5	510	3.8	8.5
CP-5	CP-41	1N7	U-15 Pu-10 Fz	77	V-20 Ti	0.196	0.016	1.9	530	6.7	19.7
CP-5	CP-41	2N8	U-15 Pu-10 Fz	79	V-20 Ti	0.193	0.016	2.0	530	6.7	20.1
CP-5	CP-41	3N9	U-15 Pu-10 Fz	84	V-20 Ti	0.189	0.016	2.1	530	6.7	21.4
CP-5	CP-43	1N13	U-15 Pu-10 Fz	73	V-20 Ti	0.199	0.015	2.3	600	6.1	17.0
CP-5	CP-50	1N16	Th-20 U	75	V-20 Ti	0.196	0.015	1.84	580	0.46	0.22
CP-5	CP-50	4N19	Th-20 U	75	V-20 Ti	0.196	0.015	1.89	595	0.47	0.23
CP-5	CP-50	2N17	Th-10 Pu-10 U	75	V-20 Ti	0.196	0.015	1.97	620	0.49	0.23
CP-5	CP-50	5N20	Th-10 Pu-10 U	75	V-20 Ti	0.196	0.015	2.00	630	0.50	0.24
CP-5	CP-50	3N18	Th-10 Pu-20 U	75	V-20 Ti	0.196	0.015	1.90	600	0.34	0.25
CP-5	CP-50	6N21	Th-10 Pu-20 U	75	V-20 Ti	0.196	0.015	1.92	605	0.32	0.24

*Vibratory compacted powders.
[a]Based on effective density.

U-Pu-Zr alloy is being irradiated in CP-5 in V-20 w/o Ti alloy tubing and has reached a calculated 7.9 a/o burnup at a maximum cladding temperature of 640°C. U-Pu-Ti alloy also jacketed in V-20 w/o Ti alloy tubing has attained a calculated 6.8 a/o burnup at maximum cladding temperatures of 560°C.

The U-Pu-Fs alloy specimens are designed to study fuel density parameters having a direct bearing on maximum attainable burnup.

Six specimens of vibrationally compacted U-Pu-Fs metal powders were removed from CP-5 after a calculated 3.8 a/o burnup. The postirradiation examination will include fission-gas recovery and analysis. The resulting data will be compared with calculated results on the probability of fission recoil gas escape.

Capsule CP-48 containing the first series of six U-Pu-Zr specimens jacketed in iron- and nickel-base alloy tubing has been removed from CP-5 after a calculated 1.7 a/o burnup. Soon after this capsule was inserted in the reactor, indirect evidence (from a thermocouple) indicated that the cladding on a specimen jacketed in Hastelloy-X had failed prematurely. Since the indicated maximum cladding temperature was only 560°C, it appeared that a defect was present in the cladding or in the sodium bond. In order to enhance the irradiation temperature of the remaining specimens, the capsule was subsequently moved to a position of higher flux in the reactor, which produced maximum clad temperatures of 660°C. In the following few weeks it was noted from thermocouple readings that the two specimens adjoining the original defective specimen developed cladding rupture. The capsule was removed from the reactor and neutron radiographed. This examination verified that two adjoining rods had failed. The capsule will be shipped to the alpha-gamma hot cell for disassembly and examination of the six specimens it contains.

Capsule CP-50 containing six Th-U and Th-U-Pu fuel alloys, jacketed in V-20 w/o Ti tubing, was inserted in a fuel thimble of CP-5. The objectives of the test are to determine the relative swelling behavior of the fuels, the restraint characteristics of the jacket, and the maximum attainable burnup before jacket failure.

c. Ceramic Fuel Irradiations in EBR-II. Tables IX (for carbide) and X (for oxide) list the ANL ceramic fuel rods under irradiation in EBR-II and summarize the operating conditions anticipated at the end of the report period. Included in Table IX are seven new capsules containing specimens of vibrationally compacted Dynapac UO_2-20 w/o PuO_2 inserted in the reactor during the month. Cladding materials are Type 304 stainless steel, Hastelloy-X, and V-20 w/o Ti. The target burnup for this new group of specimens is 5 a/o at linear heat ratings of 18 to 23 kW/ft.

TABLE IX. Status of UC-20 w/o PuC Fuel Irradiations in Progress in EBR-II

		Design Parameters				Operating Conditions			
Capsule or S/A No.	Specimen Number	Effective Density (%)	Cladding Composition (%)	Cladding OD (in.)	Cladding Thickness (in.)	kW/cc[a]	Max Cladding Temp (°C)	Burnup to a/o (U + Pu)	fiss/	ate c x 10^{-20}[a]
XG05	SMV-2	84	304 SS	0.297	0.020	2.1	645	2.6		7.3
XG05	HMV-5	80	Hastelloy-X	0.297	0.015	2.2	670	2.7		7.1
XG05	NMV-11	84	Nb-1 Zr	0.281	0.012	2.1	645	2.7		7.6
XO08	NMP-2	82	Nb-1 Zr	0.281	0.012	1.6	545	1.3		3.5
XO08	NMV-4	80	Nb-1 Zr	0.281	0.012	2.4	635	1.9		4.9
XO08	NMV-7	80	Nb-1 Zr	0.281	0.012	2.1	605	1.7		4.5
XO08	NMV-12	86	Nb-1 Zr	0.281	0.012	2.4	635	1.9		5.2
XO08	HMV-1	80	Hastelloy-X	0.297	0.015	2.1	640	1.7		4.4
XO08	HMV-4	80	Hastelloy-X	0.297	0.015	2.3	670	1.8		4.8
XO08	HWMP-1	82	Hastelloy-X + W	0.297	0.020	1.6	555	1.3		3.4
XO08	HWMV-1	83	Hastelloy-X + W	0.297	0.020	2.4	685	1.8		5.1
XO09	SMV-1	82	316 SS	0.306	0.024	1.6	570	1.2		3.3
XO09	SMP-1	80	316 SS	0.306	0.024	2.1	640	0.94		2.5
XO09	VMV-1	86	Vanadium	0.301	0.022	2.5	640	1.4		4.0

[a]Based on effective density.

TABLE X. Status of UO_2-20 w/o PuO_2 Fuel Irradiations in Progress in EBR-II

Capsule or S/A No.	Specimen Number	Design Parameters: Effective Density (%)	Cladding Composition (w/o)	Cladding OD (in.)	Cladding Thickness (in.)	Operating Conditions: kW/cc[a]	Max Cladding Temp (°C)	Burnup to Date: a/o (U + Pu)	Burnup to Date: fiss/cc x 10^{-20}[a]
X009	SOV-5	82	304 SS	0.297	0.020	1.7	555	1.2	2.5
X009	SOV-6	82	304 SS	0.297	0.020	1.7	565	1.3	2.7
X011	SOV-3	83	304 SS	0.296	0.019	1.9	610	0.52	1.1
X011	HOV-4	80	Hastelloy-X	0.295	0.014	1.8	600	0.51	1.0
X011	TVOV-1	77	V-20 Ti	0.297	0.020	1.7	575	0.50	1.0
X011	SOV-7	85	304 SS	0.296	0.019	2.0	630	0.50	1.0
X011	SOV-1	80	304 SS	0.296	0.019	1.7	590	0.50	1.0
X011	HOV-10	86	Hastelloy-X	0.295	0.014	1.9	615	0.49	1.0
X011	HOV-15	80	Hastelloy-X	0.295	0.014	1.7	590	0.49	1.0

[a]Based on effective density.

d. Oxide-Cermet Irradiations in EBR-II. Table XI lists three stainless steel-PuO_2 cermet specimens, clad in Type 304 stainless steel, which were loaded in the subassembly with the seven new oxide ceramic fuel specimens. The fuel pins were manufactured by Battelle Pacific Northwest Laboratories. The encapsulation, sodium bonding, and safety analysis of these specimens for irradiation were performed by Argonne National Laboratory. The cermets are expected to achieve 5 to 7 a/o maximum burnup at 5 to 10 kW/ft.

TABLE XI. Status of Cermet Fuel Irradiations in Capsule X011 in EBR-II

Specimen Number	Design Parameters: Fuel Composition (w/o)	Effective Density (%)	Cladding OD (in.)	Cladding Thickness (in.)	Operating Conditions: kW/cc[a]	Max Cladding Temp (°C)	Burnup to Date: a/o (U + Pu)	Burnup to Date: fiss/cc x 10^{-20}[a]
5P-9	SS-40 PuO_2	98	0.301	0.015	0.88	495	0.70	0.52
5P-12	SS-27 PuO_2	99	0.294	0.015	0.59	450	0.70	0.35
5U-14	SS-27 UO_2	98	0.298	0.013	0.45	435	0.53	0.27

[a]Based on effective density.

4. Fast-neutron Irradiation of Jacket Materials

The effects of elevated temperature coupled with fast-neutron exposure on the mechanical properties of Type 304 stainless steel, Hastelloy-X, Inconel 625, V-20 w/o Ti, and V-15 w/o Ti-7.5 w/o Cr are being investigated by their exposure to 1 x 10^{21} to 1 x 10^{23} n/cm^2. At present, a total of 26 capsules containing 60 tube-burst specimens and 296 tensile-type specimens are being irradiated in EBR-II subassemblies XA07, XA08, XO09, and XO10 at temperatures between 500 and 670°C. These specimens have accumulated maximum total neutron exposures of 5.8 x 10^{21} to 2.1 x 10^{22} n/cm^2. The status and identification of the capsules are given in Table XII.

TABLE XII. Status of Irradiations of Cladding Materials in EBR-II

		Design Parameters				Operating Conditions	
S/A No.	Capsule Number	Cladding Composition (w/o)	Type of Specimen	No. of Specimens	Specimen Environment	Max Specimen Temp (°C)	Exposure to Date (n/cm^2)
XA07	AS-9	V-20 Ti	Tensile	16	Argon-helium	590	2.1×10^{22}
XA07	AS-10	Hastelloy-X	Tensile	16	Argon-helium	590	1.9×10^{22}
XA07	AS-11	304 SS	Tensile	16	Argon-helium	590	2.0×10^{22}
XA08	AS-1	V-20 Ti	Tube-burst	12	Argon-helium	540	1.5×10^{22}
XA08	AS-2	V-20 Ti	Tube-burst	12	Argon-helium	540	1.5×10^{22}
XA08	AS-3	Hastelloy-X	Tube-burst	12	Argon-helium	540	1.6×10^{22}
XA08	AS-4	Hastelloy-X	Tube-burst	12	Argon-helium	540	1.6×10^{22}
XA08	AS-5	304 SS	Tube-burst	12	Argon-helium	540	1.6×10^{22}
XA08	AS-6	V-20 Ti	Tensile	16	Argon-helium	580	1.6×10^{22}
XA08	AS-7	Hastelloy-X	Tensile	16	Argon-helium	580	1.5×10^{22}
XA08	AS-8	304 SS	Tensile	16	Argon-helium	580	1.5×10^{22}
XA08	AS-12	V-20 Ti	Tensile	16	Argon-helium	580	1.4×10^{22}
XO09	AS-14	V-20 Ti	Tensile	13	Argon-helium	670	1.2×10^{22}
XO09	AS-15	V-20 Ti	Tensile	13	Argon-helium	670	1.1×10^{22}
XO09	AS-27	304 SS Hastelloy-X	Tensile	13	Argon-helium	670	1.2×10^{22}
XO10	AS-16	V-20 Ti	Tensile	13	Argon-helium	500	4.4×10^{21}
XO10	AS-17	V-20 Ti	Tensile	13	Argon-helium	500	4.8×10^{21}
XO10	AS-18	V-20 Ti	Tensile	13	Argon-helium	500	4.2×10^{21}
XO10	AS-19	V-20 Ti	Tensile	13	Argon-helium	500	4.4×10^{21}
XO10	AS-20	V-20 Ti	Tensile	13	Argon-helium	500	4.9×10^{21}
XO10	AS-21	V-20 Ti	Tensile	13	Argon-helium	500	5.8×10^{21}
XO10	AS-22	Hastelloy-X	Tensile	13	Argon-helium	500	5.1×10^{21}
XO10	AS-23	304 SS	Tensile	13	Argon-helium	500	5.8×10^{21}
XO10	AS-24	304 SS	Tensile	13	Argon-helium	500	4.9×10^{21}
XO10	AS-25	304 SS	Tensile	13	Argon-helium	500	4.9×10^{21}
XO10	AS-26	304 SS	Tensile	15	Argon-helium	500	4.7×10^{21}

D. General Fast Reactor Fuel Reprocessing Development

1. Skull Reclamation Process

The skull reclamation process is being developed in order to recover and purify the uranium-bearing residue or skull that is left in the crucible following the melt refining of enriched uranium-alloy fuel pins discharged from EBR-II. The uranium in the skull amounts to 5 to 10% of the original charge. Although the skull reclamation process for the EBR-II fuel does not recover plutonium, much of the chemistry and technology being accumulated in the course of this process development has potential utility for the processing of plutonium-uranium oxide and carbide fuels. The skull reclamation process is being tested with nonirradiated uranium in remotely operated plant-scale equipment (~4 kg uranium per batch) comprising a reduction furnace and a retorting furnace.

The final step in the skull reclamation process consists of retorting or solvent evaporation to recover the product uranium from a Zn-12 w/o Mg-12 w/o U ingot cast from product solution that has been transferred out of the reduction furnace. The retorting procedure consists of distilling the

Zn-Mg-U product solution under vacuum (~10 Torr) at 650 to 750°C, after which the uranium is melted (~1200°C) to form a button. A large-size (8-in. OD by 17-in. high) beryllia crucible is used in the retorting step. Eleven plant-scale retorting runs have been completed with Zn-Mg-U ingots from previous pilot-scale and plant-scale reduction furnace runs in two BeO crucibles furnished by the Brush Beryllium Company (see Progress Report for April 1966, ANL- 7204, p. 25). One crucible was used in three runs; this crucible had also been used in three earlier runs. The other crucible, previously unused, was used in the other eight runs.

Satisfactory results were achieved in all of the experiments. After the runs, the crucibles were found to be in good condition and will be used in future runs. Operation of the equipment was excellent. Uranium recoveries were satisfactory. Although a small amount of the retorting solution seeped through the crucibles, this problem is not considered to be serious since it can be remedied by improved crucible fabrication. Slight sticking of a button was encountered in one run, but this button was easily freed by gentle mechanical prying. Of the total zinc-magnesium distilled in these runs, only about 0.5% was unaccounted for.

2. Processes for Fast Reactor Fuels

Pyrochemical processing of fast breeder reactor fuels of the ceramic type (e.g., oxide or carbide) continues to be investigated (see Progress Report for April 1966, ANL-7204, pp. 25-27). In these processes, the fissile and fertile constituents of the fuel and the fission products are separated by means of liquid metal-molten salt extractions and salt-transport separations.[1] A conceptual flowsheet[2] of several steps is being investigated:

(1) An oxidative decladding step, in which the fuel is oxidized, the fuel oxides are released from the cladding, and volatile fission products are collected.

(2) An oxide reduction-partition step in which the fuel oxides are reduced to the metal form by a 90 w/o Cu-Mg alloy. The alkali, rare earth, and alkaline earth fission products remain in the molten halide salt phase ($MgCl_2$ or $MgCl_2$ plus other halide salts) which serves as a vehicle for the removal of the solid MgO formed as a byproduct of the fuel-oxide reduction. The metals formed appear in the copper-magnesium alloy.

---

[1]Salt-transport separations are based upon the selective transfer of solutes (fissile and fertile materials) from one liquid metal solution (donor) to another (acceptor) by cycling a molten salt phase which acts as a carrier between the two metal solutions. Processes utilizing salt-transport separations show promise of excellent separations of fission products from uranium and plutonium, and high recoveries of uranium and plutonium.

[2]The conceptual process flowsheet is shown in Progress Report for September 1965, ANL-7105, p. 34; see also Progress Report for November 1965, ANL-7122, p. 39.

(3) A salt-transport separation step in which the uranium, plutonium, and the noble metal and refractory metal fission products in the copper-magnesium donor alloy are separated. By cycling a molten $MgCl_2$-based salt carrier between the copper-magnesium donor alloy and zinc-magnesium acceptor alloys (different compositions), the uranium is selectively transferred to a high magnesium-low zinc acceptor alloy and the plutonium is transferred to a high zinc-low magnesium acceptor alloy. The fission products remain in the copper-magnesium alloy.

(4) Retorting operations in which the uranium and plutonium are recovered.

(5) A conversion step in which the uranium and plutonium are converted to final ceramic form (oxide or carbide).

a. Oxide Reduction-Partition Step. Two experiments have been completed in a program to determine the optimum conditions for the reduction of sintered uranium oxide pellets. In the two experiments, the same experimental conditions and reagents were used. The sintered UO_2, either in the form of a whole pellet or a powder obtained by grinding a sintered pellet to a -200 mesh powder, was suspended in a molten salt (15 m/o $MgCl_2$-37.5 m/o $CaCl_2$-42.5 m/o NaCl-5 m/o CaF_2), and reduction of the pellet or powder was attempted with Cu-6.7 w/o Mg alloy at 800°C. In the first experiment using the whole pellet (~10 g), only about 10% reduction of the pellet was achieved in $5\frac{1}{2}$ hr. In the second experiment using the powdered UO_2, about 81% reduction of the powder was achieved in $5\frac{1}{2}$ hr. In both experiments, reduction of the UO_2 was continuing after $5\frac{1}{2}$ hr, but at a reduced rate. It is anticipated that the rate of reduction will be increased by the use of more finely divided UO_2. For the next experiment, an oxidation-reduction cycle will be employed to pulverize a sintered UO_2 pellet and thereby provide the more finely divided powder. Another method of solving the problem of slow dissolution of the sintered oxide fuel would be to adopt the procedure used in the nitric acid dissolution of uranium, that is, to allow a heel of undissolved fuel to be always present in the dissolver vessel. This possibility will be considered in the near future.

In order to enhance the separation of the rare earth fission products from plutonium or uranium in the reduction-partition step, it is desirable to choose a reduction alloy which has the largest possible distribution coefficient (concentration in salt/concentration in alloy) for the rare earth elements relative to the distribution coefficients for plutonium and uranium. Copper-magnesium alloys have shown great promise for the reduction-partition step. In recent work, the distribution coefficients of plutonium and cerium between molten magnesium chloride and liquid copper-magnesium alloys were measured at 800°C. The magnesium content of the alloy was varied from 6 to 70 w/o. The cerium-plutonium separation factor,

$$\frac{(\text{w/o Ce in salt})}{(\text{w/o Pu in salt})} \Big/ \frac{(\text{w/o Ce in alloy})}{(\text{w/o Pu in alloy})},$$

was found to vary from about 310 for a Cu-6.5 w/o Mg alloy to about 38 for a Cu-70 w/o Mg alloy. The cerium-uranium separation factor (calculated from the results of earlier work) varied from about 2230 for the Cu-6.5 w/o Mg alloy to about 96 for the Cu-70 w/o Mg alloy.

Since the molten salt in this step is a waste stream, it is desirable to minimize the concentration of dissolved fissile element compounds and thereby minimize losses. A molten ternary halide salt composed of $MgCl_2$-$CaCl_2$-NaCl is being considered for this step. To achieve low plutonium (and uranium) losses, a low $MgCl_2$ concentration is required (see Progress Report for March 1966, ANL-7193, p. 36). This lowers the oxidizing power of the salt phase and thereby decreases the concentration of all reducible constituents (uranium, plutonium, and rare earth elements) in the salt. To investigate the dependence of the pertinent separation factors on $MgCl_2$ concentration, the distribution coefficients of cerium, uranium, and plutonium between a Cu-6 w/o Mg alloy and molten ternary NaCl-$CaCl_2$-$MgCl_2$ salt mixtures were measured at 800°C. The NaCl-$CaCl_2$ mole ratio was kept at unity while the $MgCl_2$ content was varied from about 1 to 100 m/o. The cerium-uranium separation factor varied from about 2200 for ~1 m/o $MgCl_2$ to 2230 at 100 m/o $MgCl_2$. The cerium-plutonium separation factor increased from about 200 at 1 m/o $MgCl_2$ to 310 at 100 m/o $MgCl_2$. These results indicate that good separations can be obtained in the region of low $MgCl_2$ concentration at which plutonium solubility in the salt is relatively low. Operation in the low $MgCl_2$ region is desirable to minimize plutonium losses to the salt phase.

b. Salt-transport Separation Step. A copper-cadmium-magnesium alloy is being considered as an alternative donor alloy for the copper-magnesium alloy for the salt-transport step (see ANL-7204, p. 26). This ternary alloy offers the possibility of lowering the operating temperature of this step from about 800 to 600°C.

A laboratory salt-transport experiment based on the crucible-within-a-crucible technique[3] was recently completed. Uranium was transferred from a 60 w/o Cu-38 w/o Cd-2 w/o Mg alloy (donor solvent) through a 50 m/o $MgCl_2$-30 m/o NaCl-20 m/o KCl salt to a 60 w/o Mg-40 w/o Zn alloy (acceptor solvent) at 700°C and at a stirring speed of 200 rpm. The donor alloy contained 5 w/o uranium initially (only 1% of the uranium was in solution). At the end of the experiment, analysis showed that, of the original uranium, about 1.9% remained in the donor alloy, about 98.5% was in the

[3]In this technique, a small crucible is suspended in the salt phase within a large crucible. The small crucible contains the acceptor solvent and the large crucible holds the donor solvent which is beneath the salt phase. The contents of both crucibles are individually stirred.

acceptor alloy and about 0.3% in the salt. The experiment was terminated after 42 hr when the rate of uranium transport had become small. Some 80% of the original uranium was transported during the first 9 hr. This experiment was not designed to obtain practical rate data but to demonstrate that the uranium transfer would occur. Calculations show that if the initial donor alloy had contained 10% uranium, then about 99.3% of the uranium would have transferred to the acceptor alloy, even under the less-than-optimum conditions in this experiment.

In previous engineering experiments on a pilot-plant scale, salt-transport separation steps were made by batch contacts (i.e., the liquid metal alloys were in adjacent vessels and the molten salt was cycled between the two vessels by alternately pressuring the bulk of the molten salt through a transfer line from one alloy to another). Continuous and semicontinuous contacting methods are now being examined. The kinetic data obtained in the batch-contact experiments (see Progress Report for March 1966, ANL-7193, pp. 37-38) have been used to calculate uranium transfer rates for mixer-settlers (a continuous contactor) in which uranium is transferred from a liquid copper-magnesium donor alloy to a liquid magnesium-zinc acceptor alloy via molten magnesium chloride. Typical calculated results for operation at 830°C with continuous salt circulation and with saturated uranium donor alloy solutions are as follows:

Volume of Each Mixer-Settler (liters)	Salt Flow Rate (liters/min)	Uranium Transfer Rate (kg/hr)
20	1	1.4
20	4	3.0
20	10	4.0
50	1	1.8
50	4	4.8
50	10	7.7
100	4	6.1
100	25	16.7

As expected, these uranium transfer rates are higher than those calculated for equivalent batch-contact equipment.

Experiments with mixer-settler equipment are planned, and the equipment to carry out the experiments is being designed.

E. Sodium Technology

1. Component and Materials Evaluation Loop (CAMEL)

a. Falex Wear Tester. An additional five machines (see Progress Report for April 1966, ANL-7204, pp. 28-31) are in construction to provide a total of nine. The parts for three units have been received from the shops

and have been partially assembled. In addition, a large part of the control circuitry for three machines which first will be installed in the 1200°F loop has been completed.

2. Sodium Quality Control Loop

The new Sodium Quality Control Loop (see Fig. 5) is a 600°F, 15-gal loop facility in which a variety of analytical instrumentation will be installed. The facility was designed so that careful and exact control of oxide impurity could be maintained. It consists of a main vessel with three small, pumped loops attached which facilitate the in-line instrumentation and supply sodium to the cold trap. Local temperature and impurity gradients are eliminated by pumping sodium from the upper region of the vessel out through the third loop and back into the vessel at a lower elevation. This return line terminates at the neck of an eductor located at the bottom of the vessel. In addition to the instrumentation loops, the facility will have provisions for taking distillation samples.

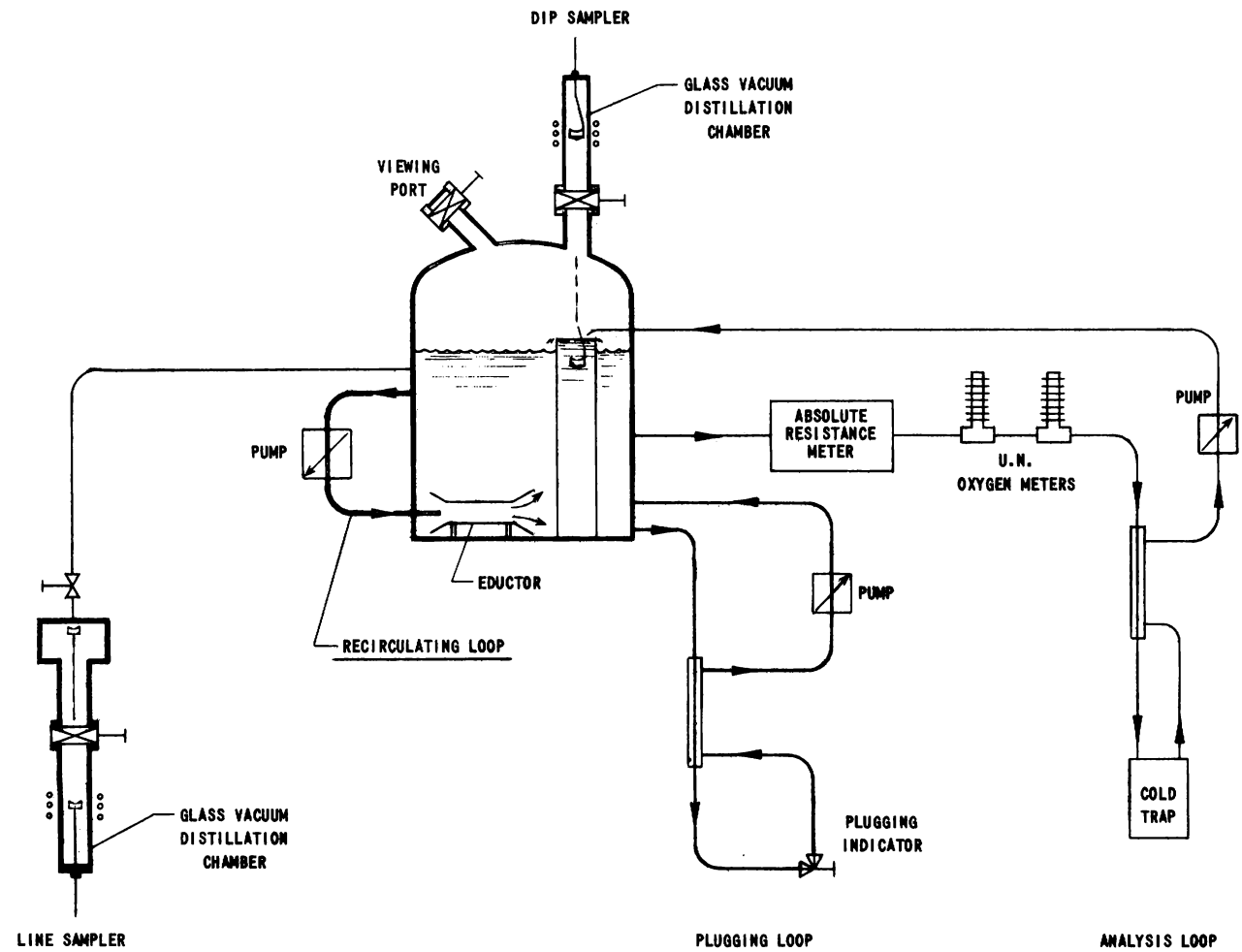

Fig. 5. Sodium Quality Control Loop

By means of the loop, it will be possible to evaluate, cross-compare, and calibrate a variety of existing in-line analytical instrumentation, and to develop and test new equipment as it becomes available. The study and evaluation will be aimed at determining accuracy, speed of response, and reliability for application of the various instruments or sampling techniques to engineering systems and loops. Analytical instrumentation and sampling techniques to be evaluated and cross-compared in this facility include the dip sampler, line sampler, new Absolute Resistance Meter, plugging indicators, and United Nuclear oxygen meters.

At present, design of all the major components of the facility is complete and fabrication work in the shop has been started. Orders have been placed for most of the items to be purchased. Work remaining, prior to completion of shop work and the actual erection of the facility, includes calculation of the heating requirements and final design of the vacuum system for the distillation samplers.

3. Static Pot Tests

a. Physiochemical Mechanics of Metals. The static pot tests (see Progress Report for March 1966, ANL-7193, pp. 40-41) of five pairs of metals partially immersed in a 1200°F sodium, and partially exposed to inert atmosphere, are nearly completed. Examination of the ball (actually the spherical head of a rod) of the ball-cone combination used for self-welding studies revealed changes of metallic properties of the rod at or near the junction of sodium and the inert atmosphere. The following observations of the rod behavior were noted:

(1) Sensitization tests as a function of height or location on the statically loaded, 5/8-in.-OD, 304 stainless steel rod indicate a measurable deleterious effect at a level about 1/2 in. above the nominal sodium level.

(2) Superficial and Rockwell C hardness tests, not only on the surface of the rod but also at 0.010 in. below the surface, show marked, measurable changes of reduced hardness at the liquid level.

(3) Cold tensile-test specimens were fabricated from various heights or lengths of the vertical static-loaded rods. Tensile tests confirmed changes in mechanical properties of the static-loaded rod at the free-surface sodium level.

(4) Impact tests with ASTM standard Charpy specimens taken above the free sodium surface level indicated an increase in toughness or ability to withstand a constant impact or load.

Positive conclusions cannot be drawn at this time due to the limited number of tests actually made.

4. Effect of Flow and Rate of Cooling on a Plugging Meter

During a 6-month period, the oxygen content of a plugging meter sodium loop varied between 3 and 37 ppm; the flow rate in the plugging loop varied between 0.256 and 0.112 gpm; the period of cooling from the time the valve was closed to plugging temperature varied from 6 to 39 min; the temperature of the main loop to which the plugging loop was attached varied from 399 to 642°F. Data were taken to determine if these variables had any effect on the plugging-meter analyses of oxygen content of the sodium.

The main loop held 12 gal of sodium and consisted of approximately 70 ft of 2-in. stainless steel pipe, well insulated and equipped with line heaters to keep the sodium temperature along the pipe constant. Clam-shell heaters supplied the largest portion of the heat at one section of the loop. An electromagnetic (EM) pump moved the sodium through a restraining valve in the loop. The intake to the plugging valve loop was on the pump side of the restraining valve, and the plugging loop emptied into the downstream side of the restraining valve. The plugging valve loop also had its individual EM pump which allowed closer control of sodium flow through the plugging valve. Both main and plugging loops were equipped with flowmeters. The time of cooling was controlled both by a fan blowing room air over the entire plugging loop and also by rate of sodium flow through the loop.

The plugging valve is a modified 1/2-in. globe valve with a cone-shaped stem fitted into a cone-shaped seat. The sodium bypass through the valve consists of 10 slots in the stem cone, 0.032 in. wide by 0.016 in. deep. The record of plugging is obtained from two pen millivoltmeters, one of which records the flow through the plugging valve and the other the temperature of the stem cone. The point at which the flow pen in the instrument deviates from a straight line is called the plugging temperature. This temperature is converted to ppm O_2 by extrapolation of the logarithmic solubility curve.

The data showed:

a. There is a decrease in flow of 0.01-0.02 gal/min from start of plugging run to plugging temperature. This decrease is probably due to: (1) sensitivity of instrument, and (2) crystals attaching themselves to the walls of the fluted passages.

b. Within the limits of these experiments, variations in sodium flow, time of cooling, concentration of oxygen, and sodium inlet temperature made no difference in the behavior of the plugging valve as a means of oxygen in sodium analysis.

II. GENERAL REACTOR TECHNOLOGY

A. Experimental Reactor and Nuclear Physics

1. Neutron Spectra in a Depleted-uranium Block

The neutron spectrum resulting from the irradiation of uranium-metal blocks by a neutron source has been the object of continuous study since the first experiments were performed by Snell et al.[4] Blocks weighing up to 10^4 kg have been fabricated from natural as well as depleted uranium, and have been used with different types of sources having both point and extended neutron distributions with a variety of spectral shapes. The neutron spectrum in the block is more sensitive to details of the scattering from U^{238} when the U^{235} content is low than when the spectrum is in a critical configuration. The effect is, of course, most pronounced in depleted uranium.

The block used in the measurements reported here was in the form of a cube, 80 cm on a side. The front 10 cm of the block was made of natural uranium and the remainder of the block was made of depleted (0.21% U^{235}) uranium. The front face of the block was oriented to receive thermal neutrons leaking from a graphite pile driven by the Argonne Thermal Source Reactor (ATSR). Thermal neutrons leaking from the graphite were absorbed in the natural uranium face and the resulting fission spectrum was used to excite the balance of the block. A boral shutter, black to thermal neutrons, could be interposed between the block and thermal source, and spectrum measurements could be made both with and without the shutter. The spectra at three positions (12.7, 27.4, and 53.3 cm along the axis) where measurements were made are expected to be free from any background neutrons not associated with the natural uranium face.

The neutron measurements were made with the aid of proton-recoil proportional counters.[5] Counters had a diameter of 2.5 or 3.7 cm and an effective length of about 7 cm, and were filled with either methane or hydrogen gas; the denser methane filling was used to reduce wall and end effects at the higher energies. In the region of measurement (from 1 keV to 1 MeV), fast-neutron spectra were observed to soften progressively as the probe moved away from the front face. Figure 6 shows the result at the 53.3-cm position together with the background spectrum taken with the boral shutter in place.

One-dimensional diffusion calculations were made using the ANL Cross Section Set 224 and compared, at each position, with the experimental results. The comparison in Fig. 7 is for the 53.3-cm position, at which place the calculated spectrum shape tends to change only slowly with

---

[4]Snell, A. H., et al., CF-589 (1943).

[5]Bennett, E. F., Fast Neutron Spectroscopy by Proton-recoil Proportional Counting, Nucl. Sci. Eng. (to be published).

distance. The spectra are softer than calculations predict (in agreement with an earlier result using a pulsed-neutron source[6]) and are quite sensitive to values of the U^{238} cross section used in the calculation.

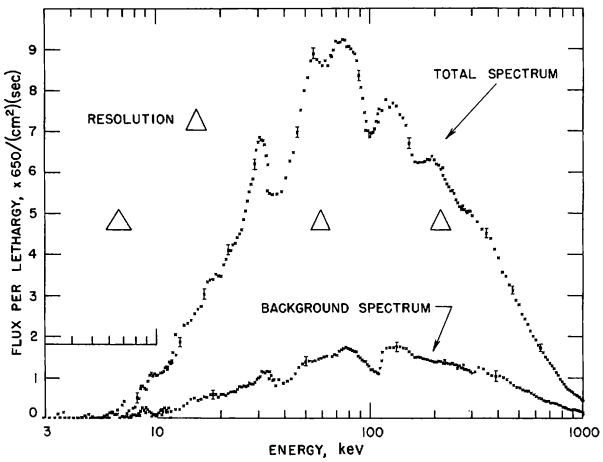

Fig. 6. Spectra from Depleted-uranium Block, 53.3 cm from Front Face

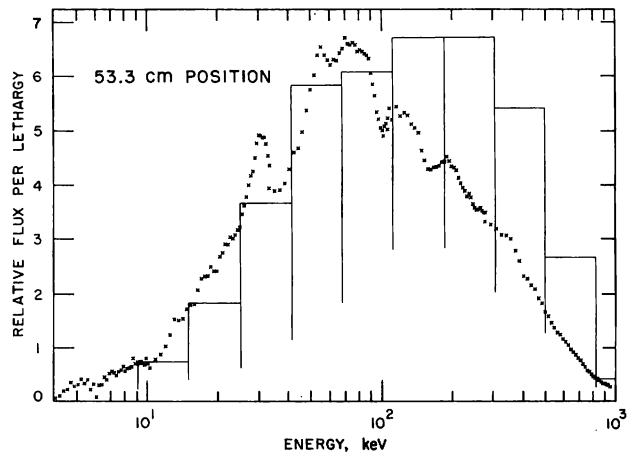

Fig. 7. Comparison of the Measured Spectrum, at 53.3 cm from the Face of the Block, with a Group Calculation

2. Neutron Scattering by Bismuth

Optical-statistical model analyses of neutron elastic and inelastic scattering cross sections for nuclei in the region near lead are particularly suitable for the study of the energy variation of model parameters and their dependences upon nuclear-structure effects such as shell closure.

Figure 8 shows the comparison of recently obtained data for the elastic scattering of neutrons by bismuth with the prediction of Moldauer's optical model for neutron scattering,[7] as modified for shell-closure effects.[8] Shown is the variation with energy of the elastic cross section and the Legendre polynomial coefficients ω_i of the angular distribution for neutron energies up to 1.5 MeV.

Figure 9 shows the angular distribution of elastically and inelastically scattered 2.5-MeV neutrons predicted according to the same model. The dashed curves indicate the effect of using a value of 1.0 for the resonance interference parameter Q.[9] The solid lines are drawn for Q = 0. The absence of dashed lines indicates that the effect of varying Q was slight.

---

[6]Kato, W. Y., et al., Fast Reactor Physics Parameters from a Pulsed Source, Pulsed Neutron Research, Vol. II, p. 373, IAEA Vienna (1965).
[7]Moldauer, P. A., Nucl. Phys. 47, 65 (1963).
[8]Vonach, W. G., Smith, A. B., and Moldauer, P. A., Phys. Rev. Letters 11, 331 (1964).
[9]Moldauer, P. A., Revs. Modern Phys. 36, 1079 (1964); Moldauer, P. A., Engelbrecht, C. A., and Duffy, G. J., ANL-6978 (1964).

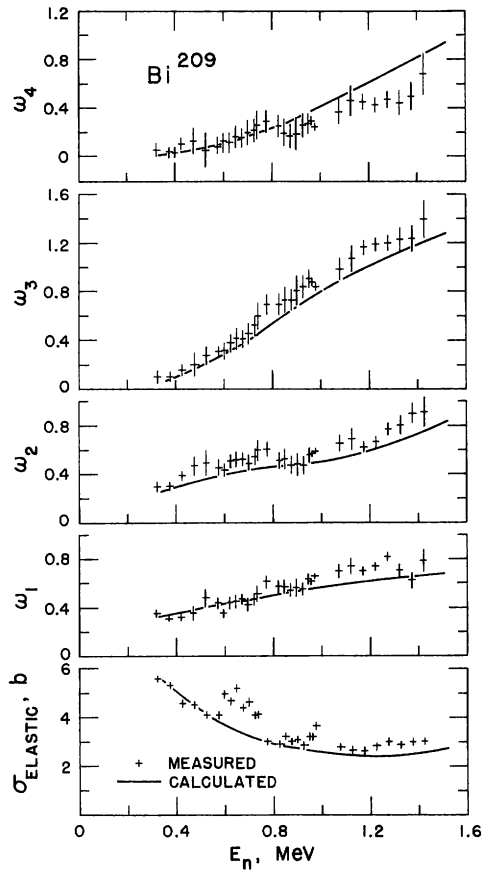

Fig. 8. Comparison of Measured and Calculated Elastic-scattering Cross Sections of Neutrons and Legendre Coefficients of the Angular Distribution for Bismuth

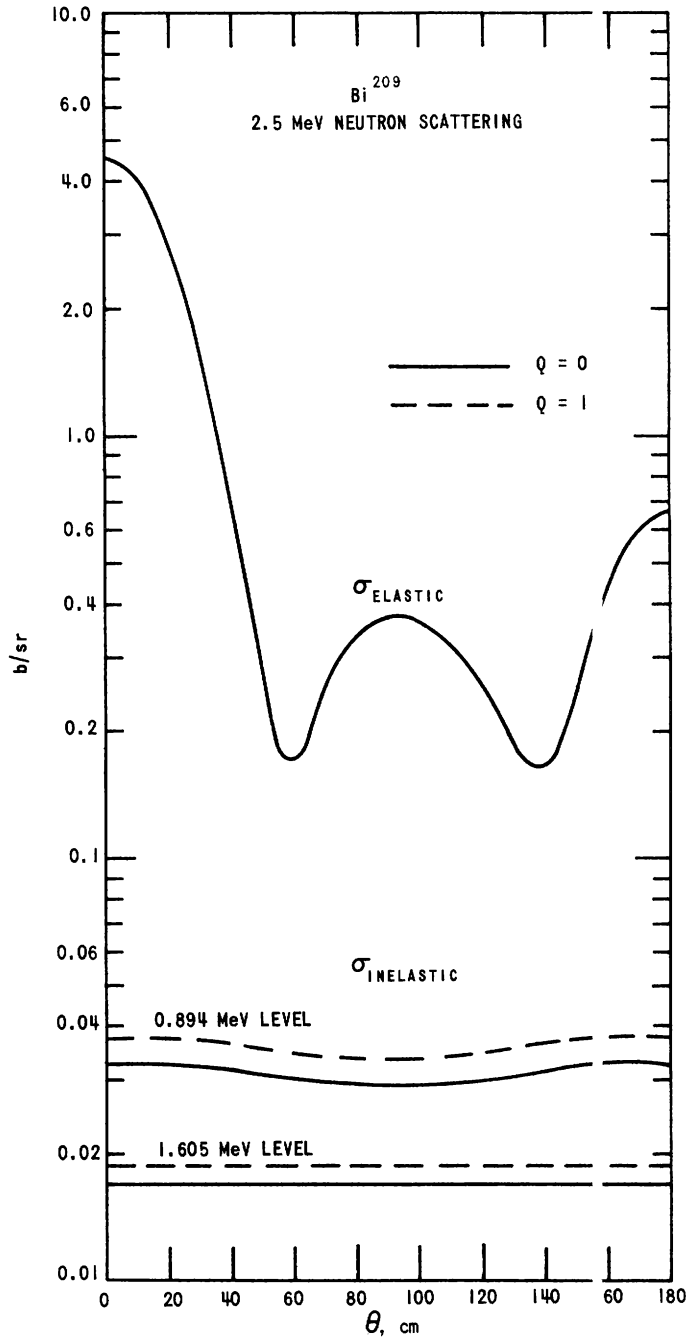

Fig. 9. Predicted Elastic- and Inelastic-scattering Cross Sections for 2.5-MeV Neutrons on Bismuth

Figure 10 shows the predicted polarizations of 1.0 and 2.5 MeV elastically scattered neutrons. Compound elastic scattering was taken into account throughout, as were width fluctuation effects.[9]

[9] Op. Cit.

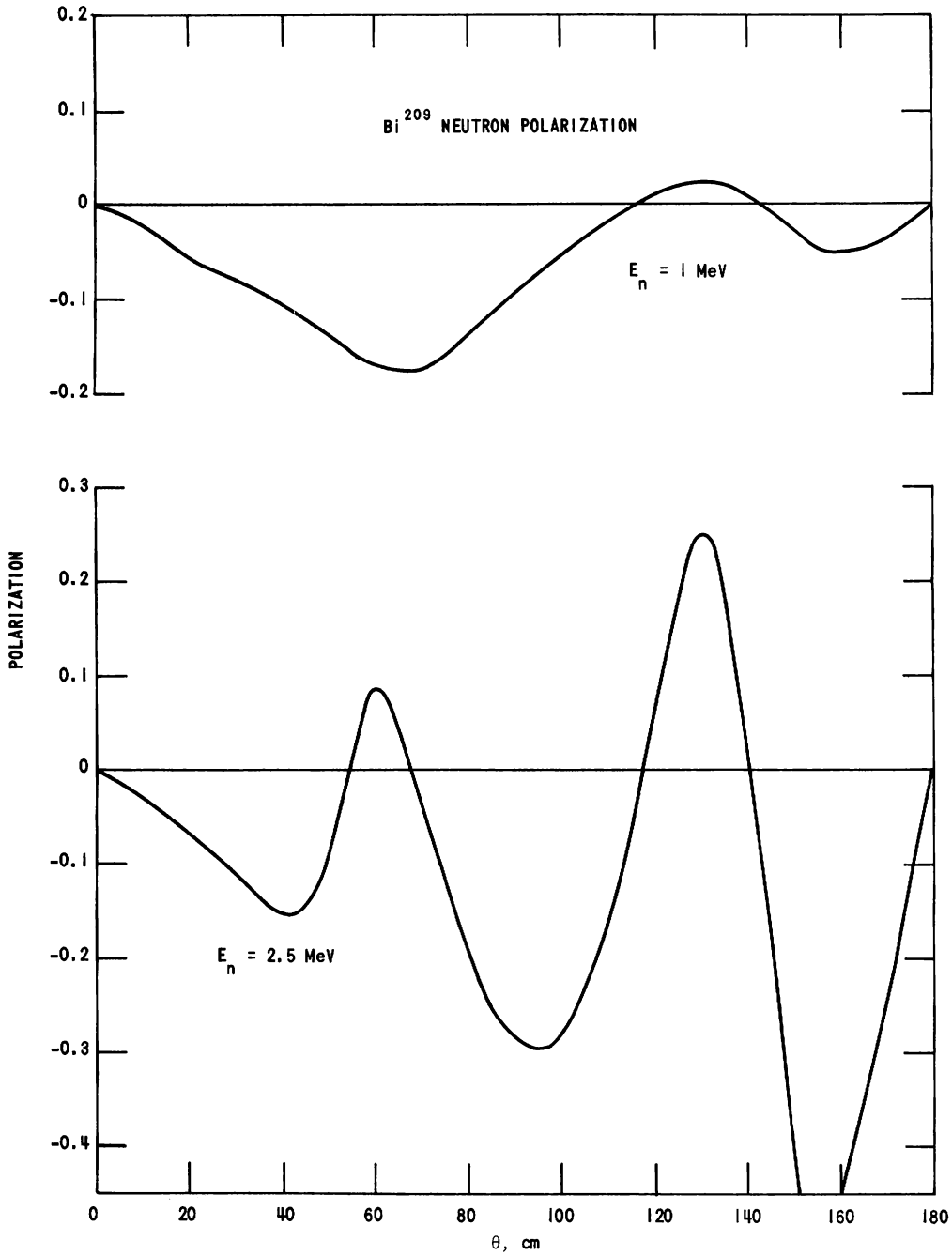

Fig. 10. Predicted Polarization of 1.0-MeV and 2.5-MeV Neutrons Elastically Scattered from Bismuth

B. Theoretical Reactor Physics

1. Evaluations of Cross Sections

A new version for Pu^{239} that incorporates the smooth fission and capture cross sections described by White[10] has been added to the MC^2 library.

[10] White, P. H., Hodgkins, J. G., and Wall, G. J., Measurement of Fission Cross Section for Neutrons of Energies in the Range 40-500 keV, IAEA Conference on Physics and Chemistry of Fission, Salzburg, Austria, March 1965.

The LIB9 and MERGE programs used in writing the MC^2 library tape have been modified to print more Hollerith information in the printed version of the library data.

2. ZPR-7 Physics Analysis

Correction factors have been calculated for the experimental measurements made of $\bar{\alpha}^{25}$ by oscillator techniques.[11] The calculations were concerned with the use of manganese and Cf^{252} as substitutes for U^{235} in the determination of the importance of absorption and fission neutrons, respectively. The correction factors were found to be small and tended to cancel each other.

3. The ARC System

a. Modifications. The present concept of the ARC System, shown schematically in Fig. 11, differs from that shown previously (see Progress Report for January 1966, ANL-7152, Fig. 28, p. 54) in that the System Control, Data Pool Loader, and Data Distribution Control of the earlier diagram have been combined into the single, unified Operating System. The present approach is consistent with the capabilities of the IBM System/360 Operating System. For example, the task of loading the Datapool with a cross-section library can be accomplished by use of suitable Job Control cards and inclusion of the data in the input job stream.

Two other changes may be noted in the neutronics modules. The code-dependent input-generation modules have now been absorbed into the corresponding diffusion- or transport-theory modules, and a set of mesh refinement modules have been added. The latter are mainly intended for expediting two-dimensional problems by using coarse space meshes in initial calculations. This task of mesh refinement is distinct from that of spatial synthesis. The modules for the latter type of problem are, as before, included among the various adjunct modules at the bottom of the diagram.

For testing the Operating System, various relatively simple standard paths are being defined which will simulate examples of most of the types of tasks required of the operating ARC System. For this purpose, a set of pseudo-modules and a corresponding set of pseudo-interface quantities have been defined. The module internal variables which are to be interface quantities are organized into data sets for storage in the DATAPØØL. A data set may be made up of an assemblage of several subscripted variables, or of a single nonsubscripted variable. These assignments will in practice depend upon the DATAPØØL organization. In the present instance, the details of the variable-data set correspondences are largely irrelevant.

---

[11] Redman, W. C., and Bretscher, M. M., Direct Measurement of Effective Capture-to-Fission Ratio at Low Flux, Trans. ANS 8, 531 (Nov 1965).

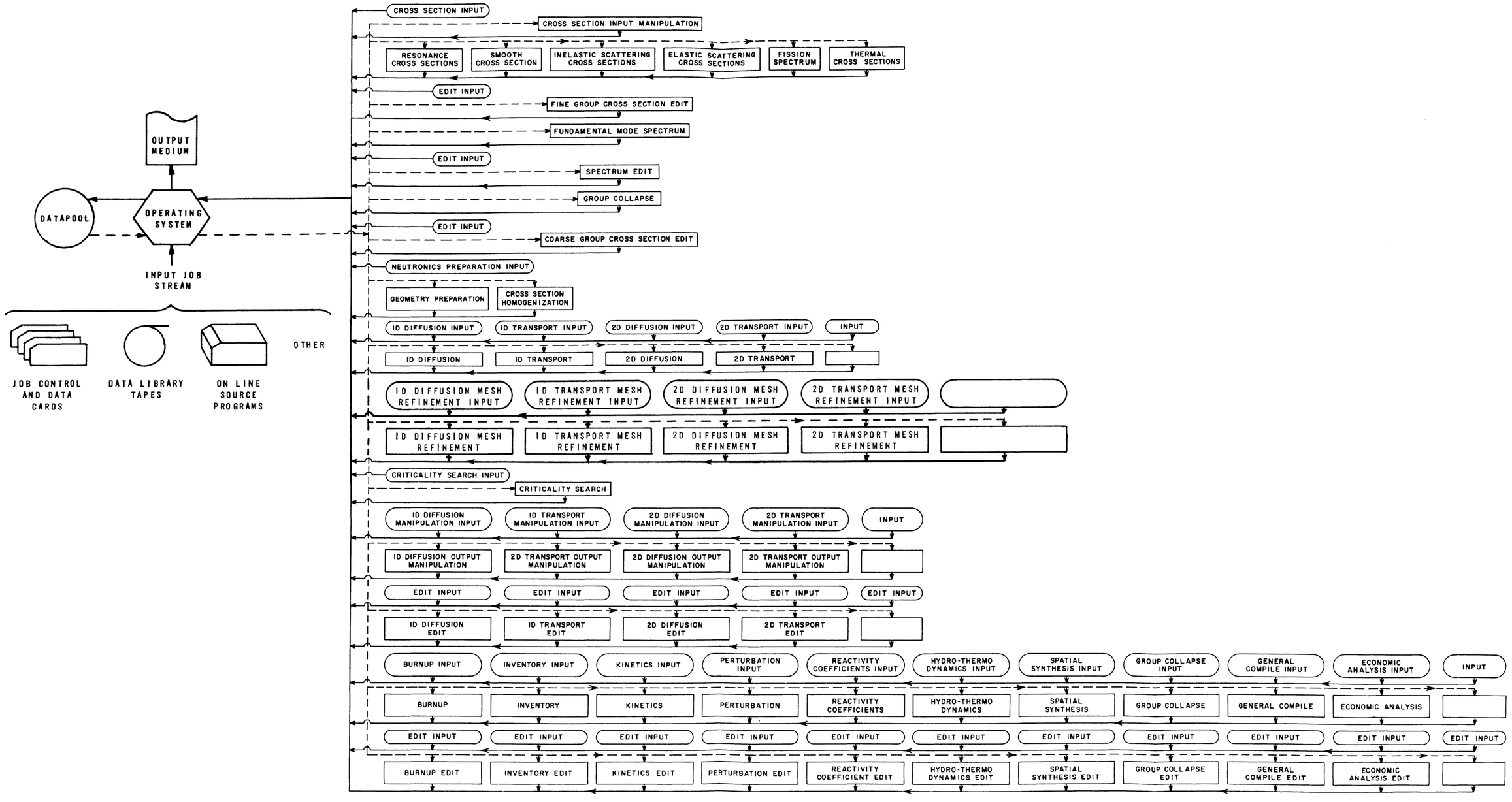

Fig. 11. Schematic Representation of the ARC System

For formal testing, the module internal details are also essentially irrelevant. For the sake of expediting the effort, the modules have been made to do something trivial and yet significant enough to provide assurance of proper handling of the data sets involved. For example, the adding of two upper interface quantities to generate a lower interface quantity is trivial and yet proof of correctness of the formal procedures.

b. Fuel Management-Burnup Package. The following capabilities have been decided upon for inclusion in the Fuel Management-Burnup Package for the Phase-I ARC System.

(i) Burnup Matrix Computation. The direct expansion and Duane's methods (see Progress Report for April 1966, ANL-7204, pp. 34-36) will be incorporated, the choice between the two procedures being made internally, in determining the burnup matrix from the coefficient matrix of the depletion equations. The depletion processes will include neutron capture, fission, (n,2n), (n,α) and (n,p) reactions, and radioactive decays through α, β^+, and β^- emissions. The nuclide-dependent fission product yield will be included, and the isomeric states of nuclides will be taken into account whenever significant. Excluded from the present considerations are the spontaneous fission, energy-dependent fission product yields, and the energy-dependent branching ratios of various nuclear transmutations.

(ii) Reactivity Control. The capabilities of searching for and determining the initial enrichment as a function of space for each irradiation step, the control (poison and/or fuel control) variation throughout the irradiation step as a function of time and space, and the length of an irradiation step to achieve a specified or a computed fuel burnup at the end of the step will be included.

(iii) Internal Fuel Management. The full capabilities of arbitrary interregion transfer of material, as described previously (see Progress Reports for February 1966, ANL-7176, pp. 51-54; for March 1966, ANL-7193, pp. 45-51), will be provided. To accommodate the presence of more than one type of fuel material, the conservation of physical volume will be taken as the basic constraint in all transfers.

(iv) External Fuel Management. The external fuel cycle will include provisions for multiple reprocessing plants, multiple external feeds, direct sale of a fraction of reprocessing plant output, and sale of the remainder of reprocessed fuel after fabrication of a fuel charge. Any fraction of a particular discharged batch may be sent to any of the reprocessing plants or be sold after cooling. Each reprocessing plant may have up to two effluents, which are divided into two classifications (normally high-reactivity and low-reactivity effluent). The selection of which members of each classification are to be used in making up each fuel material of a charge and and which are to be sold directly will be decided on the basis of

two priority systems specified by the code user. The first, an absolute priority, allows the user to specify that all of a particular member of a classification (i.e., the high- or low-reactivity effluent from a reprocessing plant or external feed) be used in making up a particular charge material in preference to any other member. All of the next most desirable member may then be used, and so on, until the requirements for that classification in that material are fulfilled. If the absolute priority level for a particular member is the same for more than one charge material, the division of that member is decided on the basis of a graded (i.e., fractional) delivery priority. If the requirements of one charge material are met while those for other materials are not, the unused fraction of the member will be distributed among those materials in proportion to the original graded priorities.

Real-time accounting will be carried throughout the cycle, and the time of each fuel movement will be recorded. Any decay present in the problem will be calculated over the external cycle. The availability of reprocessed fuel for makeup of a fuel charge will be decided on the basis of given cooling, reprocessing, refabrication, and storage times compared with the operating and shutdown times of the reactor.

(v) Equilibrium. The equilibrium calculation may be done by a repeated application of a given fuel-management policy, or, in case of a relatively simple management policy, by a direct analytical means. The equilibrium calculation for a multistage management policy will not be included for the present.

(vi) Zero-dimensional Survey Program. A zero-dimensional burnup-fuel management program will be included in the Package for survey calculations.

(vii) Interrupt Facilities. Two types of problem interrupt will be programmed. The first allows the user to interrupt the problem at any time during a burnup step, specified as a fraction of the total burn time. He may at this time dump relevant information for later use and/or respecify problem parameters, then proceed with the problem. The parameters which may be respecified depend on whether or not the interrupt occurred at the end of the burn step; the general criterion is to allow respecification of all parameters which would be available to a reactor manager at the time of interrupt.

The second type of interrupt will be the same as above except that all information necessary for restart will be dumped, followed by an edit and a problem stop. On restart the same problem parameters as above will be available for modification.

C. Instrumentation

1. High-temperature Instrument Development (Out-of-pile)

a. Flowmeters. The electromagnetic flowmeter (see Progress Report for May 1965, ANL-7046, pp. 10-11) has been completely fabricated and testing has begun. The initial tests are being carried out in an inert (helium) atmosphere at temperatures up to 650°C to determine the flowmeter impedance and signal noise levels at various temperatures without a sodium fill. In addition, the magnets are being thermally stabilized or "cured."

So far no detectable emf is generated by the meter due to thermocouple effects, even with a 50°C temperature gradient across the meter at a mean temperature of 650°C. Most of the measured meter resistance, determined without sodium present, is due to the approximately 14 ft of No. 24 AWG stainless steel lead wire being used. The equivalent flowmeter resistance was found to be ~34 ohms at 23°C and ~40 ohms at 650°C.

The entire flowmeter is being thermally cycled and soaked to "cure" the magnets. Four thermal cycles up to 690°C have been completed, with two extended 72-hr soaks at 650°C.

D. High-temperature Materials Studies

1. Ceramics

a. Uranium Monoarsenide. Uranium monoarsenide was synthesized by first reacting finely divided uranium with arsine (H_3As) gas The uranium was rendered very fine by several hydriding and dehydriding cycles. Reaction with H_3As was conducted at a temperature no higher than 300°C to mitigate dissociation of the gas. The reaction proceeded smoothly, and gravimetric analysis showed that the overall mixture has an As/U ratio of 1.20. X-ray analysis revealed the presence of two crystalline phases, UAs_2 and UH_3. On this basis the following reaction had taken place:

$$1.0\ U + 1.2\ AsH_3 \rightarrow 0.6\ UAs_2 + 0.4\ UH_3 + 1.2\ H_2 \uparrow .$$

Temperature was sufficiently low so that the unreacted uranium reacted with hydrogen to form UH_3. Three batches of a mixture of UAs_2 and UH_3 were then heated in vacuum at 1200, 1300, and 1400°C, respectively. X-ray analysis of each product revealed a single phase with the NaCl-type structure possessed by many other uranium, thorium, and plutonium monocompounds. A lattice constant value of 5.779 Å was obtained for material fired at one of the three temperatures. The resulting UAs powder was dark gray and was not pyrophoric in ambient air.

b. U-S-O System. Sulfur-saturated U_3O_8 formed by the low-temperature oxidation of US loses considerable sulfur content under oxidizing conditions in a sharp endothermic reaction at 750°C (see Progress Report for March 1966, ANL-7193, p. 66). The entire sulfur content was also lost in vacuum at the same temperature, confirming that this reaction simply involves decomposition into U_3O_8 and S species.

Samples of US_2 prepared at 400°C contained a mixture of γ and β US_2. Chemical analysis showed a S/U ratio of 1.992, with indications that oxygen contamination was slight and incorporated into the US_2 structure rather than as a separate phase. The X-ray powder pattern was very diffuse at high angles, suggesting lattice strain. When this material was heated at 800°C for 12 hr in vacuum, stoichiometry was retained and the structure was completely converted to β US_2, which had a sharp X-ray pattern. Treatment at 1285°C for 2 hr produced a material having the reported tetragonal α US_2 structure. The lattice parameters were determined to be a_0 = 10.301 Å and c_0 = 6.322 Å. Loss of sulfur, however, produced the composition $US_{1.88}$, which suggests that either α US_2 has a very wide homogeneity range or is not a true polymorph of US_2.

2. Corrosion Studies

a. Polarization Studies in Liquid-metal Environment. Experiments aimed at improved electrical insulation of zirconium electrode surfaces exposed to sodium vapor in the liquid sodium polarization cell have continued.

It was verified that a white ZrO_2 coating grown on the electrode surface in a plasma torch behaved similarly to those grown by conventional means with respect to development of electrical leakage when held overnight in vacuum at 525°C. The magnitude of the leakage developed was undesirably high.

It was found that additional Al_2O_3 insulation sprayed over the grown ZrO_2 provided insulation adequate for verification of the presence (or absence) of effect of polarizing current on corrosion in the oxygenated sodium environment. The significance of cell polarization curves may, however, be impaired by such leakage. A coating of 400- to 500-μ thickness (greater than previously tried) displayed a resistance of 10 to 20 ohms per linear inch of (0.25-in-dia rod) coated sample immersed in sodium in the range of 500°C for a three-day period.

A set of electrodes suitable for the projected polarization tests is being prepared, with shank surfaces coated in the manner described.

b. Lithium Corrosion Studies at Elevated Temperatures. The effect of silicon addition to lithium on the corrosion behavior of titanium and

tantalum at 1200°C has been previously reported (see Progress Reports for February 1966, ANL-7176, p. 57; for March 1966, ANL-7193, p. 68). It has also been reported that tantalum exhibited surprisingly good corrosion resistance when tested in a molybdenum rather than a tantalum capsule under otherwise identical test conditions. Interest has been centered on the role of silicon and molybdenum in lithium corrosion of tantalum.

In experiments with tantalum capsules and tantalum insert samples, capsule interiors were exposed to lithium and silicon-containing lithium (1.6 a/o Si), separately, at 1200°C for approximately seven days. Neutron-radiographic inspection was employed to inspect capsule seals, and to detect the position of lithium and insert samples before and after test. The tantalum and lithium images were clearly defined. Further use of this technique as a routine means of nondestructive inspection is warranted.

Test results indicated that the tantalum capsule containing lithium without additive suffered the degree of corrosion penetration reported previously. Microhardness measurements showed no abnormal surface irregularities. The corrosion resistance of tantalum in the silicon-containing lithium environment was greatly improved. Only a few shallow pits in scattered areas were observed. There were no significant microhardness differences between surface and internal areas. Microcracking had not occurred in this case as it had with the molybdenum capsule in a previous test (see ANL-7193, p. 68). There was no apparent weight change of either insert sample.

On the basis of these preliminary results, it appears that the addition of silicon to lithium retards the corrosion of tantalum under the above test conditions. Since molybdenum is only slightly soluble in lithium at this temperature, it is difficult to explain the results with the molybdenum capsule. Further study of this system and others is in progress.

3. Irradiation Testing

A summary of the present irradiations of carbides and sulfides in MTR is shown in Table XIII. All capsules are instrumented. The cladding is Nb-1 w/o Zr.

The initial results from the postirradiation examination of the specimens in capsule ANL-56-9 have been reported (see Progress Report for April 1966, ANL-7204, pp. 48-49). The metallographic examination of specimen MV-4 was started. This specimen, which was jacketed with Nb-1 w/o Zr and contained vibratorily compacted mixed UC-20 w/o PuC powders, had a circumferential crack adjacent to the bottom weld, as well as a longitudinal split extending upward from the circumferential crack. Segregation of the UC and PuC had occurred. Considerably more 20 w/o PuC was located

at the area of failure. Since the UC contained only depleted uranium, the segregation of the PuC at the bottom of the specimen caused a higher temperature and enhanced swelling in that area.

TABLE XIII. Status of Ceramic Fuel Irradiations in Progress in MTR

Capsule or S/A No.	Specimen Number	Design Parameters				Operating Conditions			
		Fuel Composition (w/o)	Effective Density (%)	Cladding OD (in.)	Cladding Thickness (in.)	kW/cc[a]	Max Clad Temp (°C)	Burnup to Date	
								a/o (U + Pu)	fiss/cc x 10^{-20}[a]
56-11	MV-2	UC-20 PuC	79	0.281	0.012	1.2	470	5.2	13.4
56-8	MV-3	UC-20 PuC	81	0.281	0.012	1.2	715	5.7	15.1
56-8	MV-5	UC-20 PuC	80	0.281	0.012	1.2	705	5.4	14.1
56-11	MV-6	UC-20 PuC	80	0.281	0.012	1.2	480	5.7	14.9
56-13	Z-4	UC-20 PuC	79	0.174	0.015	1.2	665	0.6	1.5
56-13	Z-5	UC-20 PuC	79	0.174	0.015	1.2	585	0.6	1.5
56-13	Z-7	UC-20 PuC	79	0.174	0.015	1.2	570	0.6	1.5
56-13	C-45	PuC	84	0.174	0.009	1.4	700	0.6	1.6
56-8	S-7	US	80	0.281	0.012	1.0	535	4.0	7.7
56-8	S-8	US	89	0.281	0.012	1.0	725	6.0	12.9
56-8	S-9	US	76	0.281	0.012	1.0	750	6.0	11.0
56-8	S-10	US	91	0.281	0.012	1.0	690	6.0	13.2
56-11	S-15	US	82	0.281	0.012	1.0	380	3.1	6.2
56-11	S-16	US	90	0.281	0.012	1.0	510	5.0	10.9
56-11	S-17	US	88	0.281	0.012	1.0	500	3.7	7.9
56-11	S-18	US	77	0.281	0.012	1.0	610	5.5	10.2

[a]Based on effective density.

Chemical analysis indicated that the PuC used in this specimen was hyperstoichiometric with respect to carbon. Chemical analysis also indicated that the UC was hypostoichiometric with respect to carbon, but hyperstoichiometric with respect to carbon plus oxygen. Metallographic examination verified the stoichiometry of the UC. Metallography of the PuC fraction is being done to identify the structural features present in the microstructure.

E. Other Reactor Fuels and Materials Development

1. Hydrogen in Irradiated Pressure-vessel Steel

Catastrophic delayed failure due to hydrogen embrittlement has been observed in high-strength steels, but not in structural steels like 212-B. The strength level of the steel is one of the critical parameters controlling the susceptibility of steel to hydrogen-induced delayed failure. Since irradiation raises the strength level of pressure-vessel steel, concern has been expressed that irradiation-hardened 212-B could become susceptible to hydrogen embrittlement.

a. Hydrogen Charging. Hydrogen was introduced into the steel used in these experiments by charging electrolytically in dilute sulfuric acid, the steel being the cathode.

Two different hydrogen contents of the steel were obtained. One, sufficient to cause catastrophic delayed failure in specimen 4340 at 20% of its notch tensile strength (NTS), is referred to as Charge A. The second, called High Charge, with a hydrogen content about ten times as great as Charge A, was obtained by much more severe charging conditions.

Equipment was built to measure this hydrogen. The specimens are permitted to outgas into an evacuated calibrated volume. After 24 hr at 150°C, the rate of outgassing is negligible. It has been shown[12] that baking at 150°C drives off the hydrogen responsible for delayed failure, and that a 24-hr bake practically returns the steel to its original condition. Thus the hydrogen extracted is the hydrogen that we wish to measure.

The results are reported in Table XIV. Charge A gave about 0.7-0.8 ppm (by weight) hydrogen in steel; the High Charge, although the product of the current and time is 480 times greater, gave about ten times that much.

b. Tests. In Fig. 12 the results of control tensile tests on various specimens of 212-B are plotted against the relative exposure, to fast neutrons, of the notched region of the specimens. The specimens received enough exposure to raise the transition temperature of 212-B at least 110°C. The original NDT (Notch Ductile Transition) for this steel, as determined by NRL from Charpy impact data, was in the neighborhood of -18°C. Charpy specimens of this steel subjected to this irradiation would certainly show very little impact energy at room temperature.

---

[12]Johnson, H. H., Morlet, J. G., and Troiano, A. R., Hydrogen, Crack Initiation, and Delayed Failure in Steel, Trans. Met. Soc. AIME 2 2(4), 528-536 (1958).

TABLE XIV. Hydrogen Content by Vacuum Extraction

Specimen	Pressure (mm)	Corrections[a]	Hydrogen (%)[b]	P_1 (mm H_2)	V_2 (cc H_2)	Wt H_2 in Steel (ppm)
4340-E Charge A	0.170	Negligible	92[c]	0.170	0.123	0.71
212-B Charge A	0.302	+0.020	90.7	0.292	0.188	0.87
212-W 120,000 mA-min in 4 hr	2.06	+0.040	94.9	2.00	1.29	6.0
212-Y 120,000 mA-min in 20 hr	2.92	+0.050	95[c]	2.82	1.82	8.5
212-X 120,000 mA-min in 20 hr. Broken, aged 2 days.	2.04	+0.010	95[c]	1.94	1.25	5.8
212-B As-received	0.035	+0.005	Small[c]	<0.02	<0.01	<0.05

[a]Estimated initial losses.
[b]Remainder: helium purge gas and air inleakage.
[c]Estimated.

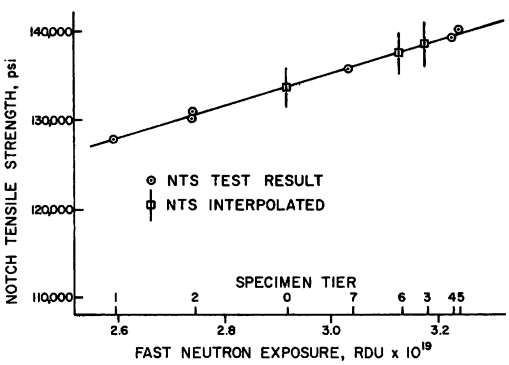

Fig. 12. 212-B Notch Tensile Strength vs. Neutron Exposure

The increase in the notch tensile strength of 212-B due to the irradiation was from 22 to 34%. The 20% difference in flux rate over the length of the capsule was enough to produce a spread of about 9% in NTS. Over this fairly short range the dependence of NTS versus RDU (Radiation Dose Units) exposure is practically linear.

In Fig. 13 the stress-strain curve for a typical irradiated notch tensile specimen is shown. The others would look similar, with the elongation to fracture being less as the NTS is increased by irradiation. Curves for Charge A notched specimens are so little different from the control curves that they have been omitted.

In the same figure the effect of the high hydrogen charge is shown. The high charge caused the notched specimen to lose about half its elongation, and almost all of its reduction in area. With this specimen the same curve was developed through the elastic range, but it broke before the onset

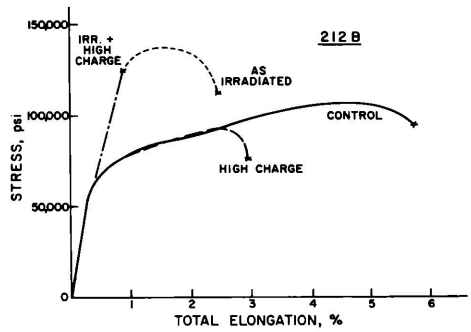

Fig. 13. Engineering Stress-strain Curves of 212-B Notched Tensile Specimens

of plastic flow. This type of behavior is typical. Tensile test results, based on a broad range of hydrogen contents, all fall on the same curve. The lower the hydrogen content the further along the curve before failure.

Figure 14 shows a high-charge specimen at high magnification, but the fracture surface is so jagged that parts of it are out of focus. The hydrogen must cause the cracking that leads to this type of fracture surface.

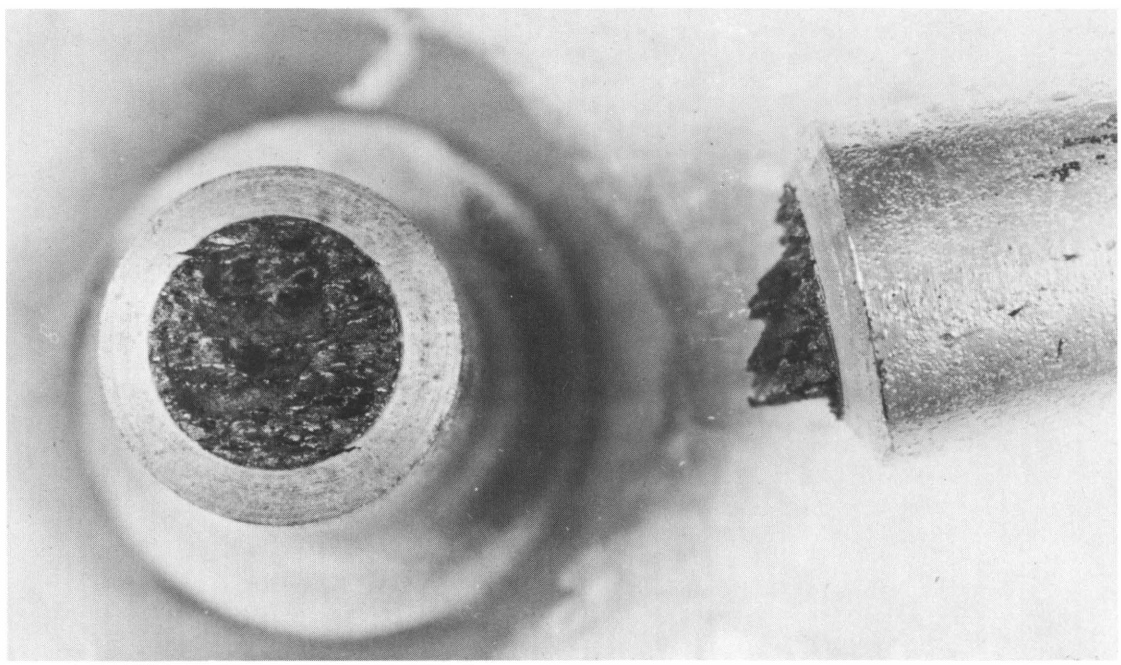

Fig. 14. Fracture Surface of High Charge Specimen at High Magnification

Pictures of the fracture faces of irradiated 212-B show an interesting contrast. Figure 15 is a specimen that was broken in delayed failure, but not hydrogenated. Most of the fracture surface is brittle, as would be the case for the same material broken in tension.

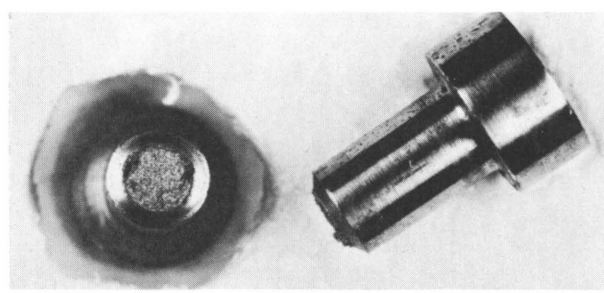

Fig. 15. Fracture Surface from Stress-rupture Test of Irradiated 212-B (As irradiated)

Figure 16 shows the results of a tensile test of an irradiated specimen with Charge A. There is a thin dark ring at the notch root, and the rest of the broken surface has a typical brittle appearance. Figure 17 is of the specimen

discussed in the preceding paragraphs, irradiated and hydrogenated, and tested in tension as indicated in Fig. 13. It looks like a flat brittle fracture, with none of the jagged appearance of the high-charge control specimens. The combination of high hydrogen content and irradiation-embrittled steel results in a fracture that looks granular, suggesting that a crack would propagate rapidly once initiated in such material.

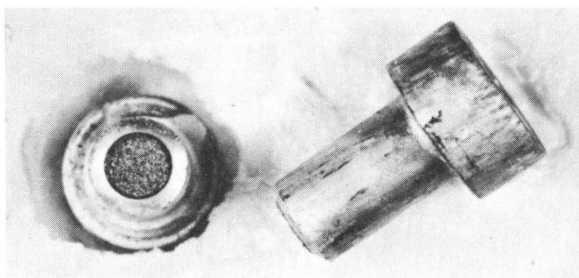

Fig. 16. Fracture Surface from Tensile Test of Irradiated 212-B (Charge A)

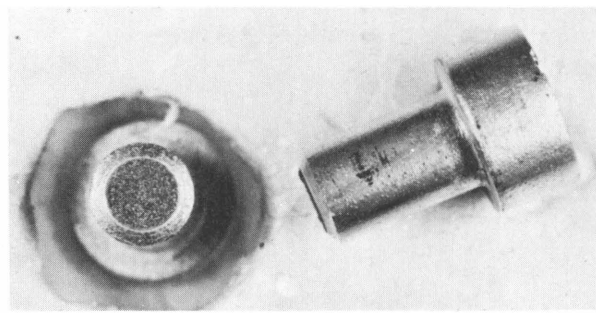

Fig. 17. Fracture Surface from Tensile Test of Irradiated 212-B (High charge)

The data from tensile and stress-rupture tests are correlated by plotting the applied stress as a percent of the unhydrogenated notch tensile strength for each test, as in Fig. 18. The notch tensile strength of a hydrogenated specimen is indicated by a square, as a percent of the unhydrogenated NTS. Thus, under Charge A Unirradiated a square shows that the charged NTS was about 96% of the uncharged NTS. The time to failure, in hours, is indicated for each stress-rupture test. An X is used to indicate a test that did not fail in 100 hr. The lower critical stress (LCS) must be above the X for a given condition.

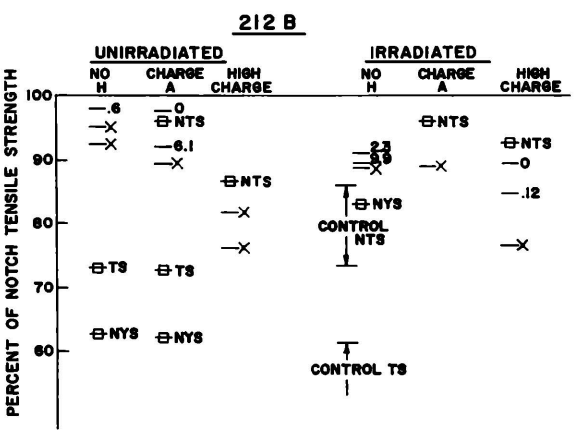

Fig. 18. Correlation of Tensile and Stress-rupture test results

A trend can be discerned. In each case a narrow band in which delayed failure was observed lies between the notch tensile strength and the lower critical stress. The band is broader for steels with higher strength level or heavier hydrogen charge. However, the delayed failure range of stresses seems to lie between about 90 and 95% of the charged NTS for the same charging condition. In no case is the catastrophic strength loss so typical of hardened 4340 observed.

c. Discussion. Irradiated Charge A specimens showed no particular effect attributable to hydrogen. It is evident that Charge A does not introduce enough hydrogen into 212-B to cause significant embrittlement.

Vacuum extraction analysis indicated that the hydrogen content of these test specimens was about 0.9 ppm, typical of the concentrations calculated as being possible for a thick, unclad pressure vessel. Harries and Broomfield concluded that the primary source of hydrogen in such a vessel would be corrosion by the reactor water.[13] They give equilibrium concentrations for various water temperatures and vessel wall thicknesses, and these concentrations range from less than 0.1 to 1.3 ppm. The Westinghouse analysis on the Yankee plant[14] indicates such a range for operating conditions, and one about three times as high after prolonged shutdown.

Hydrogen contents of this order are not sufficient to cause deterioration in properties of vessel steels in their design stress range. No difference in performance at stresses below the yield stress would be expected.

The High Charge condition was selected because it caused a significant loss in mechanical properties of the 212-B. It is far more severe than that necessary to embrittle high-strength steels completely, and is twice as high in mA-min (charging current X time) as the condition used by Cain and Troiano[15] to embrittle normalized steel. Based on vacuum extraction, these high charge specimens contained about 8 ppm hydrogen, more than one would expect to find in practice due to any aqueous corrosion reaction. In any reactor system that operates at elevated temperature this concentration could never be maintained.

Our results are compared with Cain's in Fig. 19. He studied a pearlitic 4620 steel for application in a hydrogen sulfide environment. Delayed failure was observed under high charge conditions in about 0.2 hr. A lower critical stress of 100,000 psi, or about 68% NTS, was found. This steel had a tensile strength of 100,000 psi and a notch tensile strength of 150,000 psi. This is almost the strength range of the irradiated 212-B tested. Despite the high charge and the fact that the irradiated steel was brittle, it showed no sharp drop-off or great reduction in its lower critical stress. In fact, the LCS is about 80% of the NTS.

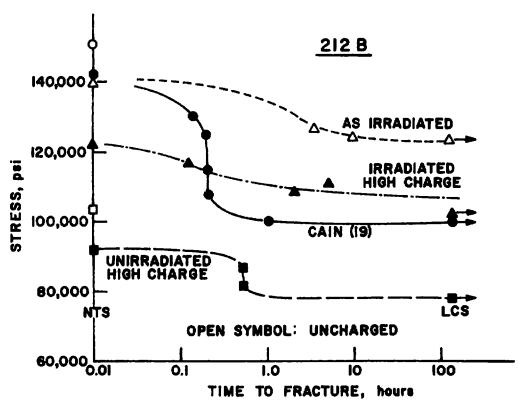

Fig. 19. Delayed Failure of High Charge 212-B

[13]Harries, D. R., and Broomfield, G. H., Hydrogen Embrittlement of Steel Pressure Vessels in Pressurized Water Reactor Systems, J. Nucl. Materials 9(3), 327 (1963).

[14]Evaluation of YANKEE Vessel Cladding Penetrations, WCAP-2855, Westinghouse Atomic Power Division, Pittsburgh (October 15, 1965).

[15]Cain, W. M., and Troiano, A. R., Steel Structure and Hydrogen Embrittlement, Petroleum Engineer (May 1965).

Thus, for this pearlitic steel 212-B the pattern of the delayed-failure behavior shows a lower critical stress at about 90% of the charged NTS. This range is typical even for uncharged specimens. However, the NTS itself is lowered by hydrogen. This behavior suggests that either the hydrogen does not diffuse as well in lower-strength steel, or if it diffuses it does not build up critical concentrations.

d. Safety of Reactor Pressure Vessels. One of the purposes of this study was to consider the possibility of catastrophic hydrogen embrittlement in a nuclear reactor pressure vessel. It is generally agreed that ductile steels used for reactor vessels are of low enough strength that the hydrogen concentrations needed to embrittle them are beyond reality in practice. These experiments indicate that this is the case, since even with a high artificial charge the loss in notch tensile strength is in the neighborhood of 10%. The LCS is only another 10% below that. This is not catastrophic.

The Pressure Vessel Code requires designers to keep the maximum stress in the structure to below the yield strength. It certainly means that designers can keep stress levels from reaching the failure range (>80% NTS). This is not a valid design criterion, however. Empirical tests reflect only their exact conditions, and detailed stress analysis would be required to relate these tests to design.

No information was found in the literature on the effect of neutron irradiation on the hydrogenated tensile and stress-rupture behavior of 212-B. This work shows little effect. The reduction in notch tensile strength is about the same percentage of the NTS irradiated as unirradiated. Since irradiation increases the yield, and tensile and notch tensile strengths, the loss due to hydrogen does not even bring these parameters back to their original levels. The net effect is still one of strengthening, but because of the rise in NDT due to neutron embrittlement, vessels are generally not designed to operate to exposures as high as those used in this experiment.

As for hydrogen embrittlement itself, it becomes clear that vessel designs must continue to avoid sharp corners, and be inspected to avoid cracks or flaws that could act as stress raisers. Next, the processes by which hydrogen enters steel must be studied so that more confident predictions of hydrogen content can be made.

As long as these concentrations are in the range of 1 to 2 ppm by weight, and radiation levels stay low enough to satisfy NDT criteria, the necessary conditions for catastrophic delayed failure do not exist in 212-B reactor pressure vessels.

e. Conclusions

(i) Delayed failure due to hydrogen can occur in lower-strength steels, but the lower critical stress level does not drop below 75% of the notch tensile strength or less, even with the high hydrogen content used.

(ii) Charging 212-B with hydrogen results in a lowering of the notch tensile strength itself that is a direct function of the hydrogen content.

(iii) Delayed-failure tests reveal a lower critical stress level at about 90% of the charged notch tensile strength for 212-B, independent of the strength level.

(iv) The above characteristics are observed in 212-B irradiated to 3×10^{19} RDU in which the NDT has been raised to 66°C above room temperature. Irradiation raises the notch tensile strength, and the hydrogenated results are changed in proportion. Irradiation does not change the microstructure.

(v) Even if a mechanism were available for building up a few ppm concentration of hydrogen in a reactor pressure vessel wall, the conditions for catastrophic delayed brittle failure do not exist in practice.

(vi) The differences in behavior of low-strength steel (i, ii, and iii above) could be attributed to poorer diffusion of hydrogen. This might be due to less lattice expansion for a given load, geometry, and stress field. It could also be related to the ferrite and pearlite microstructure as opposed to that of tempered martensite.

(vii) Delayed failure occurs in as-irradiated 212-B, but it is not catastrophic, and the pattern is comparable to the control and charged material.

2. Nondestructive Testing

a. Elastic Moduli of High-temperature Materials by Ultrasonics. The variations of room-temperature elastic properties of V-15 w/o Ti-7.5 w/o Cr as a function of annealing temperature are being studied (see Progress Report for February 1966, ANL-7176, pp. 60-61). Results obtained to date are shown in Table XV as averages for four specimens.

The values of Young's modulus E and shear (rigidity) modulus μ show a slight increase with increasing annealing temperature, while Poisson's ratio σ decreases. The largest difference between values of Young's modulus is 0.83×10^{11} dynes/cm^2, or about 6.5%.

TABLE XV. Room-temperature Elastic Properties of V-15 w/o Ti-7.5 w/o Cr as a Function of Annealing Temperature

Heat Treatment	Density (g/cm^3)	Longitudinal Velocity (10^5 cm/sec)	Shear Velocity (10^5 cm/sec)	σ	μ $\left(10^{11}\frac{dyne}{cm^2}\right)$	E $\left(10^{11}\frac{dyne}{cm^2}\right)$	E $\left(10^3\frac{kg}{mm^2}\right)$
As-rolled	5.878 ± 0.001	6.08 ± 0.04	2.75 ± 0.01	0.371 ± 0.002	4.45 ± 0.03	12.19 ± 0.09	12.42 ± 0.09
700°C Anneal	5.88 ± 0.01	6.12 ± 0.02	2.748 ± 0.008	0.374 ± 0.004	4.44 ± 0.03	12.20 ± 0.09	12.44 ± 0.09
900°C Anneal	5.89 ± 0.01	6.008 ± 0.004	2.771 ± 0.007	0.365 ± 0.001	4.52 ± 0.02	12.35 ± 0.07	12.60 ± 0.07
1250°C Anneal	5.91 ± 0.01	6.10 ± 0.01	2.827 ± 0.006	0.363 ± 0.002	4.72 ± 0.02	12.88 ± 0.07	13.14 ± 0.07
1500°C Anneal	5.93 ± 0.01	6.02 ± 0.02	2.845 ± 0.005	0.356 ± 0.001	4.80 ± 0.01	13.02 ± 0.06	13.28 ± 0.06

A rod of V-15 w/o Ti-7.5 w/o Cr has been machined for use in the 1100°C furnace. The dimensions of the index region of the rod were chosen to be the same as those of a V-20 w/o Ti (TV-20) rod that was measured some time ago,[16] because it was assumed that the elastic properties of the two materials would not be too different. However, the echo pattern in this rod is markedly different from that in the TV-20 rod. The main reason is that shear waves are much more highly attenuated in the ternary alloy than they were in the binary. The longitudinal waves are attenuated more too, but not as much as the shear waves. As a result, the trailing pulses[16] are not clearly resolved; it is hard to distinguish them from spurious trailing pulses generated in the unthreaded portions of the large-diameter end of the rod and from the high noise level of pulses scattered from internal sources in the rod. As a result, the bar may have to be remachined before a high-temperature run can be made; the matter will be studied further. The cause of the high shear wave attenuation is not yet apparent.

b. Ultrasonic Instrument and Transducer Development. Two further samples of porous nickel were received from the manufacturer. Both are 1.27 cm in diameter and 2.22 cm long. One sample is 70.6% dense (-325 mesh), the other 67.3% dense (-500 mesh). Sample length in the past was 1.27 cm. By increasing the sample length, it is hoped that the amplitude of unwanted echoes from this material, when utilized as a backing member in ultrasonic transducer probes, will be significantly reduced. The fine-particle sample (-500 mesh) was ordered to evaluate the effect of finer particles on the longitudinal wave velocity. Any increase in longitudinal wave velocity will allow use of lower-density material, which will more effectively attenuate the ultrasound.

Four transducer probes were fabricated. Two contain the nickel samples received this month. The other two have Fiberglas-loaded and tungsten-loaded epoxy backings, respectively. Except for the backing material, the probes are identical. Evaluation of these probes is in progress.

[16] Peterson, R. G., A Facility for Studying the Elastic Moduli as a Function of Temperature by an Ultrasonic Method; Measurements of Vanadium-20 w/o Titanium, ANL-7119 (to be published).

A longitudinal wave velocity of about 3.56×10^5 cm/sec for the -500 mesh, 67.3% dense nickel sample was measured prior to fabrication. The resultant acoustic impedance (Z) is then about 21×10^6 kg/m^2-sec. Since a Z value of about 34×10^6 kg/m^2-sec is necessary, a higher-density sample of this material is required.

Electronic circuitry for a pulse Schlieren system is under construction. All other components for this system have been ordered and received.

c. Development of a Neutron Image Intensification System. More extensive gamma radiation tests have been completed on the new 15-cm neutron image intensifier tube. A cobalt-60 source was used to provide a known gamma background during neutron imaging tests. No difficulty in resolution degradation nor in contrast capability was noted for cobalt-60 gamma-background intensities as high as 2400 R/hr at the tube face. At gamma intensities of 9600 R/hr an image distortion was observed, but the high-contrast resolution capability of the neutron television system appeared unchanged. Contrast-sensitivity capability of about 10% could be observed through the 9600-R/hr gamma background. Fuel-irradiation-capsule neutron images at that gamma level were not appreciably degraded. These data, therefore, appear well in line with previously reported information that gamma intensities at least as high as 4000 R/hr at the intensifier tube would cause little neutron image degradation with the neutron intensity available at the Juggernaut reactor neutron radiographic facility.

d. Development of Infrared Systems for Nondestructive Testing. Analysis of the indium antimonide infrared detection system for locating unbonded areas in EBR-II capsules has continued. Detector delay time, sample velocity, and minimum unbond length were determined.

The optimum sensitivity was obtained by a procedure in which the instantaneous temperature of the surface at the trailing edge of the heat source is monitored as the sample is moved in front of the detector spot at a maximum scan speed of 0.5 cm/sec. Surface emissivity is an important factor in system performance. High emissivities are necessary to permit detection of small changes in temperature. The color of the EBR-II capsule was dark gray, rendering a surface treatment unnecessary for the test.

The minimum unbonded length detected by the system was 2 mm. The length and position of the unbonded areas were determined by X radiography. Correlation between X radiographs and infrared traces were good.

F. Engineering Development

1. Boiling Liquid-metal Technology

a. Niobium-1% Zirconium Loop. A power failure caused a small rupture in the sodium hot trap. This has been repaired. Fresh sodium has been circulated in the hot trap at 1300°F, and the main loop is now ready for sodium filling. As soon as the vacuum chamber has passed the final leak check, low-temperature operation of the main loop will begin.

b. Heater Experiments

(i) Electron-bombardment Heater Experiment. Approximately 150 hr of testing with the present 0.030-in.-dia thoriated-tungsten cathode have been achieved. Heat fluxes exceeding 300,000 Btu/hr-ft^2, with peak sodium temperatures to 1350°F, have been supplied to the anode during both steady-state and transient testing. This includes an emission current ranging up to 3.55 A and a cathode-to-anode voltage approaching 7700 V. This information is pertinent to the design of a reliable high-temperature, high-heat-flux electron-bombardment heater for use in the Nb-1% Zr loop.

Negotiations with an outside vendor pertaining to a special service contract have been completed. This work (to run 2 months) will produce information necessary to the final design of a transient electron-bombardment heater.

2. General Heat Transfer

a. Heat Transfer in Double-pipe Heat Exchangers

(i) Countercurrent Turbulent Liquid-metal Flow. A computer program for the reduction of experimental data has been written and "debugged." Leak testing of the loop with test section installed, and calibration of thermocouples and flow rate measuring orifices are in progress.

3. Electric Master-Slave Manipulators

Assembly and preliminary testing of the experimental Electric Master-Slave Manipulator, ANL Mark E4A, has begun. The master arm has been made much lighter than the slave arm to reduce inertia and friction, thus improving the overall sensitivity of the manipulator. For light loads the force at the slave tongs can be selected to be equal to or twice the force exerted by the operator at the master handle. For larger loads, the operator can select a force boost of 5, which enables him to exert the full 50-lb capacity of the manipulator with one hand. Although the force feedback to the operator is reduced, the vitally important factor of bilateral response is maintained.

The sensitivity of the manipulator is considerably improved over that of Mark E3 at all load levels. It is planned to measure all parameters when the manipulator has been completely checked out. Although the servo control system was set up to be quite stable on the bench, the overall stability of the servo and manipulator mechanical components is lower than is needed. Steps are being taken to improve the stability.

Major design work is nearing completion on the slave arm for the Mark E4B manipulator, powered with the new cup-type servo motors, which will have a load capacity of over 100 lb (see Progress Report for March 1966, ANL-7193, p. 75). About 50 percent of the fabrication for the slave arm is completed. The master arm, which is essentially a duplicate of the one for the Mark E4A manipulator, is about 80 percent fabricated. The Mark E4B together with the Mark E4A will make up a working pair of manipulators.

The low inertia cup-motor to be used on the Mark E4B manipulator is difficult to stabilize in a force reflecting servo system. Current feedback was found to be considerably better than voltage feedback in a single-field control system. Further improvement has been achieved with a two-field control system, but it has not yet been stabilized adequately for all load conditions.

G. Chemical Separations

1. Fluidization and Volatility Separations Processes

a. Recovery of Uranium and Plutonium from Low-enrichment Fuels: Laboratory Support Work

(i) Fluorination of UO_2-PuO_2-Fission Product Pellets. Studies are being performed in a 2-in.-dia fluid-bed reactor to determine optimum conditions for fluorinating UO_2-PuO_2 pellets containing fission products. Recent experiments involved the use of BrF_5 as a selective fluorinating agent for uranium-plutonium mixtures. In the reaction, uranium is oxidized to volatile UF_6 while plutonium is converted to PuF_4, a solid. The plutonium remains in the fluid bed as nonvolatile PuF_4 and may be recovered by converting the PuF_4 to volatile PuF_6 by fluorination with fluorine at temperatures of 300 to 550°C.

A less desirable alternative for plutonium recovery is by leaching the fluid bed with a solution of nitric acid. The leaching step is not an integral step in the all-volatility process currently under development, but was investigated to demonstrate the added process versatility in the plutonium removal step when BrF_5 is used as an agent for the selective volatilization of uranium.

Samples of alumina fluid beds which had been taken during previous runs after the BrF_5 fluorination step had been completed (see Progress Reports for January and February 1966, ANL-7152, pp. 67-68, and ANL-7176, p. 65) were blended to prepare the material for leaching studies. The blended mixture contained 0.3 w/o uranium and 0.19 w/o plutonium. Leaching tests, performed at 100°C with 6N nitric acid for periods of 1, 2, 3, and 5 hr, indicated that uranium and plutonium in the alumina bed can be readily leached with 6N HNO_3; greater than 99% of the uranium and plutonium was leached in 2 hr, and over 99.9% was leached in 5 hr.

In the design of fluid-bed equipment, it is necessary to apply kinetic rate data, frequently obtained in an entirely different system, to predict reaction rates in large-scale equipment. Kinetic data for the U_3O_8-BrF_5 reaction obtained during previous tests in the 2-in.-dia fluid-bed reactor were compared with data obtained from thermobalance experiments (see Progress Report for January 1966, ANL-7152, p. 68). Data from the fluid-bed experiments were analyzed by the same method as employed in the analysis of the thermobalance data, namely, by a diminishing-sphere model wherein the rate-controlling step is assumed to be reaction at the surface of the sphere. Very good agreement of the rate constants calculated from the fluid-bed and thermobalance systems was obtained.

(ii) Neptunium Fluoride Chemistry. Laboratory-scale studies of the reaction of NpF_4 with BrF_5 are being carried out to determine the behavior of neptunium when oxidized nuclear fuel is contacted with BrF_5. Initial experiments were concerned with identification of the product of the NpF_4-BrF_5 reaction and determination of the rate of the reaction. Preliminary data indicate that at temperatures of 325 to 500°C NpF_4 reacts with BrF_5 to form a volatile neptunium compound, presumably NpF_6. The rates of the reaction were significantly lower (by factors of 10^{-1} to 10^{-2}) than those measured for the UF_4-BrF_5 reaction.

b. Recovery of Uranium and Plutonium from Low-enrichment Fuels: Engineering Work

(i) Engineering-scale Alpha Facility. Current work involves the recovery of residual amounts of plutonium in the final alumina bed and in process-equipment lines and vessels from the first three runs. The plutonium in the equipment lines and vessels was deposited as a result of chemical reaction, thermal decomposition, or alpha decomposition. During the recovery operation, all parts of the process equipment were exposed to 90 to 100% fluorine at temperatures above 250°C. In the initial part of the recovery operation, the final alumina bed from the third run was fluorinated for 6 hr at 350 to 550°C and for 6 hr at 550°C with 90 v/o fluorine on total gas recycle. This bed material included the finely powdered material which had been retained in the upper portions of the reactor and which contained

significant amounts of plutonium (see Progress Report for April 1966, ANL-7204, p. 64). Refluorination of the bed resulted in the reduction of the plutonium concentration from 0.22 to 0.06 w/o. It appears that the plutonium in the fines is readily removed by fluorination. Preliminary data indicate that the treatment was effective for removing plutonium from the upper portions of the fluid-bed reactor.

(ii) Process Development Studies for Uranium Dioxide Fuels. A series of experiments were performed in a 1.5-in.-dia fluid-bed reactor to investigate the effect of the addition of small quantities of BrF_5 to a fluorine gas stream on the rate of fluorination of U_3O_8 fines in fluidized beds of alumina. Qualitative estimates of the rate of fluorination of U_3O_8 at 200°C were made for feed gases containing 2.6 v/o BrF_5 in nitrogen, 12.8 v/o fluorine in nitrogen, and a mixture of 2.2 v/o BrF_5 and 12.5 v/o fluorine in nitrogen. Preliminary data indicate, at the reactant concentrations used in these tests, that the fluorination rate of U_3O_8 fines is higher with the mixed reactant feed than for BrF_5 or fluorine alone. Experiments with higher concentrations of BrF_5 in fluorine will be made to evaluate further these effects.

(iii) Studies with Irradiated UO_2-PuO_2 Fuels. Three experiments have been completed on the processing of UO_2-PuO_2 fuel in a bench-scale fluid-bed unit. Two experiments involved unirradiated Zircaloy-2-clad UO_2-PuO_2 fuel material, and the other Zircaloy-2-clad UO_2-PuO_2 fuel irradiated to 5300 MWd/t and cooled 22 months. In these experiments, the cladding was chemically removed from the oxide fuel by reaction of the cladding with 50 to 70 v/o HCl in nitrogen for 2 to 3 hr at approximately 430°C. The fuel was then fluorinated by two-zone oxidation-fluorination for 3.2 hr at 460°C followed by direct fluorination with 90 v/o fluorine at 450 to 550°C. Chemical analyses of the final alumina beds indicated that the plutonium retention on the bed material was only slightly higher for the experiment with irradiated fuel than for experiments with unirradiated charges. The results with the irradiated fuel were similar to those obtained in bench-scale experiments with unirradiated fuel containing added fission product elements (see Progress Report for January 1966, ANL-7152 p. 66), and tend to confirm the validity of those results. The results with irradiated fuel indicate that >99% removals of plutonium from the bed should be possible with several reuses of the alumina bed.

H. Plutonium Recycle Experiment (EBWR)

1. Theoretical Calculations

Measurements have been made of the boric acid worth, nine-rod bank-worth shutdown margin, and minimum boric acid concentration required to produce eight-rod shutdown for full loading at room temperature.

The reactivity worth of a change in boric acid concentration was obtained from the difference in critical settings of the central rod. The differential worth of the central rod was obtained from period measurements. The bank worth was then obtained from the difference in the critical height of the nine-rod bank resulting from the boric acid dilution. The results of the measurements of the boric acid worth and the bank worth are given in Table XVI.

TABLE XVI. Boric Acid and Nine-rod Bank Worths

Boric Acid (g/gal)		Nine-rod Bank (in.)		Reactivity Change (%)	Boric Acid Worth (%Δk/g/gal)	Nine-rod Bank Worth (%Δk/in.)
Range	Change	Range	Change			
6.68 - 7.56	0.88 ± 0.03	18.65 - 21.30	2.65 ± 0.04	1.10 ± 0.10	-1.25 ± 0.16	0.42 ± 0.04
5.84 - 6.68	0.84 ± 0.03	16.60 - 18.65	2.05 ± 0.04	1.09 ± 0.12	-1.29 ± 0.18	0.53 ± 0.07
5.20 - 5.84	0.64 ± 0.03	15.12 - 16.60	1.45 ± 0.04	0.929 ± 0.095	-1.45 ± 0.22	0.63 ± 0.08
4.67 - 5.20	0.53 ± 0.03	14.10 - 15.12	1.02 ± 0.04	0.746 ± 0.076	-1.41 ± 0.22	0.73 ± 0.10
4.18 - 4.67	0.49 ± 0.03	13.22 - 14.10	0.88 ± 0.04	0.678 ± 0.064	-1.38 ± 0.21	0.77 ± 0.11
3.70 - 4.18	0.48 ± 0.03	12.45 - 13.22	0.77 ± 0.04	0.662 ± 0.068	-1.38 ± 0.23	0.86 ± 0.13
3.32 - 3.70	0.38 ± 0.03	11.80 - 12.45	0.65 ± 0.04	0.571 ± 0.060	-1.50 ± 0.28	0.88 ± 0.15
3.00 - 3.32	0.32 ± 0.03	11.31 - 11.80	0.49 ± 0.04	0.431 ± 0.045	-1.34 ± 0.26	0.88 ± 0.16
2.80 - 3.00	0.20 ± 0.03	11.00 - 11.31	0.31 ± 0.04	0.319 ± 0.034	-1.59 ± 0.41	1.03 ± 0.24

Because of the magnitude of the unavoidable experimental errors a dependence of the boric acid worth upon boric acid concentration cannot be easily discerned. The boric acid worth for concentrations between 7.5 and 2.8 g/gal averages to -1.40 ± 0.25% k/g/gal. The nine-rod bank worth tends to increase as the bank is lowered. Factors that may contribute to this effect are: the lower boric acid concentration, the greater leakage from the increasingly flattened core, and the increasing axial curvature of the flux.

For several boric acid concentrations, the critical height of the nine-rod bank and the critical height of the eight-rod bank when the central rod was at its maximum permissible height were obtained. The concentration at which the eight-rod bank height extrapolates to zero is the minimum boric acid concentration allowed. This intercept was found to be 2.75 ± 0.02 g/gal. Because it is forbidden to reduce the boric acid concentration below the level for which eight-rod shutdown is assured, the shutdown margin cannot be measured directly. The multiplication constant for the fully rodded and unpoisoned reactor must thus be determined by using information from the nine-rod bank-worth measurements and the boric acid worth for concentrations above 2.75 cm/gal. The shutdown margin is the complement of this constant. With the reactor critical at 2.8 g/gal when the nine-rod bank is at 11 in. and by use of the assumptions that the boric acid worth is 1.40 ± 0.25% k/g/gal and the bank worth is 0.90 ± 0.20% k/in., our estimate of the shutdown margin is 6 ± 3% k.

Because of the large uncertainty in this estimate of the shutdown margin, a two-dimensional, four-group computation was made using the 20-GRAND program. Spectrum-dependent cross sections for each type of

fuel were obtained by use of the GAM and THERMØS codes. The computation yielded a shutdown margin of 3.4% k, which is just within the uncertainty of the experimental estimate. For the computed shutdown margin, the operating power is expected to be about 30 MW. The effect of using spike assemblies, left over from the 100-MW operation of EBWR, upon the shutdown requirements is being investigated in connection with their potential use as a means of lowering the shutdown margin to allow operation at higher powers.

III. ADVANCED SYSTEMS RESEARCH AND DEVELOPMENT

A. Argonne Advanced Research Reactor (AARR)

1. General Plant Design

a. Architect-Engineer. The architect-engineer, Burns & Roe of New York, continued Title I activity. They have received all information and criteria necessary for completion of Title I design, including all requirements for conformance with the PSAR. The Title I report is scheduled to be issued on September 1, 1966.

b. Reactor Design. The Preliminary Safety Analysis Report (PSAR) generated questions involving the general safety of the reactor concept. The design shown in the PSAR indicates control drives mounted on the top of the reactor vessel, with the core structure suspended from the vessel cover.

A new design study was recently completed that evaluated the arrangement of the reactor internals and the control rod drives, particularly with respect to safety, reliability and maintenance, cost, and fuel or core handling. In the new arrangement, the control rod drives have been located below the reactor vessel (this is the best arrangement for reactor safety). The core package is removable as a unit or, should it be necessary, can be disassembled within the reactor vessel. (A functional description of the core package is given in Progress Report for December 1965, ANL-7132, p. 70.)

2. Reactor Physics Experiments

Experimentation continued with the uniform 1215/1620 loading of 1215 standard fuel foils and 1620 boron-stainless steel poison strips (see Progress Report for February 1966, ANL-7176, pp. 73-75). More precise measurements were made of the azimuthal power distribution in the vicinity of control-blade followers for a radial in-core blade. The followers involved were: 0.2-in.-thick stainless steel; 0.2-in.-thick aluminum; and 0.15-in.-thick aluminum. The aluminum follower of reduced thickness was included to increase the water gap and to simulate more accurately the design control-channel water thickness. These new measurements indicate that the azimuthal power peaking in fuel near control-blade followers is little affected by the use of a stainless steel rather than an aluminum follower. In the case of the thin aluminum follower, there was increased activation in the control channel itself, but little additional peaking in nearby fuel. The power peaking was most pronounced within the first 1/2 cm of fuel at the control channel. Approximately, the azimuthal maximum-to-average power ratio near the control-blade follower was $1\frac{1}{4}$.

A new procedure for determining reactivity-control worths of fixed-size samples of neutron absorbers makes use of the availability of the DDP-24 computer for on-line data analysis. Previously, data were obtained by the methods of rising period or flux drift. The computer reproduces data for sample worths to within one part in 50, whether the sample is inserted or withdrawn. Data given in Table XVII are from on-line computer analysis of sample insertion, which typically corresponded to a reduction in reactivity. Data are given for sets of three identical samples positioned with their vertical centers at the midplane of the active core. The centers of the widths of the samples were at radii of 9.5, 15.7, and 21.9 cm from the vertical axis of the internal thermal column (ITC). All

TABLE XVII. Measured Reactivity-control Worths in the Fuel Region for the Full Uniform Loading of the AARR Critical Assembly[a]

Sample Description	Sample Thickness (in.)	Sample Weight (g)	Reactivity-control Worth of Sample (10^{-2}%)
Boral (B_4C-Al)[b]	0.200	17.859	6.03
Boron-stainless steel (1.01 w/o B)	0.200	53.955	2.21
Cadmium	0.200	62.703	2.80
	0.100	31.352	2.10
Dysprosium	0.010	3.056	1.38
Europium oxide-stainless steel (31 w/o Eu)	0.156	43.299	6.56
Gadolinium oxide-stainless steel (0.7 w/o Gd)	0.200	56.052	0.935
Hafnium-zirconium (97.5 w/o Hf)	0.200	92.274	6.12
	0.119	55.132	4.61
	0.100	46.137	4.31
Nickel	0.200	63.722	0.43
Stainless steel (Type 304)	0.200	56.868	0.27
Uranium-aluminum (17.444 w/o U; 93.17% U^{235})	0.182	19.914	-0.54
Water	0.200	21.657	-0.40

[a]The reference material is 0.2-in.-thick aluminum.

[b]In this case the clad thickness is included; the absorber thickness was 0.168 in.; the listed w/o boron is based on an average of the total clad sample.

samples were 2.18 cm x 2.18 cm, with thicknesses indicated in Table XVII. When the sample thickness was less than 0.2 in., it was shimmed to a total thickness of 0.2 in. by the addition of aluminum sheet on one side. The samples were inserted by the motion of long, dummy aluminum control blades which were chambered to contain the samples; these dummy blades were in one radial control-blade channel.

Preparations are being made for the first graded-fuel loading. An evaluation of the available supply of special thin fuel foils indicates that of the total of 11 graded-fuel regions, 7 will be matched to within 5% of the current desired average composition, and 4 will be matched to within 5-10%.

3. Theoretical Reactor Physics

It was noted (see Progress Report for March 1966, ANL-7193, p. 84) that, to a good approximation, the peak thermal-neutron flux in the ITC was determined by the total thermal power from the reactor core, and that it was not sensitive to the detailed radial power distribution. However, both the peak neutron flux in the ITC and the gross radial power distribution near the ITC were affected significantly by the loading of the ITC. Table XVIII shows the influence of the ITC contents on the gross radial power distribution. A fixed graded-fuel loading was present, namely, the reference loading set for the reference 7-cm ITC unperturbed by aluminum diluent or sample

TABLE XVIII. Calculated Radial Power Distribution near Inner Edge of Reactor Core as Function of ITC Loading

(Relative values for constant total reactor power)[a]

Radius (cm)	ITC Characteristics			
	100% H_2O; no Boron	25% Al; no Boron	25% Al; 1 g B	50% Al; 1 g B
6.83[b]	76.5	70.8	64.2	53.9
7.20	76.2	72.3	66.9	59.1
7.56	75.0	73.3	69.3	64.7
7.73	74.1	73.4	70.2	67.2
7.90	74.0	74.3	71.7	70.3
8.06	68.9	70.0	68.2	68.2
8.22	60.6	62.0	60.8	61.8

[a]Actually, these values are the relative rates of production of fission-spectrum neutrons, not power density. There is little difference between these distributions and the power distributions, however.

[b]This is the inner edge of the fuel zone.

absorber. Note that the peak power density near the ITC was lowered significantly in the case of an ITC fully loaded with samples, and that there is a shift in the radial location of this peak to a position farther from the ITC. Consequently, special attention is needed to match the graded-fuel loading at the inner edge of the reactor core to the ITC loadings planned for a given core cycle, so as not to exceed heat-transfer limits. The economics and safety aspects of tailoring the reactor loading in this fashion are under study.

Two soluble poisons have been evaluated with respect to their use for backup reactivity control. The total reactivity-control worth of boron in the ITC and in the outer beryllium reflector rapidly saturates with increasing concentration of boron. Boron in the reactor core, however, presents almost a constant differential worth up to a concentration of at least 10 g B per liter of water. The total reactivity-control worth of boron dissolved uniformly in the water of the reactor is approximately 6% for $2\frac{1}{2}$ g B/liter, and 15% for 10 g B/liter, excluding the reactivity losses due to boron in the axial reflectors. Of the latter total (15%), approximately 2/3 arises from poisoning of the reactor core zone.

In spite of its very large capture cross section for thermal neutrons, gadolinium does not offer any real advantages in comparison with boron. The neutron poisoning of the inner and outer reflectors saturates very rapidly. The above-thermal microscopic capture cross section of gadolinium is only two to five times as large as that of boron, however, and the much larger atom density of boron compensates for the lower cross section of the boron in the heavily absorbing reactor core. For example, a concentration of $2\frac{1}{2}$ g gadolinium per liter of water in the entire reactor is calculated to reduce reactivity by $7\frac{1}{2}$%, exclusive of the reactivity loss resulting from the poisoning of the axial reflectors.

Other rare-earth poisons are being reviewed for their usefulness and their cost as soluble poisons for backup reactivity control.

4. Mark-I Core Development

a. Experimental Studies of Heat Transfer. The steady-state heat transfer program is intended to measure the effect of channel spacing, flow, inlet water temperature, pressure, power upon pressure differential within the channel, void distribution, and critical heat flux. These measurements are being made with electrically heated, rectangular test sections that simulate the flat-plate geometrical arrangement of the AARR core.

Figure 20 illustrates the basic dimensions of the test section used. Section A-A depicts the planned shape of the flow channel; section B-B shows the estimated shape of the flow channel during the tests. This shape resulted from incorrect backup of the test section and was detected during initial adiabatic test runs.

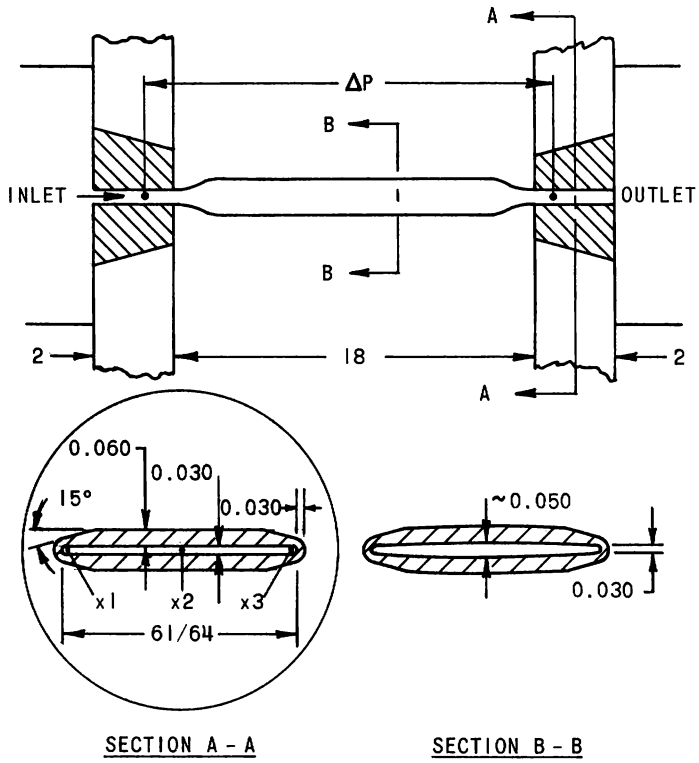

NOTE: "x" shows approximate locations of thermocouples. Numbers relate location of water temperature listed in Table XIX.

Fig. 20. 0.030-in. Test Section

Inconsistencies within the data have appeared. Anomalies, such as measured adiabatic pressure drops of only 30% of calculated and excessive distortion in the temperature profile across the coolant channel, have pointed to a possible dimensional error. The tests were run regardless of this condition in order to check instrumentation and the burnout detector-power supply response.

After the tests during which physical burnout of the test section occurred, the nonmelted portion of the test section was sectioned and the flow channel remeasured. The channel had distorted under pressure; the center spacing was now about 0.050 in., although the spacing at the corners remained about 0.030 in. (see Fig. 20). The backup plates, which were to prevent this type of distortion, were inspected. A slight dimensional error was found that allowed the backup plates to bottom on a guide bar before touching the test-section assembly. The test-section assembly procedure has been changed and additional preoperational tests instituted to prevent future occurrences of this trouble.

A complete series of steady-state tests were run at nominal exit pressures of 615 and 675 psia on the 0.030-in. flow-gap test section. In these tests, the total power, inlet coolant temperature and exit pressure were set. Then the inlet coolant flow was progressively reduced until burnout was detected, whereupon the power was rapidly reduced to save the test section. Measurements at each flow rate included the axial temperature distribution on the outer test-section wall, axial voltage variation, pressure drop across the length of test section, coolant temperature across the channel at a point $1\frac{1}{4}$ in. downstream from the end of the heated portion but still within the 0.030-in. channel, and the exit bulk temperature downstream from the 0.030-in. channel. The data will have to be reviewed in detail, but a preliminary survey of the data is given here.

Figure 21 shows the variation of pressure drop across the test section as a function of coolant flow rate for the nominal exit pressure of 675 psia. Figure 22 shows actual measured burnout points and the

Zenkevich-Subbotin burnout prediction curve for a 0.030-in. and a 0.040-in. channel. The axial maximum-to-average power density estimated for the test data and used in Fig. 22 was 1.4:1. These two curves summarize the type of information expected from the steady-state heat transfer program. The curves of Fig. 21 are used to evaluate flow instability in parallel channels and those in Fig. 22 to predict maximum power at constant flow.

The burnout detector worked well, allowing ~95 runs and 23 burnout points before actual physical burnout of the test section occurred Table XIX gives burnout data.

In reviewing the test data, it is important to bear in mind that at 100 MW the average and maximum operating heat flux at steady state is 5.1×10^5 Btu/hr-ft^2 and 2×10^6 Btu/hr-ft^2, respectively, whereas the nominal mass velocity is ~10×10^6 lb/hr-ft^2. The design inlet water temperature and exit pressure are 135°F and ~650 psia. The estimated

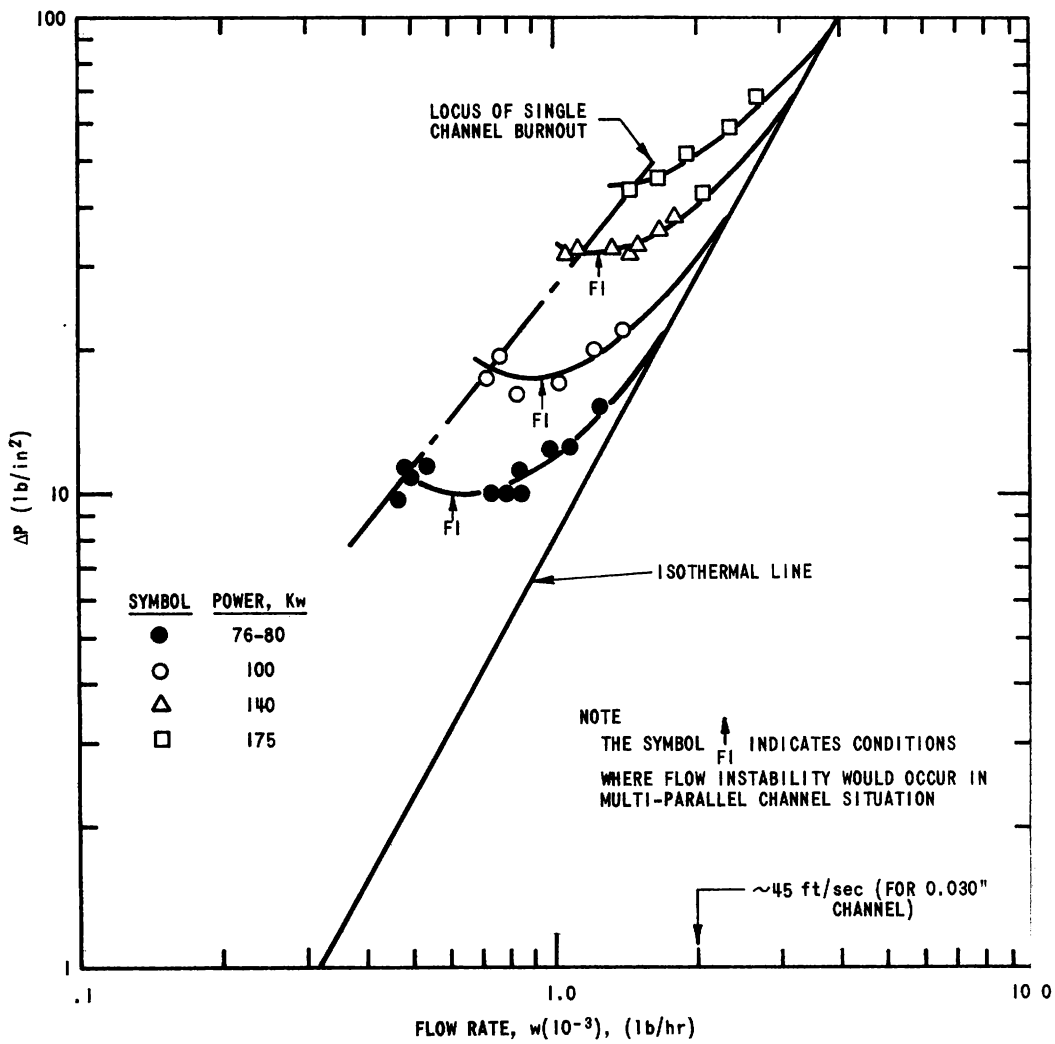

Fig. 21. Measured Pressure Drop-flow Rate Characteristic for 0.030-in. Test Section with Distortion for Exit Pressure of ~675 psia

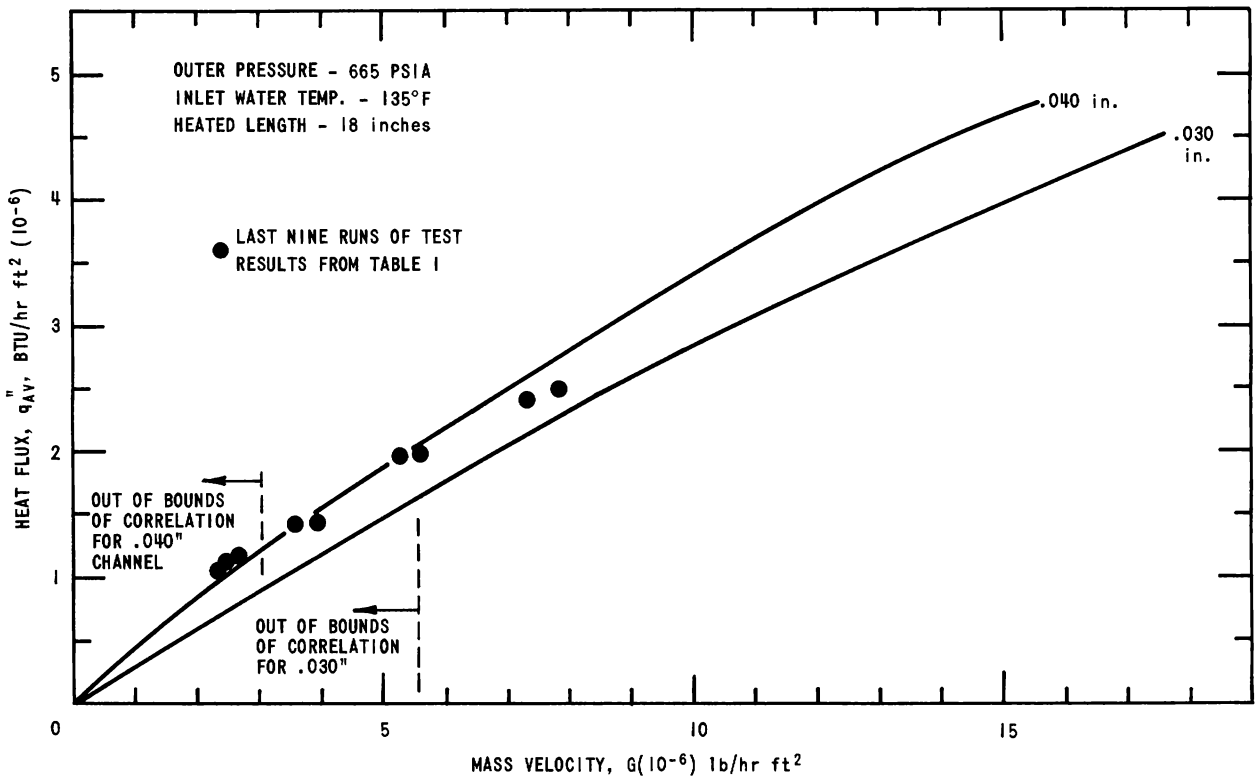

Fig. 22. Estimated Burnout Conditions for AARR Test Section Based on Zenkevich-Subbotin Correlation

TABLE XIX. Operating Conditions Coincident with Indicated Test-section Burnout

Run No.	Water Temperatures (°F) at Inlet	1[a]	2[a]	3[a]	Outlet	Outlet Pressure (psia)	Pressure Drop ΔP (lb/in.^{2})	Flow Rate W[lb/hr/(10^{-3})]	Inlet Mass Velocity [lb/hr/ft^2 (10^{-6})]	Power (kW)	Average Heat Flux [Btu/hr/ft^2 (10^{-6})]
B013	122.9	474.6	390.8	474.9	484.0	616.0	10.75	0.60	3.0	73.4	1.04
B021	117.8	480.5	464.5	482.5	488.8	639.7	11.25	0.56	2.8	76.2	1.08
B028	123.7	485.8	452.6	485.4	491.5	631.9	16.5	0.78	3.9	98.0	1.39
B030	124.8	480.3	445.8	482.0	486.0	605.2	16.25	0.81	4.1	96.8	1.37
B031	124.7	481.25	420.4	480.6	489.0	617.4	17.25	0.85	4.2	99.3	1.40
B034	127.2	483.4	437.2	481.6	484.0	604.7	21.25	1.08	5.4	113.4	1.60
B035	126.0	485.6	435.0	484.8	485.2	609.2	21.75	0.95	4.8	113.0	1.60
B037	127.8	483.7	450.1	484.4	485.65	618.4	29.25	1.12	5.6	131.1	1.85
B038	125.2	484.95	450.8	484.6	486.0	619.2	29.50	1.19	5.9	132.0	1.87
B041	113.5	476.45	361.4	472.5	454.3	617.7	20.25	0.82	4.1	109.6	1.55
B042	113.5	474.0	366.6	477.5	459.0	629.7	20.0	0.85	4.3	111.3	1.57
B043	118.5	478.4	379.0	479.8	460.8	606.0	20.0	0.78	3.9	110.4	1.56
B045	113.0	462.0	401.6	461.4	462.0	617.2	10.0	0.52	2.6	75.9	1.07
B050	113.5	473.8	367.5	470.7	461.8	627.4	10.0	0.63	3.2	77.4	1.09
B053	113.0	470.85	348.8	470.7	484.0	672.2	10.75	0.49	2.46	78.0	1.10
B054	113.2	481.2	381.4	481.9	487.7	672.4	9.75	0.465	2.328	76.44	1.08
B056	131.3	480.0	371.1	482.6	489.8	677.2	12.0	0.5338	2.673	82.0	1.16
B057	138.5	481.1	387.8	484.9	493.0	687.9	11.25	0.4878	2.442	75.95	1.07
B059	143.0	481.6	361.8	481.5	484.0	678.4	19.5	0.7771	3.891	100.76	1.42
B061	133.3	490.6	421.9	493.0	496.7	686.0	17.5	0.7200	3.604	100.1	1.42
B064	133.3	489.5	387.8	491.0	494.4	670	32.0	1.056	5.286	139.4	1.97
B068	139.2	489.0	423.4	493.2	496.7	683	32.5	1.118	5.597	139.7	1.98
B072	137.8	493.3	433.0	495.1	475.8	658.6	45.5	1.468	7.352	171.5	2.42

[a]See Fig. 20 for location.

maximum-to-average heat flux with the test section was ~1.4. Therefore, the maximum heat flux for each burnout point listed is ~1.4 times the average heat flux listed in Table XIX.

The test data may be used for the AARR in situations requiring an assessment of the impact upon reactor operation if excessive deformation

of this type occurred in the reactor. For example, the data depicted in Fig. 21 indicate that a channel with a shape herein attained would be subject to a flow-instability limitation for the low power-low flow rates before the critical heat flux condition would be reached. The data also indicate that a critical heat flux limit would occur before flow instability at the high power-high flow rate condition. This type of data illustrates the reason for conducting the tests with particular emphasis on pressure drop-flow rate characteristics.

Void measurements have not been satisfactory when at power because of alignment difficulties with the void-measuring equipment. Changes in test-section-assembly procedure and position of measurement have been instituted in an attempt to correct these difficulties.

The 0.050-in.-gap test section has been assembled and is being installed in the loop.

b. Fuel and Control-rod Design

(i) Stress and Hydraulic Analysis

(α) Pressure-distribution Studies and Fluid Dynamic Modeling. Preliminary estimates of the steady-state pressure as a function of "reference channel" and axial position have been made, including one or more postulated conditions for the fuel-plate subassembly, control blades, safety blade, and core shroud (see Table XX). These estimates are to be used for interim evaluations of the static loading of structural components in the core. Since the dimensions of the reflector and ITC are not yet clear, the pressure drops across these components have not yet been estimated.

TABLE XX. Summary of ΔP Calculations

I. ΔP across fuel plate assembly
Flow rate = 18,500 gpm
a. 70% of total area with U = 45 ft/sec
ΔP = 85.5 psi
b. 30% of total area with U = 51 ft/sec
ΔP = 88.2 psi

II. ΔP across control blades
Total flow through control blades and safety blades = 2200 gpm
a. Blade not in contact with channel
ΔP = 193 psi
b. Blade in contact with channel
ΔP = 109.8 psi

III. ΔP across safety blades
Total flow rate as shown in I
a. Blade not in contact with channel
ΔP = 199 psi
b. Blade in contact with channel
ΔP = 112.2 psi

IV. ΔP across core shroud
Assume V = 52.5 ft/sec
ΔP = 103 psi

(β) Control-rod Dynamics. Understanding of the conditions for lateral stability and possible oscillations of the control blade under a suddenly applied longitudinal force is desired. The preliminary mathematical analysis for the dynamic response of the control blade is basically complete. Further efforts are being directed toward the inclusion of hydrodynamic loading. Because of the potential complexity and coupling of this type of loading with the control-blade motion, computer requirements are being considered. It would be desirable for the parametric survey effort to be performed on an analog computer, but the decision for the final simulation will wait for an evaluation of the extent to which nonlinearities are expected to influence the problem.

For example, the piston-type damper, to be used in decelerating the control blade following a scram, has been modeled assuming a constant-area port through which the hydraulic fluid moves. It is assumed that a scram spring is also acting throughout the stroke of the damper. The resulting differential equation of motion is nonlinear. However, via a transformation, a solution can be obtained as an integral which can be evaluated numerically.

The initial effort to describe a fluid dynamic model (much oversimplified) for the purpose of explaining possible flow-induced oscillations of the control blades (and/or fuel subassemblies) included the assumptions of (1) one-dimensional flow, (2) incompressible fluid, and (3) no cross flow between channels formed by the control blade.

An expression for the pressure distribution, in the form of a partial differential equation, was derived by applying the momentum and continuity equations to an elemental volume from one of the channels. For the special case of steady-state flow, e.g., the case in which the blade is bowed due to a thermal gradient along its length, but not oscillating, the differential equation is separable and can be solved by integration.

The shearing stress along the bounding walls was modeled on the basis of results from documented experimental tests which have shown that for turbulent flow, the friction pressure drop varies as the velocity to the n^{th} power, n ranging from 1.72 (smooth wall) to 2.0 (rough wall). Therefore, the resulting expression for the pressure distribution is in terms of two unknown constants: K, a constant of proportionality, and n, the power to which the flow velocity is raised.

The transverse force intensity acting on the control blade is equal to the width of the blade times the distributed pressure difference across the blade.

For a preliminary investigation, it might be assumed that the steady-state pressure distribution can be used to represent the pressure distribution occurring during unsteady flow. With this assumption, the derived equations can be used in the dynamic response analysis of the control blades.

(γ) General Engineering Analysis of Structural Problems. In the process of evaluating the magnitude of the structural mechanics problems to lend guiding direction to the mechanics-research activity thermal thrusts, support-plate grid analyses, section properties, plate analyses appropriate to anticipated shroud configurations, plastic analysis of plates as required to establish deformation pattern of fuel elements were computed.

(δ) Material Properties. The effective mechanical properties at room temperature (to account for sandwich structure and orientation) were determined for samples taken from a depleted-uranium fuel plate. A reasonable average effective elastic modulus of 24×10^6 psi and a Poisson's ratio of 1/4 were determined.

(ii) Stress Tests. Much experimental work will be required to confirm certain intermediate conclusions about the gross deformation behavior of the "rhomboidal" fuel assembly. The problems emphasized here are primarily a result of a "kind of anistropy" of the moment of inertia of the cross section of the assembly, which could cause deformation components normal to the direction of lateral loading and/or traverse temperature gradient. Sufficient computations were performed to enable the determination of the moment of inertia for any orientation of applied bending moments. The minimum and maximum values were found to be about 0.90 $in.^4$ and 2.73 $in.^4$, respectively. The mutually perpendicular orientations of these moments of inertia are located about 6° from the lines bisecting the 60 and 120° angles between the two major axes of symmetry of the assembly. These data imply that subsequent stiffness (EI) calculations may be based on uniform material properties of the fuel-element cross section.

(iii) Hydraulics Tests—General Purpose Test Loop. The construction of a General Purpose Hydraulic Loop (GPHL) is complete. Hydraulic requirements of AARR fuel and control-rod test programs will be met by the loop as designed, but a more extreme range of conditions is possible by changing the pumping arrangement from series to parallel. The maximum capabilities under both modes of pumping are listed in Table XXI.

Actual testing of AARR fuel and control-rod components will take place within a test chamber fabricated from 12-in. Schedule 100, Type 304 stainless steel pipe. The chamber has four 4-in. dia, high-pressure, high-temperature viewing ports, and provision is made for

instrumenting test sections through the bottom flange. A major feature is a "Y" attachment containing a fluid channel selector which will allow reading the outputs of up to 48 Pitot-static tubes located within the flow channels of an AARR fuel assembly. These data and others will be transmitted to the control panel for recording and/or readout.

TABLE XXI. GPHL Operating Capabilities

Description	Pumps in Tandem	Pumps in Parallel
Flow, gpm	800	1600
Head, psi	350	175
Loop Pressure (design), psig	1250	1250
Max Operating Pressure, psig	1230	1230
Water Temp (design), °F	500	500
Max Operating Temp, °F	450	450
Min Operating Temp, °F	110	110

A fixture for support of a single full-size AARR fuel assembly within the test chamber was designed and fabricated. The chamber has sufficient room to accommodate several such fuel assemblies at one time, but no multiple-assembly fixture has been fabricated as yet.

c. Fuel Material Fabrication Development

(i) Nondestructive Evaluation of UO_2 Distribution. Possible techniques for making nondestructive tests as regards the homogeneity of dispersion of UO_2 in a UO_2-SS cermet has been conducted by the Illinois Institute of Technology Research Institute under contract with the AARR project.

Because of the small difference in density between the UO_2 (~10 g/cc) and stainless steel (~8 g/cc), it was necessary to use a technique that would give a better resolution between the two materials than that obtained with the usual methods of X-ray attenuation. It seemed possible to obtain a very acceptable resolution through use of the 120-keV radiation from Co^{57}. The 120-keV energy is slightly above the uranium "K" ring absorption edge at 116 keV. Thus the absorption coefficient of UO_2 is nearly a relative maximum when exposed to the 120-keV gamma rays. The relatively low absorption coefficient of stainless steel and the high absorption coefficient of the UO_2 at this energy level are sufficiently different to produce a difference in net 120-keV gamma-ray attenuation that will provide a high degree of contrast in the readout equipment. Further improvements in resolution of UO_2 particles in the stainless steel matrix graphic readout appears to be possible with a differentiating amplifier that has been developed by UKAERE Harwell. This special amplifier and its associated readout equipment has been ordered; delivery is expected in early June.

Evaluation of the basic Co^{57} photomultiplier gamma-attenuation equipment with conventional amplifiers and strip-chart readout has demonstrated the ability of a 1-μCi source to differentiate variations in fuel loading of less than 2% (i.e., 0.8 w/o UO_2 in the core) in a 0.03-sq in. area of fuel plate. A difference in clad thickness of 0.001 in. produced a difference in transmittance of 0.6%. Raising the source strength by a factor of 10-100 is expected to permit the use of a smaller scanning aperture, increase scanning speed, and reduction in the effect of background "noise." Such use will give increased speed and accuracy in the process of homogeneity measurement and evaluation.

(ii) Irradiations Test Program. Irradiation testing of the all-stainless-steel brazed-joint samples has been completed. The three-plate microassembly and the three 37 w/o UO_2-SS-0.16% B^{nat} (ZrB_2) fuel plates have completed one cycle of irradiation testing and will be irradiated for one more cycle. Additional fuel-plate specimens containing 37 w/o UO_2-SS-0.25% B^{nat} (ZrB_2) and 37 w/o UO_2-SS-0.16% B^{nat} (4 w/o B-Si glass beads) will also be irradiated.

A portion of the hot-cell evaluation by Phillips Company of the irradiation performance of the basic 37 w/o UO_2-SS cermet fuel irradiated in January-March 1965, has been completed. Analysis to date indicates that the use of UO_2 of 35% theoretical density yielded gross reduction in fuel-plate swelling at burnups of two times the average burnup expected in the AARR 100-MW Mark-I core. The studies have shown that swelling in the fuel plates will continue at a relatively insignificant amount at the AARR irradiation temperatures until the burnup reaches 25 x 10^{20} fiss/cc. Above 25 x 10^{20} fiss/cc the rate of swelling in the fuel plate is expected to increase to approximately 1.2-1.6% ΔV per each a/o burnup. These results, although encouraging for the UO_2-SS cermet, must still be confirmed for the burnable poison-bearing materials currently being tested.

d. Control-rod Drop Tests. Several drop tests were performed in the AARR control-rod mockup test facility to demonstrate control-blade scram and equipment performance. The data analyzed to date indicate a rather noticeable impact between the piston and the bottom of the dash pot. The redesign of the dash pot is necessary to improve its operating characteristics.

5. Component Design and Testing

a. Reactor Vessel

(i) Configuration. Major design revisions of the core package, fuel handling, and location of control rod drives have necessitated a modification of the physical profile of the reactor vessel. Figure 23 illustrates the modified vessel design which includes: (a) a new core- and reflector-support structure, (2) provisions for bottom control-rod drives, and

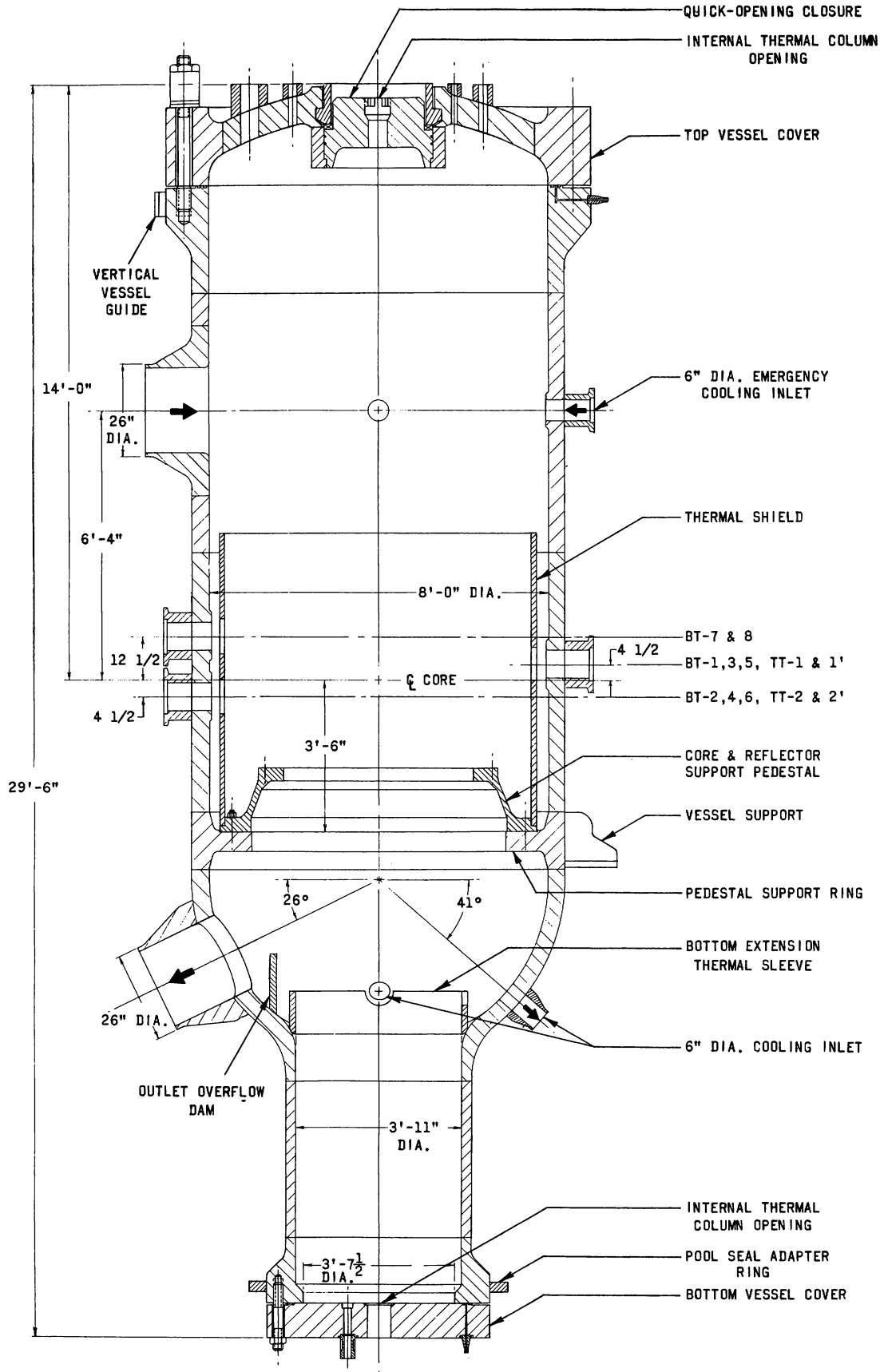

Fig. 23. AARR Pressure Vessel Profile

(3) a domed closure (see Progress Report for March 1966, ANL-7193, p. 85). The central, quick-opening closure designed for the original flat-head closure (Progress Report for October 1965, ANL-7115, p. 71) was retained for fuel-loading operations.

(ii) Stress Analyses. Numerous machine calculations were completed to assess the stress conditions in the vessel regions affected by the design revisions. The stress states in the portions of the vessel listed below are now known to meet the minimum requirements of Section III of the ASME Code "Nuclear vessels" under idealized temperature gradients:

a. entire vessel shell section between the flange closures;

b. upper vessel-closure flange;

c. closure bolting.

Calculations are in progress to determine the stresses in the irregularly perforated, flanged domed cover. Preliminary results of calculations indicate that four vertical-facility holes yielding access to the beryllium reflector are too close to the central quick-opening closure. The calculated stresses are above the ultimate strengths of the materials (such as SA212B, SS304, and Inconel) considered for the fabrication of the vessel. Alleviation of the stress condition will be attempted by relocation of the four nozzles.

Other calculations are in progress to determine maximum metal stress at the beam tube-nozzle area for Inconel under maximum thermal gradients and nuclear heat generation.

(iii) Vessel Specifications. A second interim vessel specification and revised drawings were prepared after receipt of vendors' comments on the preliminary specifications (see ANL-7176, p. 80). The newer specifications and drawings incorporate a number of design changes necessitated by the change from top to bottom rod drive. Additional design studies and stress calculations were initiated to alleviate the following two problems, defined in the vendors' responses to the inquiry:

a. stress-corrosion cracking of austenitic stainless steel cladding materials;

b. radiation damage to the vessel walls and beam tube nozzles.

An ad hoc committee was appointed to review the existing information on Inconel 600 alloy as a possible AARR pressure vessel material. A preliminary report was issued, recommending certain essential irradiation and corrosion programs. Inconel could be used either as welded-on cladding (on carbon steel) with solid Inconel beam tube nozzles or solid Inconel alloy construction throughout.

The recommendation for a solid Inconel vessel wall is based on the apparent radiation-damage resistance of this alloy. A search for additional data on the radiation effects of Inconel is under way to augment the meager published data. Measurements of neutron flux in the AARR critical facility are expected to give better definition of the radiation-damage spectrum at the vessel wall adjacent to the neutron window (needed for outside instrumentation) and at the beam tube nozzles. Both areas are located in a region of high flux of fast neutrons. For example, a fast flux (>0.1 MeV) of approximately 1 x 10^9 nV is estimated at 100-MW operation at the inside surface of the vessel wall adjacent to the neutron window. Exposure to this level of radiation now aggravates the selection of reactor vessel materials by introducing problems in radiation damage, particularly as regards nil-ductility-temperature (NDT). Meanwhile, three pieces of Inconel, 60 in. long by 16 in. wide by $4\frac{1}{2}$ in. thick, are on order to furnish the data required in the event that a solid (or partially solid) vessel wall is accepted for fabrication.

Alternatively, enlarged belt-line vessel sections, up to 120 in. in diameter, are under study. The vessel sections of larger diameter incorporate $12\frac{1}{2}$-in.-ID beam tube nozzles which permit a 3-in. radial annulus for water for thermalizing the damaging neutron fluxes on the nozzle walls.

b. Experimental Facilities. An updated thermal analysis of the AARR beam tubes has been completed. The original design study (see Progress Report for March 1964, ANL-6880) was based on an earlier version of the reactor core, namely, an aluminum instead of a stainless steel core. The results of the earlier study, although valid for the aluminum core, are much too conservative for the present design; therefore, to obtain more appropriate information for design, a re-examination of the beam tubes was initiated. The new study, made for a standard 5-in.-ID beam tube and a lower coolant temperature (135°F) at the beam tube inlet, now accounts for the lower heat generation associated with the stainless steel core.

The results of a steady-state thermal analysis are shown in Table XXII for the total heat generated in the portion of the beam tube and jacket within the beryllium reflector for both 100-MW and 240-MW reactor operation. The total heat generation was computed for a 5-in.-ID tube,

TABLE XXII. Total Heat Generated (kW)

Tube	100 MW		240 MW	
	Beam Tube	Jacket	Beam Tube	Jacket
Through Tubes	11.2	1.8	26.9	4.4
Blind Tubes BT-1, 3, 4, 6	9.7	1.6	23.3	3.8
Blind Tubes BT-2, 5	7.2	1.1	17.2	2.8

0.45-in. cylindrical wall thickness, and an 0.225-in. hemispherical wall thickness at the tip. In the analysis, the average coolant temperature rise was based on a flow rate of 24,600 lb/hr 50 gpm at 135°F, an annulus between the tube and jacket of 0.125 in., and a transfer of all jacket heat inward to the coolant. The average temperature rise, $\overline{\Delta T}$, and associated outlet coolant temperature are shown in Table XXIII for both 100-MW and 240-MW operation.

TABLE XXIII. Calculated Temperatures

Tube	Heat Input (kW)		$\overline{\Delta T}$ (°F)		Avg Outlet Temp (°F)	
	100 MW	240 MW	100 MW	240 MW	100 MW	240 MW
Through Tubes*	6.5	15.7	~1	3	136	138
BT-1, 3, 4, 6	11.3	27.1	2	5	137	140
BT-2, 5	8.3	20.0	~2	4	137	139

*To axial midpoint of through tube only, i.e., Table XXII values are halved.

For comparison, the coolant temperature rise, ΔT, along the axial line (hot line) of the beam tube closest to and facing the core was also computed. This analysis was made because the annular space between the beam tube and jacket may be fluted, in which case circumferential mixing would be prevented. The temperature rise was assumed proportional to the average heating rate over the length of the hot line of the tube. Table XXIV shows the results.

TABLE XXIV. Calculated Hot-line Temperatures

Tube	$T/\overline{\Delta T}$	ΔT (°F)		Outlet Temp (°F)	
		100 MW	240 MW	100 MW	240 MW
Through Tube*	1.64	2	5	137	140
BT-1, 3, 4, 6	2.57	6	13	141	148

*To axial midpoint of through tube only.

The location of the peak heat flux in the blind beam tubes was determined in order to verify that the coolant flow velocity is adequate for the region of peak flux. Because of the variation in the thickness of the blind tube tip and distance from the core center, the location of the peak heat flux is not obvious, except that it lies on the tube surface (i.e., axial hot line) facing the core. Figure 24 shows a plot of the local heat flux (normalized to the flux at the juncture of the cylinder and hemispherical tip) in the region of the tube tip. For convenience, the location of the normalized heat flux at any point is also referred to its angular displacement from the juncture

of the cylinder and hemispherical tip; at the juncture, the angle is 0. The plot shows the peak heat flux occurring at approximately a 5° displacement, at which it is slightly (4%) greater than the flux at the juncture. At this point (for tubes BT-1, 3, 4, 6), the distance from the center of the core is 35.4 cm and the heating rate is 7.7 W/g for beryllium. For aluminum, the heating rate corrected for flux peaking (1.3) and gamma-energy absorption (1.1) is 11 W/g at 240-MW operation.

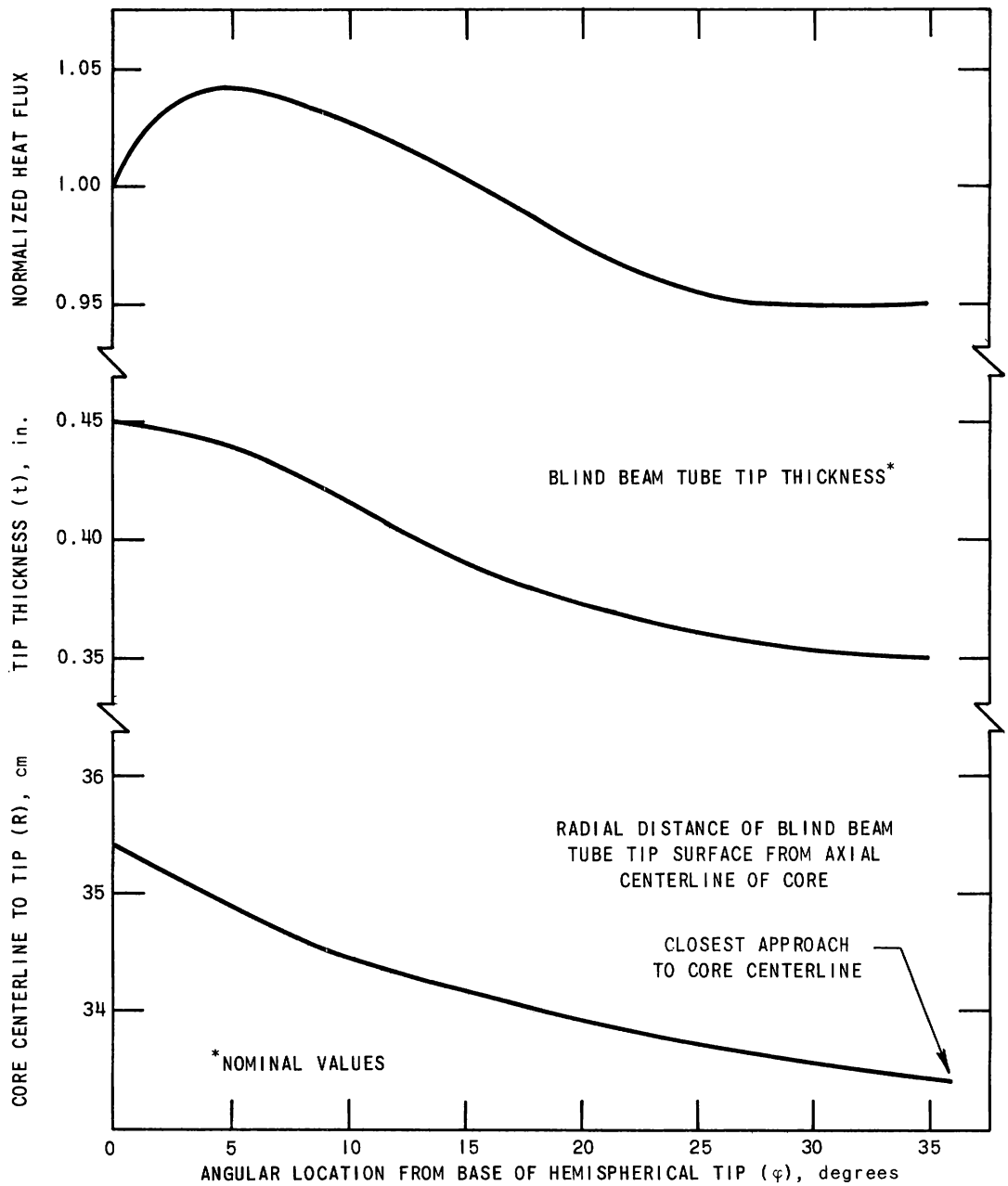

Fig. 24. Normalized Heat Flux vs. Position on Blind Beam Tube Hemispherical Tip

Assuming one dimensional heat flow, the computed heat flux at the juncture (hot side) is 111,000 Btu/hr-sq ft for 240-MW operation and

46,200 Btu/hr/sq ft for 100-MW operation. Allowing an added 8% for possible increased heating rate due to thermal growth toward the core center, the peak heat flux is 125,000 Btu/hr/sq ft at 240 MW and 52,500 Btu/hr/sq ft at 100 MW. These peak heat fluxes were used to determine the temperature drops over the fluid film, oxide film, and metal to obtain the maximum surface temperature and maximum metal wall temperature (inside surface).

A summary of the results of the fluid-film temperature drop calculations is shown in Table XXV for the blind tubes, $\Delta T(BT)$ and for the through tubes, $\Delta T(TT)$. The coolant flow for all cases was 24,600 lb/hr.

TABLE XXV. Fluid-film Calculations

Reactor Power (MW)	h (Btu/hr/sq ft/°F)	q"(BT-1, 3, 4, 6) (Btu/hr/sq ft)	q"(TT) (Btu/hr/sq ft)	ΔT(BT) (°F)	ΔT(TT * (°F)
240	2,065	125,000	60,500	61	30
100	2,065	52,500	25,200	26	13

*At axial midpoint of through tube.

Estimates of the temperature drop across a potential oxide coating on the beam tube surface are based on the experimental results of corrosion tests on aluminum. The water-oxide film interface temperature has been shown to be an important quantity in determining the rate of oxide formation.[17] Experimental results obtained under temperature condition closely resembling those expected for the beam tube were used to obtain temperature drops across the oxide film, with results as follows:

Surface Temp T_s (°F)	Exposure (hr)	Heat Flux (Btu/hr/sq ft)	Oxide Temp Drop ΔT_x (°F)	Data Source
190	1527	400,000	12.6	ANL-7152
260	1507	820,000	130	ANL-7115

The exposure period for this data did not include thermal cycling, which could possibly result in spallation. These results, when ratioed to the expected beam tube heat fluxes, yield the oxide-film temperature drops which are summarized in Table XXVI.

TABLE XXVI. Oxide-film Temperatures

		Tubes BT-1, 3, 4, 6		TT	
Reactor Power (MW)	Inlet Water (°F)	Water-Oxide Interface (°F)	ΔT_x (°F)	Water-Oxide Interface (°F)	ΔT_x (°F)
240	135	209	20	170	2
100	135	167	3	150	1
100	190	217	8	203	4

[17]Griess, J. C., et al., Effect of Heat Flux on Corrosion of Aluminum by Water, ORNL-3230 (Dec 1964).

The temperature drops (ΔT_m) through the beam tube walls are shown in Table XXVII for 6061-T6 aluminum. A conductivity of 100 Btu/hr/ft/°F was conservatively selected for all cases.

TABLE XXVII. Temperature Drops through Walls of Beam Tube

	BT-1, 3, 4, 6		TT	
Reactor Power (MW)	Heat Flux (Btu/hr/sq ft)	ΔT_m (°F)	Heat Flux (Btu/hr/sq ft)	ΔT_m (°F)
240	125,000	24	60,500	12
100	52,500	11	25,200	5

A summary of the beam tube hot-spot surface temperatures is given in Table XXVIII for a coolant flow rate of 24,600 lb/hr and an inlet temperature of 135°F. The metal wall temperature given refers to the inside surface of the beam tube wall, which is assumed insulated. Local water temperatures were obtained from Table XXIV.

TABLE XXVIII. Summary of Hot-spot Temperatures

	Blind Tube Temperatures (°F)			Through Tube Temperatures (°F)		
Reactor Power (MW)	Local Water	Oxide-H_2O Interface	Tube Metal	Local Water	Oxide-H_2O Interface	Tube Metal
240	148	209	253	140	170	184
100	141	167	181	137	150	156
100	196	217	236	192	203	212

c. Material Compatibility and Corrosion. The stainless steel specimen used in the test with a heat flux of 4×10^6 Btu/hr-ft^2 (see Progress Report for February 1966, ANL-7176, p. 85) has been partially examined. The water-cooled surface developed a very thin, dark film, which was apparently too thin to interfere measurably with heat transfer. Visually, there appears to be no localized attack on the specimen, but at this time, the metallographic examination is incomplete.

The second test with a stainless specimen has been started. In addition to a heat flux of 2×10^6 Btu/hr-ft^2, other test conditions are:

Flow rate, fps	45
Pressure, psig	
Specimen inlet	750
Specimen outlet	705
Water temperature, °F	
Specimen inlet	229.5
Specimen outlet	273.0

Also exposed in the loop are beryllium and aluminum specimens in a quantity rendering the ratio beryllium:aluminum:stainless steel heat transfer surface about the same as in the AARR design.

The temperatures observed on the specimen at the start of the test, and other pertinent thermal data are as follows:

Distance from Inlet End (in.)	Thermocouple Temperature (°F)	Temperature of Water Interface (°F)	Bulk Water Temperature (°F)	Fluid Film Coefficient (Btu/hr/ft²/°F)
1.25	454.0	345.5	236.0	19,000
2.25	465.0	356.5	245.0	18,700
3.25	464.0	355.5	252.0	18,400
4.25	471.0	362.5	258.0	18,200
5.25	475.0	366.5	265.0	18,700
5.50	484.0	373.5	267.0	18,500
6.25	482.0	375.5	272.0	18,400

After 720 hr the temperature of the specimen had not changed, indicating no detectable buildup of corrosion products on the water-cooled surface. The test will continue for three months (1 core life for the 100-MW core).

The isothermal loop test, in which various crevice and galvanically coupled specimens are exposed, was continued. Within the next month, this test will be terminated, and the corrosion specimens examined.

6. Control Studies

a. System Dynamics Analysis. Revised calculations of the AARR transient behavior when subjected to various perturbations of reactor steady-state conditions are in progress. These calculations are accomplished by the analog computer program used for PSAR analyses (see Progress Report for December 1964, ANL-6997), changed to include the latest estimates of relevant neutronic properties of the reactor. Comparisons of current values and those used for the bulk of previous PSAR calculations are shown in Table XXIX.

TABLE XXIX. Changes in Neutronic Properties of the AARR

	Doppler Effect*	Prompt Neutron Lifetime (μs)	Effective Delayed Neutron Fraction
PSAR Value	$\frac{\Delta P}{\Delta T} = -\frac{3 \times 10^{-3}}{T}$	10	0.0078
Current Value	$\frac{\Delta P}{\Delta T} = 0$	20	0.0072

*In the given expressions for the Doppler effect, ΔP = reactivity change (in absolute units), T = fuel temperature in degrees Kelvin, and ΔT = change in fuel temperature (in °K) from 273°K.

Revised calculations of reactor transients in response to positive step function and 33-ms ramp function reactivity insertions have been completed over the input reactivity range from \$0.25 to \$1.50. These calculations were made for a simulated initial reactor power level of 100 MW and no safety-system action was assumed during the course of the transients. Preliminary examination of the data and comparison with the previously obtained results for equal values of input reactivity, expressed in dollar units, indicate the following:

i. The peak power reached during the initial power burst is reduced below previously obtained values, especially for step-function reactivity insertions which exceed prompt critical.

ii. The initial power burst is broadened; for example, peak power occurs nearly 10 ms later than it did previously for step-function reactivity insertions.

iii. The energy released and fuel-plate temperatures obtained show a small general increase above previously calculated values.

iv. A slight decrease in the inherent, self-limiting capability of the reactor to protect itself from core damage due to rapid reactivity insertions is indicated by the calculations. For example, the threshold value of step-function reactivity just sufficient to cause hot-spot steam blanketing has been reduced from the previously obtained value of \$0.90 to approximately \$0.85.

These data will be examined further to provide more detailed and expanded conclusions for AARR reactivity-parameter studies.

b. Computer Control Study. A study has been initiated to investigate the feasibility and desirability of incorporating a digital computer into the plant instrumentation and control system. The study is divided into two separate phases. Phase one is a technical and economic feasibility study, covering many different plant-operating modes and digital-equipment configurations, to determine the desired extent of use of digital equipment in plant operation.

Phase two will be a comprehensive study of the particular digital-equipment participation selected during phase one. The objective of phase two is the establishment of the detailed requirements for an on-line digital computer.

Burns & Roe, Inc. will perform the major portion of the phase one study. Their effort will be supplemented in the area of reactor physics by Argonne personnel.

B. Liquid Metal Fast Breeder Reactor (LMFBR)

1. 1000-MWe Follow-on Study Program

The bid package covering the Nuclear Steam Supply System, which was sent to prospective contractors in April, has been expanded to include the Energy Conversion System (turbine-generator). The return date for proposals has been extended two weeks.

Other minor modifications were made in the package at the same time.

C. Magnetohydrodynamics

1. Condensing Injector Studies

Instrumentation of the Freon Refrigerant-11 condensing injector and test loop facility is complete. The portable Sciaky power supply is ready for service. Circulation has been initiated in the loop, and also power has been put to the heater sections. Preliminary startups and brief check-out runs have been made. No major difficulties have been encountered with the test loop. Continuing efforts have been directed toward analysis of the high-velocity condensing injector processes.

2. Effects of Interfacial Transport Processes on Film Condensation

A prototype test section for the study of the effects of interfacial transport processes on film condensation (see Progress Report for April 1966, ANL-7204, p. 73) is being designed and constructed for the purpose of developing instrumentation to measure both film thickness and wave structure, as well as interfacial sheer stress. Film thickness and wave structure will be measured by conductance probes mounted flush with the surface over which the film flows. An audio-frequency carrier signal will be used to measure changes in the film conductance, which reflects film characteristics over a localized region. Probe size and spacing will be varied to improve sensitivity of measurement over a maximum range of film thicknesses while still reflecting conditions over a minimum region of the film. Interfacial shear stress will be determined by measuring the velocity profile in the gas and then extrapolating to the film surface. Various configurations of the vapor and liquid inlets to the test section will also be constructed and tested to determine the configuration which will reduce entrance effects to a minimum. Preliminary tests will be done with the air-water loop.

Concurrent with these preliminary tests is the completed design of the boiler and condenser for the primary steam-water test loop.

IV. NUCLEAR SAFETY

A. Reactor Kinetics

1. Irradiated Fast Reactor Oxide Fuel Pins

Four uranium oxide fuel pins, of which two each were irradiated to 0.7 a/o and 3 a/o nominal burnup, respectively, in the Materials Testing Reactor, have been loaded into transparent TREAT meltdown capsules. Sample responses will be recorded by direct high-speed color photography. The four pins are from a batch of 14, half-length, EBR-II-size pins (see Progress Report for February 1966, ANL-7176, p. 86).

In addition to the previous (see ANL-7176, pp. 86-7) nondestructive examinations of 14 samples, continuous gamma-ray scans were taken along the axis, and X-ray photographs were taken of these four pins. The gamma scans provide a record for comparison with the previous neutron radiographs and for comparison with gamma scans of pins exposed in the TREAT tests. The X-ray photographs do not provide a picture of voids inside the oxide fuel as do the neutron radiographs, but do give a clearer representation of edges and small details of oxide fuel shapes inside the cladding. Fission gas samples, burnup samples, and ceramographic samples were taken from the control pins for study.

Data desired from the first photographically recorded meltdown experiments with irradiated oxide pins included information on (a) the phenomenology of slumping under transient heating (for example, on the possible movement of fuel down the central voids resulting from irradiation), (b) the behavior of irradiated oxide upon transient heating to failure (does frothing or fragmentation occur due to internally trapped fission gases?), (c) the thermal characteristics of the fuel-cladding "gaps" after irradiation (is heat transfer from the fuel to the cladding relatively uniform?--is the magnitude of the fuel-cladding thermal resistance changed from that typical of the unirradiated fuel studied earlier?), and (d) the phenomenology of pin failure and fuel motion associated with failure. Each pin is to be exposed to a preliminary, low-energy transient, appreciably below the failure threshold, which will produce a maximum cladding surface temperature below 1000°C. This test will provide information about the thermal resistance of the fuel-cladding gap in an excursion.

2. TREAT Meltdown Tests with Metallic Fuel in Flowing Sodium

The Mark-I integral sodium loop containing a single, 4.1% enriched EBR-II pin inside a ring of six dummy pins, which was exposed to a 1.67% k_{ex} transient (see Progress Report for April 1966, ANL-7204, p. 76), has been returned for disassembly and inspection of the sample.

A second loop was loaded with a 6% enriched pin and exposed to a TREAT excursion initiated with 2% k_{ex} to ensure sample failure. Because of the higher initial reactivity of the excursion and the higher enrichment of the sample, the energy input into a gram of sample fuel alloy is calculated to be 100% greater during the power peak of the excursion than that obtained in the earlier 1.67% k_{ex} transient test.

Transient records indicated a vigorous sample failure ~ 50 ms before the time of maximum power; at that time the flow, as measured on the electromagnetic flowmeter at the test-section inlet, dropped abruptly from about 4 m/sec to no flow. Simultaneously, the pressure transducer on the inlet registered a spike of about a millisecond width estimated to be ~24 atm from extrapolations of the transducer calibration. As flow of coolant resumed and reached approximately the original value, about 230 ms after the initial spike, another pressure spike of comparable magnitude occurred, accompanied by an abrupt flow reversal. It appears that for this type of high-energy input transient, the bursting of the sample pin inside the confined 7-pin test section stops flow, producing a "water hammer." Determination of the relative roles played in subsequent events by sodium entering at the inlet of the loop and sodium in the loop returning to the region of the pin failure after expulsion requires study of the sample remains and detailed analyses of the transient records.

3. Mark-II Integral Sodium Loop

Specifications have been established for an advanced (Mark-II) integral sodium loop for use in TREAT meltdown experiments on small clusters of fuel elements in flowing sodium. Although the experience gained through use of the Mark-I loop with metallic samples was used as a basis for the new loop design, the layout of the Mark-II loop is quite different. The new design provides higher pressure and temperatures, special remote handling, and more complete instrumentation for transient sodium behavior. The basic specifications provide for:

a. steady-state operating temperature of 500°C;

b. a test section capable of handling a cluster of 19 EBR-II-size pins;

c. integral, remotely operated sodium dump tank;

d. fast-response pressure-transducer assemblies mounted at both test-section inlet and outlet;

e. electromagnetic flowmeters at both test-section inlet and outlet;

f. insertion of sheathed thermocouples into the loop test section;

g. design pressure in excess of 70 atm at operating temperature;

h. loop sections in series, rather than in counterflow harp geometry;

i. pump section with pressure rating matching that of the rest of the loop.

4. Fast Reactor Safety

a. Coolant (Water) Expulsion Studies. The compilation and reduction of data for the water-expulsion studies continues. The height versus time information from the high-speed motion pictures has been obtained, and a computer program is being written to smooth and differentiate the raw data in order to obtain velocities and accelerations. Preliminary indications are that expulsion velocities ranged from about 2 to 8 m/sec. It is anticipated that the computer program will be operational in 3 to 6 weeks.

The expulsion apparatus will be slightly modified to permit tests at subatmospheric pressure. Since the specific volume of water vapor markedly increases with decreasing pressure, it is expected that the resulting pressure transients following heating surges will differ significantly from the runs at atmospheric pressure.

b. Superheat Experiment. Assembly of the experiment continues. The initial superheat test vessel has been assembled. The power lines, instrumentation lead wires, etc., are being brought through the walls of the containment vessel to the superheat test vessel. Fabrication of the gas-purification system is completed.

c. Critical-flow Studies. In a study of critical flow and the velocity of sound in two-phase one-component droplet flow, a one-dimensional propagation-velocity model was formulated by assuming the flow pattern to be mist flow. Unlike previous models, the present model is not restricted to the assumption of thermodynamic equilibrium between the vapor and liquid phase (that is, of equal temperatures and velocities). Two extreme cases were investigated:

(i) Disturbances which occur in much shorter times than the relaxation time of the mixtures, i.e., no mass and momentum transfer between the phases;

(ii) The system remaining in equilibrium through the disturbance, i.e., infinitely fast reacting system.

For high vapor fractions by weight, case (i) led to calculated propagation velocities nearly independent of the mixture quality and approximately equal to the velocity of sound in saturated vapor. On the other hand,

case (ii) indicated that the moisture content can greatly affect the propagation velocity. In this case, the velocity decreases with decreasing mixture quality, resulting in considerably lower values than the propagation velocity obtained for the all-vapor case.

When relaxation phenomena, which result from temperature and velocity lags between the phases, are included in the analysis, good agreement is illustrated between predicted values and actual two-phase critical flow and velocity of sound data obtained in the high-quality region.

5. Containment Program

The first stage of a hydrodynamic analysis undertaken in connection with the concept of primary containment by energy absorption was completed. A fluid dynamical analysis for an idealized reactor system having spherical symmetry was made to determine the effect of the destructive component of an energy release due to a nuclear accident on a primary containment system.

The destructive component was assumed equivalent to that produced by the detonation of a bare TNT charge. Most of the resistance to the explosive energy is offered by the concrete biological shield in which nonprestressed, unbonded, high-strength steel strands are embedded. The new concept for nuclear reactor containment is based upon the enormous energy-absorbing capabilities of the strands.

The hydrodynamical equations of motion, which constitute a set of nonlinear partial differential equations, were integrated numerically by the CDC 3600 computer. The propagation of shock discontinuities was treated by a common form of the artificial viscosity technique of J. von Neumann and R. D. Richtmeyer.

A sample problem simulated a typical sodium reactor installation. The TNT charge was 2 ft in diameter, weighed 375 lb, and was surrounded by a 5-ft-thick layer of water. The water was surrounded by a 1-ft-thick layer of argon, and the entire system was enclosed in a 6-ft-thick shell of concrete reinforced by high-strength steel strands.

The rate of strain to which the steel strands would be subjected, related to the impulse which is a result of the pressure acting on the biological shield serving as an energy-absorbing basket, was desired. A pressure-time curve for the inside face of the concrete structure was obtained from the analysis. The magnitude of the impulse is equivalent to the area under this pressure-time curve.

For the reactor system described above, the maximum strain rate to which any steel strand would be subjected was determined to be

12.32 sec^{-1}. This is classified in the extreme lower range of moderate rate of strain (10^0-10^3 sec^{-1}).

R. F. Klinger conducted strain-rate tests on the high-strength steel SAE 4340 in the range from the annealed condition (119,000 psi) to a nominal ultimate strength of 220,000 psi. The range of strain rates for his tests was 10^{-5} $sec^{-1} < \dot{\epsilon} < 10^1$ sec^{-1}. His results indicate that, in general, the strength properties increase with increasing strain rate. Moreover, the strain rate-effect becomes markedly less as the strength level of the steel is increased. In fact, the 220,000-psi steels (same ultimate stress range as for the steel strands) showed either no change or a slight loss in strength (< 3%) with increasing strain rate. No significant effect on the total elongation at any strength level was noted.

The significance of the above discussion is that the new containment concept is rendered entirely feasible. The new concept of primary containment is based upon the energy absorbing capability of the steel strands which, in turn, is dependent upon the strength and elongation properties of these strands. Both properties are functions of the strain rate. Since the strength and elongation of the SAE 4340 steel in the 220,000 psi range do not change appreciably for a strain rate less than 10^1 sec^{-1}, the values of these properties obtained by static testing procedures (at a strain rate of 10^{-3} sec^{-1}) could be used for design purposes for this example problem.

General information as to the manner in which the destructive component propagates and changes with time was obtained by monitoring the pressure at various critical locations in the reactor system and by following the movement of the interfaces between fluids. This information was obtained in the form of pressure-time curves and location-time curves.

B. TREAT

1. Operations

A single EBR-II pin was destructively tested in flowing sodium in a packaged sodium loop (see Sect. IV.A.2).

A sample of mixed PuO_2-UO_2 SEFOR fuel, covered with a cadmium filter, was subjected to four transient irradiations. A capsule containing one normal and one sodium-logged SEFOR UO_2 fuel sample was subjected to six transient irradiations. Both samples have been returned to the General Electric Company for examination.

2. Large TREAT Loop

A revision of the Large TREAT Loop Hazards report is being made. Study of a model for the meltdown and pressure-pulse generation was

acceptable on the basis of a range of possible reactivity additions. In addition, the second pressure-pulse mechanism, which may result from the return of sodium in contact with the fuel subsequent to fuel disintegration, was allowed for in the model. New calculations were made for this model.

The upper structure of the loop will be modified to incorporate the elimination of the surge suppressor. The surge suppressor will be held on standby for use if it is needed in the future.

C. Chemical and Associated Energy-transfer Problems in Reactor Safety

1. Equation-of-state Data by a Modified Exploding-wire Technique

Metal vapors, which are dielectrics at low pressure, become conductors at higher densities. This result is related to the overlap of the wave functions of the outer electrons in the atoms with the reduction in the interatomic distances.

The behavior of mixed vapor systems appears to be analogous to that of doped semiconductors and it may, therefore, be possible to improve the conductivity of vapors with techniques used in MHD devices, arc current rectifiers, and others. Improved conductivity of the vapor would permit higher energy inputs and higher temperatures to be achieved in exploding-wire experiments, to produce the vapor, before falling density inhibits the energy input.

Since negative ions are much larger than positive ions for a given vapor, electron transfer is more likely between a neutral species and a negative ion than between a neutral species and a positive ion of the same species. Accordingly, the most predominant species in the vapor should be capable of forming stable negative ions, and a minimum energy should be necessary to remove the electron from the donor. In other words, it is desirable to minimize the quantity $(I_d - A_m)$, where I_d is the donor ionization energy and A_m is the electron affinity of the acceptor.

Consideration of the properties of metal vapors indicates that the most desirable system would be mercury vapor "doped" with cesium, since $I_{Cs} = 3.87$ eV is the minimum known for metals, and $A_{Hg} = 1.79$ eV is the maximum known for metals. In addition, the vapor pressure characteristics of metals are satisfactory. The difference $I_{Cs} - A_{Hg} = 2.08$ eV is significantly less than for any single-species ionization potential. This system has been considered for MHD cycles for other reasons.

Experimental data in the literature indicate that the logarithm of the electrical conductivity increases linearly with metal density at constant

temperature for densities above one-half the room-temperature density. If the onset of metallic conductivity for mercury vapor is expected to take place at about 20% of the normal liquid density, a temperature of 1400°C and a pressure of about 500 atm would be needed unless a phase transition, caused by the onset of conduction, would lower the temperature and pressure. These conditions are sufficiently beyond present-day technology as to discourage any experiments but those intended to investigate fundamental behavior.

2. Metal-Water Reactions

a. Photographic Studies of Aluminum-clad Fuel Plate Samples in TREAT. A series of twenty experiments gave additional information on the in-pile behavior of aluminum-clad fuel materials. (Previous experiments were reported in Progress Reports for May 1964 and August 1965, ANL-6904, p. 106, and ANL-7090, p. 76.) In the present experiments samples of fuel were submerged in water in a transparent capsule and exposed to transient bursts of neutrons in the TREAT reactor. High-speed color motion pictures were taken of the samples during the transients. In several cases sample temperatures were measured by means of thermocouples. After the TREAT transients, gas samples were analyzed mass spectrometrically for hydrogen to determine the extent of chemical reaction.

Two types of fuel samples were studied. One, Spert 1-D fuel, was a 23 w/o fully enriched uranium-aluminum alloy, 0.020 in. thick and clad with 0.020-in.-thick 6061 aluminum. The second, HFIR fuel, was fully enriched 41.45 w/o U_3O_8-aluminum cermet, 0.030 in. thick and clad with 0.010-in.-thick 6061 aluminum. Results with the two types of fuels are summarized in Tables XXX and XXXI.

TABLE XXX. Summary of Spert-type Fuel Experiments

Exp. No.	Transient Number	Integrated Power (MW-sec)	Period (sec)	Fission Energy Input (cal/g)	Aluminum Reacted (%)	Comment
MWT-1	848	31	0.265	76	0	Calibration run
MWT-2	849	65	0.261	197	0	Calibration run
MWT-14	947	70	0.285	212	0	Boiling of water; no sample reaction
MWT-3	850	147	0.139	445	0	Corner melted
MWT-8	929	157	0.162	485	<1	Melted into globule
MWT-4	851	159	0.139	481	0	Melted into globule
MWT-7-1	897	69	0.265	209	0	Boiling of water; no sample reaction
MWT-7-2	898	163	0.140	493	0.25	Two-thirds of the sample melted
MWT-13	939	176	0.115	532	0.8	Melted into globule[a]
MWT-9	930	177	0.113	536	1.2	Melted and formed hull-shaped mass
MWT-10	931	205	0.108	621	5.3	Al_2O_3 clouded water
MWT-11	932	220	0.108	666	13.6	Fragmented
MWT-12	938	230	0.108	696	10.6	Fragmented
MWT-18	956	248	0.109	751	37	2040°C measured; sample fragmented
MWT-19	967	233	0.108	706	<3	Dropped into water

[a] Thermocouple failed after indicating 1400°C.

TABLE XXXI. Summary of HFIR-type Fuel Experiments

Exp. No.	Transient Number	Integrated Power (MW-sec)	Period (sec)	Fission Energy Input (cal/g)	Aluminum Reacted (%)	Comment
MWT-5	862	21	0.270	170	0	Calibration
MWT-6	863	65	0.265	530	0.2	Cladding partially molten; blow hole
MWT-15	948	81.5	0.285	662	1.8	Sample melted;[a] UO_2 layer visible
MWT-16	952	85.5	0.280	694	1.7	Cladding molten
MWT-17	955	99	0.280	805	12	2170-2370°C; fragmented; UO_2 layer visibl
MWT-20	968	108	0.228	877	3	Dropped in water; UO_2 layer visible

[a] Thermocouple failed after indicating 1400°C.

The two fuel types showed qualitatively similar behavior in the extents of metal-water reaction. In each case no significant reaction was observed until a threshold energy was reached; then the extent of reaction increased fairly rapidly with increasing energy input. For the Spert-type fuel, for example, the threshold was at about 600 cal/g (see also ANL-6904, p. 106). An increase in energy from 620 to 750 cal/g increased the extent of reaction from about 5 to 37%. Less data are available for HFIR-type fuels, but a similar effect at higher energies is observed. It should be noted that the reactor period, which is a measure of the rate of energy input to the fuel sample, varied from 0.108 to 0.265 sec in the runs with Spert fuel and from 0.228 to 0.285 sec in the runs with HFIR fuel. In this range of reactor periods (0.1 to 0.3 sec) the heat losses from the samples were large; the temperature reached by a sample was consequently strongly dependent on the reactor period. Thus, the difference in energy thresholds between the two types of fuel samples is probably a result of differences in reactor periods. Previous experiments in TREAT with HFIR fuel at periods from 0.10 to 0.15 sec (see ANL-7090, p. 75) indicated a threshold energy that is in good agreement with the Spert data.

After the first transients in which complete sample melting was obtained, the sample adhered to the alumina support pins. Since the samples were relatively immobile even though melted, a technique was developed to obtain temperature data during the transient by use of 0.010-in. thermocouple wire. As noted in Tables XXX and XXXI, the thermocouples in experiments MWT-13 (Spert) and MWT-15 (HFIR) indicated approximately 1400°C, the region of melting of the Chromel-Alumel wires used as thermocouples and consequently not necessarily the maximum sample temperature.

In experiments MWT-17 (HFIR) and MWT-18 (Spert) W-5% Re/W-26% Re thermocouples were used. Sample breakup coincided with a temperature approximately equal to the boiling point of aluminum (namely, 2270°C). In MWT-17, intermittent contact was apparently made between the sample and the thermocouple junction. It may tentatively be suggested that when the temperature of such samples exceeds a lower limit of about 1400°C, significant aluminum-water reaction will occur; however, the lack of temperature uniformity observed in the samples during the TREAT transients precludes exact measurement of this lower temperature limit. Nonuniform temperatures are clearly evident in the films taken of the samples during the tests.

The general sequence of events as observed in the motion picture taken during the transients is outlined below:

i) Power rises.[17]

ii) Water boils.

iii) Melting occurs: Spert fuel melts to globule; HFIR fuel slumps and develops holes.

iv) Glowing observed; bubbles of hydrogen form.

v) HFIR samples fuse to globules.

vi) Brightness increases and ignition occurs, as indicated by oxide smoke producing a cloudiness of the water.

vii) Sample fragments.

viii) Sample burns until quenched.

It is interesting to note that fragmentation occurs after ignition. The fragmentation apparently results from the water column driving the sample against the bottom of the vessel. The water is initially forced upward forming a bubble; the collapse of the bubble forces the return of the water to the bottom of the vessel, thereby fragmenting the sample. A similar phenomenon was observed when metal particles at the bottom of a water column were heated with a laser beam.[18] In that work it was observed that the particles were forced to the bottom of the vessel quite violently, often with sample break-up resulting.

---

[17]Seen on film as counting marks.

[18]Chemical Engineering Division Semiannual Report, January-June 1964, ANL-6900, p. 253.

A thermite reaction between aluminum and U_3O_8 would be expected to occur in the experiments with HFIR fuel samples. In previous laboratory studies with 40 w/o U_3O_8-aluminum compacts, a thermite reaction was observed for samples heated to 1000°C. Self-heating rates of about 100 to 200°C/sec were measured.[19] During the TREAT transients, the HFIR fuel plates (41.45 w/o U_3O_8) were subjected to heating rates which were at least greater by an order of magnitude than the rates attributable to the thermite reaction. Thus, it is not surprising that no evidence of the thermite reaction was observable on the temperature records of the experiments. However, in experiments MWT-15, -17, and -20, a layer of brown UO_2 (identified by X-ray diffraction) was visible on the edge of the samples, indicating that the thermite reaction did occur with these samples.

The last two experiments of the series, MWT-19 and -20, were designed to observe the behavior of a molten fuel sample dropping into water. The samples were heated while suspended above the water column and were released after the aluminum cladding reached its melting point (660°C). In both experiments parts of the sample, after dropping into the water, became incandescent and hydrogen was released; however, only a small fraction of the aluminum reacted with the water. In both experiments the energy input was of such magnitude that 20 to 30% of the aluminum would have reacted had the samples been placed in the water prior to heating as in the previous experiments. The cermet sample in MWT-20 had a layer of brown UO_2 on one edge. The UO_2 appeared to have been molten, thereby indicating a temperature, at least locally, of 2800°C or higher.

Analysis of the films is continuing to help clarify the relations among reactor power, temperature, fuel behavior, and other parameters.

b. High-temperature, High-pressure Furnace Studies. Experiments designed to study the reactions of fuel cladding under conditions simulating the environment in a water-cooled power reactor following a loss-of-coolant accident have continued. The studies are carried out in a furnace designed for a maximum pressure of 1000 psig and sample temperatures as high as 1700°C (see Progress Report for November 1964, ANL-6977, p. 82). The furnace consists of two zones: an internal steam-filled zone that is surrounded by an alumina tube, and an external zone that is argon filled. The argon-filled zone contains molybdenum heater windings and insulation. The pressures in the two zones are automatically matched to avoid stresses on the alumina tube. Water is introduced into the lower part of the steam zone by a positive-displacement pump and is converted to steam. At the start of an experiment, the sample is elevated

[19]Chemical Engineering Division Semiannual Report, January-June 1964, ANL-6900, p. 253.

from a moderate-temperature section, where reaction with steam is negligible, into the high-temperature section. Some unreacted steam and the hydrogen produced by the metal-steam reaction are continuously removed from the upper part of the steam zone (high-temperature section) through an outlet valve. The extent and the rate of metal-steam reaction are determined by continuously monitoring the amount of hydrogen collected. Upon completion of an experiment, the sample is lowered to its initial position.

Previous studies of the reaction of single Zircaloy-2-clad and type 304 stainless steel-clad, UO_2-core fuel rods with high temperature steam (see Progress Report for July 1965, ANL-7082, p. 67) have been extended to include bundles of 4 rods. In the previous experiments, the fuel rod was held in the lower part of the furnace, with the top of the rod at a temperature of about 900°C. At the start of an experiment the 8-in. long fuel rod (3/8-in. OD, 0.025-in. cladding thickness) was raised at the rate of 1 in./min (total of 8 in.) until the upper part of the rod was in the hot zone (1500°C). After insertion, the fuel rod was held in the hot zone for 2 min and then rapidly removed. The results of these single-rod experiments showed that the fuel rod surface temperature rose to about 1600°C (100°C above the furnace temperature) at the hot end for both types of cladding. Under these conditions the stainless steel cladding reacted about twice as fast as the Zircaloy-2 cladding

In the present experiments, a 4-rod fuel bundle in a square array with 0.6-in. center-to-center spacing was exposed to 1 atm steam. The steam flow was increased from 10 g/min (the rate for the experiments with single rods) to 25 g/min to insure that the reaction was not steam limited. Other experimental conditions were not altered from those used in the earlier experiments.

A photograph of a 4-rod bundle (type 304 stainless steel cladding) after exposure to 1 atm steam is shown in Fig. 25. The holder is

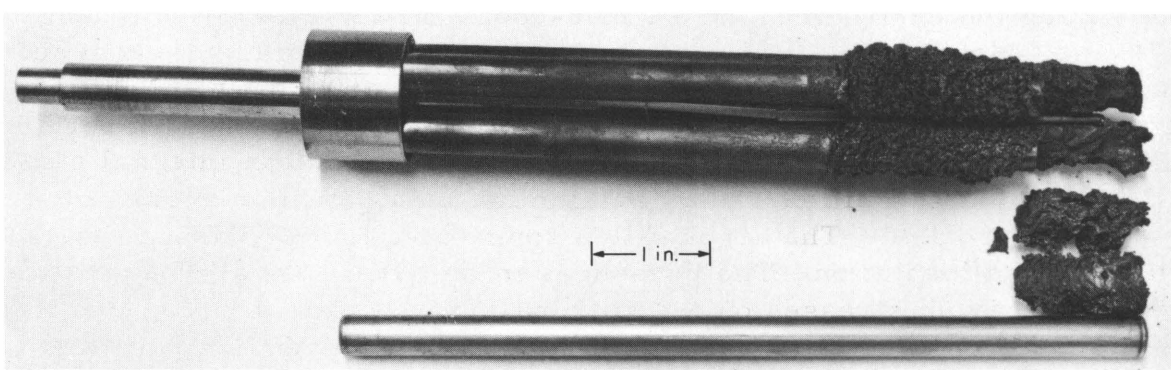

Fig. 25. Four-rod Bundle of Type 304 Stainless Steel-clad, UO_2-core Fuel after Exposure to One atm Steam at 1600°C. (Unexposed fuel rod also shown for comparison.)

shown at the bottom and an unexposed fuel rod on the right. Figure 26 is a close-up view showing the area near the boundary (which was at a temperature of about 1400°C) between the rapid "frothing" reaction and the slow "corrosion" reaction. In the area of rapid reaction, the expansion of the reaction products into the steam flow channel is evident, with bridging between rods occurring in some areas. The amount of hydrogen evolved per fuel rod was about the same as that observed in similar experiments with single fuel rods (i.e., the total amount of hydrogen evolved was approximately four times the amount evolved in the experiments with single rods).

Fig. 26. Close-up View of a Four-rod Bundle of the Type 304 Stainless Steel-clad, UO_2-core Fuel Rods in Fig. 25.

The residue from a 4-rod bundle (with Zircaloy-2 cladding) after exposure to high-temperature steam is shown in Fig. 27, along with an unexposed rod. The holder is at the left. Although the fuel elements were badly damaged, a large portion of the fuel was still encased in tubes of oxidized Zircaloy. Some of the damage to the cladding occurred while the test section was being removed from the furnace. Self-heating of the Zircaloy-2-clad elements was apparent; during the run the temperature of the hot end of the sample exceeded 1700°C (more than 200°C above the furnace temperature). The hydrogen evolved per fuel rod was about twice that observed in the single-rod experiment, which would be expected because of the higher temperatures reached by the 4-rod bundle.

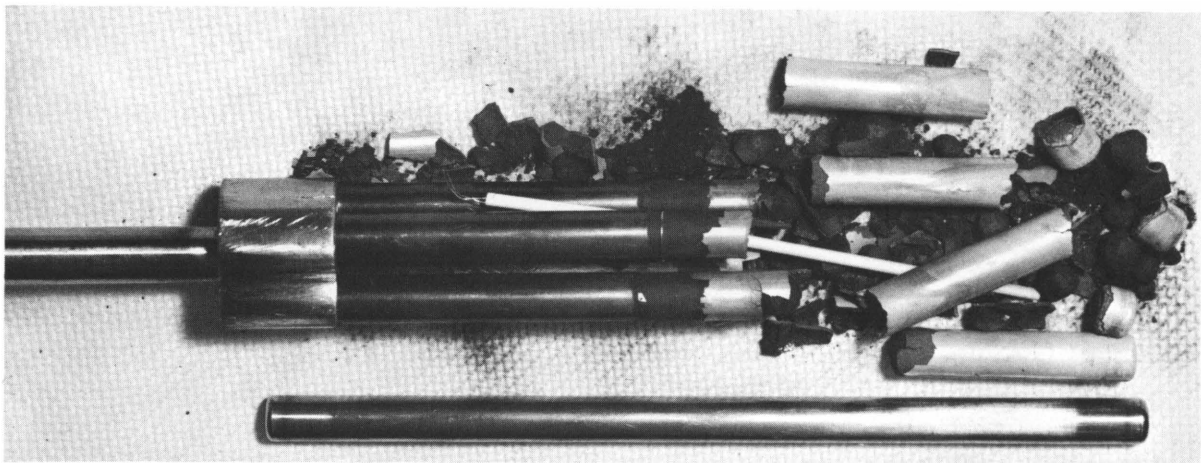

Fig. 27. Four-rod Bundle of Zircaloy-2-clad, UO_2-core Fuel after Exposure to One atm Steam at Temperatures Greater Than 1700°C. (Unexposed fuel rod also shown for comparison.)

D. Plutonium Volatility Safety

1. Chemistry of Tellurium Fluorides

Studies of the reactions of volatile tellurium fluorides have been initiated to determine the conditions under which tellurium is fixed on a solid and to investigate the kinetics and stoichiometry of the reaction. Preliminary studies of the sorption of tellurium hexafluoride on activated alumina at 25 to 100°C indicated that TeF_6 is in part reversibly sorbable when TeF_6 sorption is carried out at 100°C or below. Further studies are planned to measure the extent of sorption and desorption of TeF_6 on activated alumina at temperatures up to 400°C.

2. Disposal of Gaseous Fluoride Volatility Reagents.

The studies on environmental contamination control for fluoride volatility processing involve the development of methods for the treatment of gas streams containing plutonium hexafluoride and fission product fluorides, as well as treatment of gas streams containing reagents such as fluorine and bromine fluorides. A series of tests have been performed in a 2-in.-dia fluid-bed reactor to evaluate the use of a fluidized bed of activated alumina as a means for disposal of fluorine (initial tests with this experimental system were reported in Progress Report for April 1966, ANL-7204, p. 86). In current tests at bed temperatures of 300 to 400°C, the concentration of fluorine in the effluent gas from the fluid-bed reactor preceding breakthrough of fluorine has been less than 5 ppm. The efficiency of removal of fluorine from the inlet gas stream has therefore been ~99.99%. A factorially designed experiment is planned to study the effect of temperature, gas concentration, gas velocity, bed-particle size, and bed height on the efficiency of fluorine removal and on the extent of conversion of alumina to aluminum fluoride.

V. PUBLICATIONS

Papers

Nonisothermal Reaction of Uranium with Water by the Condense : Discharge Method
Louis Baker
Nucl. Sci. Eng. 25, 116-130 (June 1966)

High Temperature-High Pressure Cell for Measuring Densities of Metals by a Radiation Counting Technique
I. G. Dillon, P. A. Nelson, and B. S. Swanson
Rev. Sci. Instr. 37, 614-619 (May 1966)

Phase Relations in the Uranium-Uranium Dioxide System at Hig ı Temperatures
R. K. Edwards and A. E. Martin
Proc. IAEA Symp. on Thermodynamics with Emphasis ɔn Nuclear Materials and Atomic Transport in Solids, Vie ına, July 22-27, 1965. Intern. Atomic Energy Agency, Vieni a, 1966, Vol. 2, pp. 423-430

Fluidized-Packed Beds
John D. Gabor
Chem. Eng. Progr. Symp. Ser. 62(62), 32-41 (1966)

Reaction of Uranium with Water as Initiated by a Power Excursiɔn in a Nuclear Reactor (TREAT)
R. O. Ivins, R. C. Liimatainen, and F. J. Testa
Nucl. Sci. Eng. 25, 131-140 (June 1966)

Isothermal Reaction of Uranium with Steam between 400 and 160ɔ°C
R. E. Wilson, C. R. Barnes, R. A. Koonz, and Louis Baker
Nucl. Sci. Eng. 25, 109-115 (June 1966)

Current Practices in Handling and Storing Solid Radioactive Wa: te from Reactors
C. E. Stevenson
Nucl. Safety 7(2), 231-235 (Winter 1965-1966)

Vibratory Compaction. II. Compaction of Angular Shapes
J. E. Ayer and F. E. Soppet
J. Am. Ceram. Soc. 49, 207-210 (April 1966)

Phase Relations and Structures in Uranium-Plutonium-Fissium Alloys
O. L. Kruger
J. Nucl. Mater. 19(1), 29 (April 1966)

Preparation of the Sulfides and Phosphides of Plutonium
O. L. Kruger and J. B. Moser
J. Inorg. Nucl. Chem. 28, 825-832 (March 1966)

Refractory Metal Tubing Inspection Using Ultrasonic and Pulsed Eddy Current Methods
C. J. Renken and R. H. Selner
Mater. Eval. 24, 257-262 (May 1966)

Corrosion Behavior of Steels and Nickel Alloys in Superheated Steam
W. E. Ruther, R. R. Schlueter, R. H. Lee, and R. K. Hart
Corrosion 22, 147-155 (May 1966)

Incorporation of Nonstandard Input/Output Devices into FORTRAN Systems
C. E. Cohn
Comm. Assoc. Computing Mach. 9, 343-344 (May 1966)

Conference on Neutron Cross Section Technology
C. N. Kelber
Nucl. News 9, 22-23 (May 1966)

Mathematical and Practical Aspects of Heat Transfer in Double Pipe Heat Exchangers
R. P. Stein
Proc. Third Intern. Heat Transfer Conf., Chicago, August 7-12, 1966. AIChE, New York, 1966, Vol. 1, p. 139

Elastic and Inelastic Scattering of Fast Neutrons from Ag, In, and Cd
W. G. Vonach and A. B. Smith
Nucl. Phys. 78(2), 389-408 (1966)

Thermoelastic Stresses and Deformations in Reactor Fuel Plates
C. K. Youngdahl
Nucl. Eng. Design 3(2), 205-222 (February-March 1966)

The Sleeve Induction Motor for High-Performance Servomechanisms
D. E. Wiegand
IEEE Trans. IGA-2(2), 151-157 (March-April 1966)

The following appeared in Power Reactor Technology, 8(4) (Fall 1965):

Liquid-Metal MHD Topping Cycles
Michael Petrick
199-207

Evaluating Heavy-Atom Cross Sections for Plutonium Recycle Calculations
E. M. Pennington
210-211

Critical and Exponential Experiments with Plutonium
K. E. Plumlee
211-214

ANL Reports